2014

Mutations in a Mechanosensitive Channel Enable Intravascular Metaststic Cell Survival

Paul William Furlow

MUTATIONS IN A MECHANOSENSITIVE CHANNEL ENABLE INTRAVASCULAR METASTSTIC CELL SURVIVAL

A Thesis Presented to the Faculty of

The Rockefeller University

in Partial Fulfillment of the Requirements for

the degree of Doctor of Philosophy

by

Paul William Furlow

June 2014

MUTATIONS IN A MECHANOSENSITIVE CHANNEL ENABLE INTRAVASCULAR METASTSTIC CELL SURVIVAL

Paul William Furlow, Ph.D.

The Rockefeller University 2014

Next-generation sequencing technology has revolutionized cancer biology by accelerating the unbiased discovery of mutations across human cancers[1-4]. Despite this advance, it remains unknown whether there exist mutations that function specifically to drive steps in the metastatic cascade independent from, or perhaps even to the detriment of, tumor initiation and growth[5]. The development and implementation of a discovery framework that integrates next-generation RNA-sequencing with *in vivo* selection, has identified recurrent non-synonymous amino acid mutations that are enriched in metastatic breast cancer cells and predicted to significantly alter protein function. The pro-metastatic role of one of these mutations—a nonsense alteration that yields a truncated pannexin-1 ($PANX1^{1-89}$) plasma membrane megachannel subunit—was functionally characterized. $PANX1^{1-89}$ forms a multimeric complex with wild-type PANX1 at the plasma membrane and augments PANX1 channel activity to promote cancer cell survival soon after cells enter the microvasculature of metastatic target organs, where they become physically deformed within vessels. Enhanced ATP release from PANX1 channels, which are activated during membrane stretch, acts as a cell autonomous survival signal during lethal cellular deformation. Functional characterization of additional nonsense and missense PANX1

mutations detected in epithelial cancers of the colon, lung, and prostate reveals that these mutations also enhance PANX1-mediated ATP release. One such truncating colorectal cancer variant is also shown to promote survival during cellular deformation as well as *in vivo* intravascular survival, dissemination and metastatic liver colonization by colon cancer cells. Finally, pharmacological treatment of mice with a PANX1 inhibitor suppresses breast cancer metastasis to the lungs, implicating PANX1 as a therapeutic target in cancer. These findings reveal that mutational augmentation of PANX1 channel activity during mechanical trauma enables cancer cells to overcome a major metastasis suppressive barrier—cell death in the microvasculature.

To my grandfather, Bill Cowell (1926-2007)

“Things have gone pretty well!”

- Bill Cowell, *Memories* 1998

ACKNOWLEDGEMENTS

I would first and foremost like to thank my mentor, colleague and friend, Sohail. Your investment, faith and confidence in this work made it not only possible, but also a true joy. In addition, I deeply thank the entire Tavazoie Lab for all their assistance, support and advice. I would like to give a special mention to the work of Steven Zhang, Nils Halberg, Hani Goodarzi, Claudio Alarcon and Creed Mangrum, who have all helped tremendously in moving this project forward. I also would like to thank our computational collaborators from Weill Cornell Medical College, Dr. Olivier Elemento and Dr. T. David Soong, whose expertise in sequencing analysis was critical to our success. I thank Dr. Connie Zhao of the Rockefeller Genomics Resource Center and Jenny Xiang of the WCMC Genomics Resources Core Facility for their assistance with next-generation RNA-sequencing. To Dr. Sarat Chandarlapaty of MSKCC, thank you for providing the MDA-MB-468, BT549 and HCC1806 breast cancer cell lines. To Dr. Val Shestopalov of the Bascom Palmer Eye Institute, a sincere thank you for sending the PANX1-KO mice up from Miami. To Nora Pencheva, Jason Ross, Zander Nguyen and Ryan Notti, thank you for your comments and improvements on the earlier drafts of these results.

To my Faculty Advisory Committee, Dr. Tarun Kapoor, Dr. David Allis and Dr. Olivier Elemento, thank you all for your time, advice and guidance. I look forward to a continued correspondence as colleagues in the years to come. To my

gracious external examiner Dr. Andy Minn, thank you for 1) creating the MDA-LM2 lines years ago and 2) taking time away from your clinical duties to make the trip up from The University of Pennsylvania to provide valuable feedback on this work.

To Dr. Olaf Anderson, Ruth Gotian and the entire faculty and staff of the Weill Cornell/Rockefeller University/Sloan-Kettering Tri-Institutional MD-PhD program, a very big thank you for taking a chance on a budding scientist from the Upper Peninsula of Michigan, and for all your support, advice and, most importantly, the many good times along the way. I could not imagine a better place to train. I certainly would like to thank the support of NIH MSTP grant GM07739, and the taxpayers of the United States of America.

On a more personal note, I thank my best friend and rock, Jennie. I love you for so many reasons, but your unconditional support and encouragement during these years turned the lows into highs and made the highs even higher. To Mom, Dad and Stephanie, without you, this would not have happened—thank you for your love and motivation. To my many friends in New York City and beyond, we sure managed to have a good bit of fun during this!

TABLE OF CONENTS

LIST OF FIGURES

LIST OF TABLES

CHAPTER I: INTRODUCTION

Despite significant advances in mammographic screening, surgery and medical therapy, breast cancer remains a tremendously devastating problem. It is consistently the leading cancer among females in the United States[6], predicted to afflict one out of every eight US women over the course of their lives[1]. Fortunately, early identification and treatment of a localized mass provides a relative 5-year survival rate of 98.6%[6]. However, if at the time of diagnosis the cells within the primary tumor have already acquired the ability to metastasize, or disseminate through the body to form secondary tumors in distal organs, this rate drops to 23.3%[6]. In fact, 90% of all solid tumor-related deaths are caused by metastasis, not primary tumor burden[7]. These statistics highlight the need for additional research into the molecular basis of metastasis. By asking whether specific genetic changes exist that function to promote metastatic dissemination and colonization independent from, or perhaps even to the detriment of, tumorigenesis, the cellular mechanisms that result in the majority of cancer-related death may be revealed. An understanding of these mechanisms may offer a new opportunity for the development of therapeutic agents that can effectively prolong the life, in both duration and quality, of those cancer patients otherwise without curative options.

The metastatic process would seem to be an impossible journey for a single cell to complete. To leave its origin in the primary tumor and travel through the bloodstream to take up residence in a noncontiguous organ, a malignant cell must successfully overcome a number of challenges. The ability to complete this

stepwise sequence of events, known as the “metastatic cascade”, requires a primary tumor cell to be fully equipped to invade through the extracellular matrix, migrate towards the blood vessels or lymphatics, intravasate into those vessels, survive embolization in the circulation, adhere to small vessels at the secondary site, extravasate into the secondary organ, survive the foreign microenvironment, and reinitiate unregulated proliferation for secondary tumor growth[7] (Fig. 1). It is remarkable that a successful metastatic cell harbors a genetic landscape that grants it each and every one of the countless phenotypes required to complete this journey[3]. For this reason, metastasis is accomplished by only the subpopulations of cells within a primary tumor that possess all of the traits required to complete the process[8-10]. It is then critical to understand how such traits are acquired through genetic and/or epigenetic alterations that arise over the evolution of a metastatic primary tumor.

Somatic mutations arise at random in every cell that divides. Normally, these alterations are repaired, otherwise the afflicted cell undergoes apoptosis[1]. In rare instances, a mutation will persist and provide the cell with a growth advantage by altering the function of a protein that is crucial for key cell biological processes, such as cell cycle regulation, differentiation, apoptosis or DNA repair[5,9]. Genes affected by such mutations are classified as oncogenes or tumor suppressors[5]. A selective proliferative advantage results when a spontaneous mutation “turns-on” an oncogene or “turns-off” a tumor suppressor. Mutations of this nature, often referred to as “driver mutations”, promote the clonal expansion of the cell without regard to the

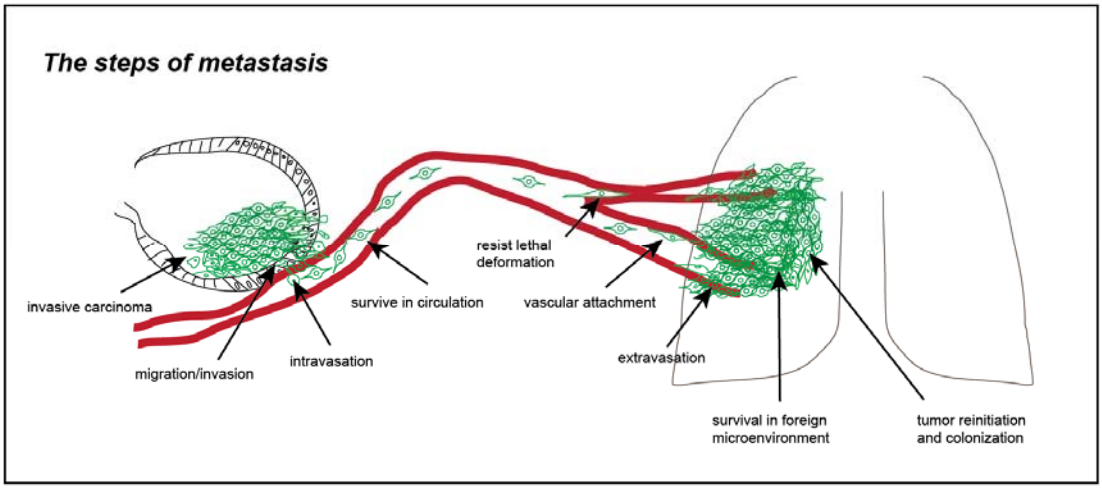

Figure 1. The steps of metastasis. The selective process a primary tumor cell must be genetically equipped to complete in order to successfully metastasize and colonize distant organs such as the lungs (left-to-right). Each step in the process acts as a selective bottleneck due to the physical and molecular demands on the cancer cell as well as the characteristics of the external environment. For this reason, the formation of metastases can be prevented at many points along a cell's journey, suggesting that the ability to metastasize must be inherent in cells at the primary tumor site.

Figure 2. The mutationally driven clonal expansion of tumors. a, The random acquisition of driver mutations (D1-4) alters the evolutionary trajectory of dividing cells, thereby creating subclones with unique traits (A, B). **b**, Successive waves of proliferative driver mutations result in accelerated cell division causing the expansion of subclones that comprise a tumor. When tumors acquire the ability to invade through the basement membrane they become carcinomas. Late in cancer progression, subclones arise that have acquired all the traits necessary to successfully metastasize. In theory, metastatic subclones may show unchanged, increased or even decreased rates of proliferation and therefore variable frequencies within a primary tumor.

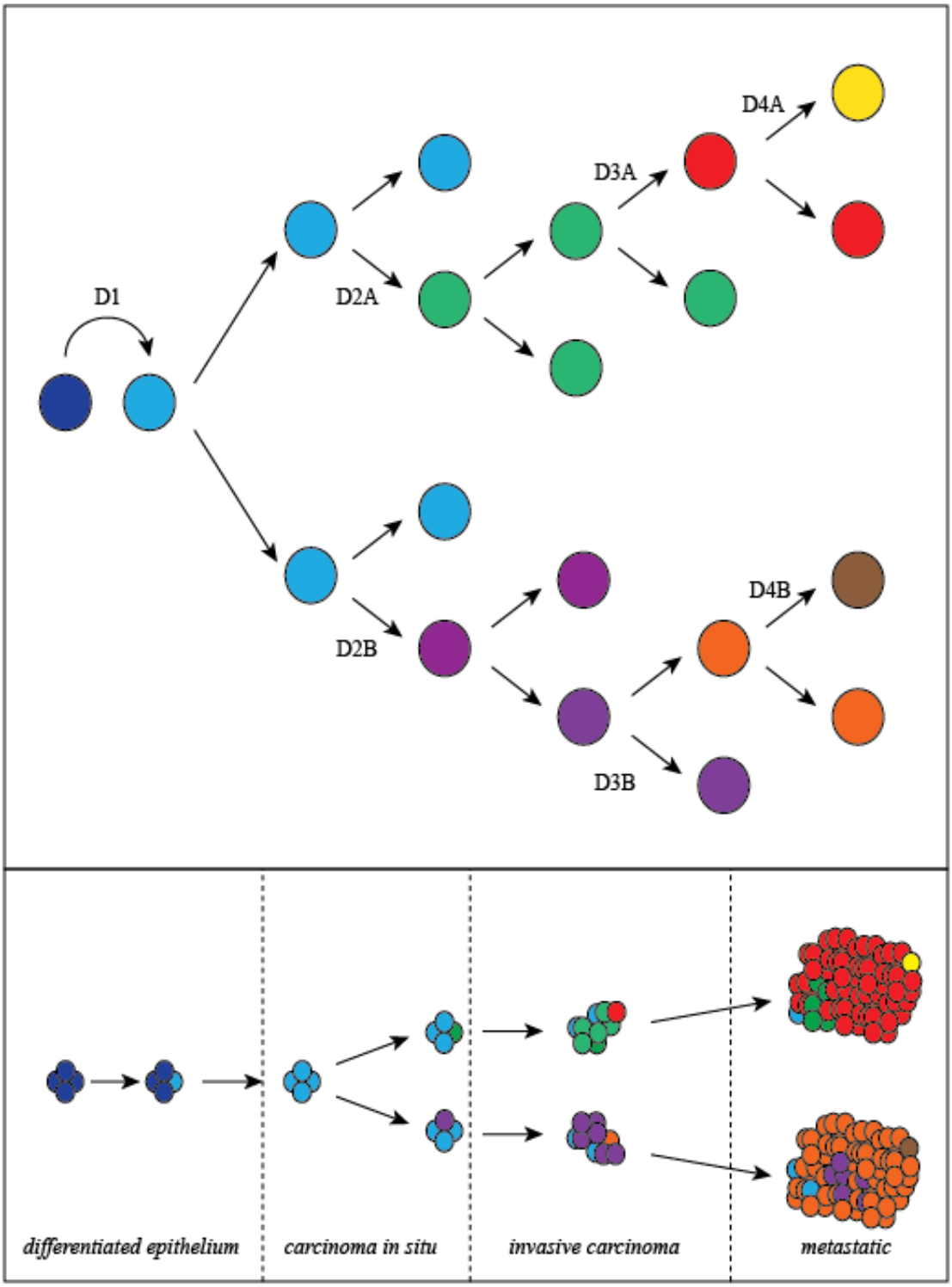
D1
D2A
D2B
D3A
D3B
D4A
D4B
differentiated epithelium
carcinoma in situ
invasive carcinoma
metastatic

normal tissue surrounding it[11] (Fig. 2). The genetic instability inherent to this deregulated cell growth supports the subsequent acquisition of additional driver mutations within the original clone[9,11] (Fig. 2). A classic example of this concept is illustrated by the progression of colorectal cancer, where the mutational inactivation of the tumor suppressor APC leads to the slow development of a small adenoma and the subsequent mutational activation of the KRAS oncogene increases the proliferative rate of cells, yielding a large adenoma[5] (Fig. 3). Continued unchecked, proliferation results in the accumulation of additional random mutations that eventually grant a subclone of cells within the large adenoma the ability to breach the basement membrane and invade the surrounding stroma, at which point the tumor becomes a carcinoma[5] (Figs. 2 and 3). It is generally believed that the ability of a cell to complete each step of the metastatic cascade is conferred by the successive waves of mutation-driven clonal expansion leading to the formation of a metastatic primary tumor[8] (Fig. 2). If this holds true, the mutations present in the highest percentage of primary tumor cells are likely to have been the earliest initiators of a patient's cancer, whereas those found at a lower frequency would be more likely to promote the phenotypes characteristic of a metastatic cell[2]. While researchers have come to learn much about the mutations that provide a cell with a tumor-initiating growth advantage, insight into those later mutations that might act specifically to enhance a cell's metastatic capacity remains limited.

To effectively study metastasis, the cancer biologist must isolate the rare metastatic cells within a heterogeneous cancer cell population from the many

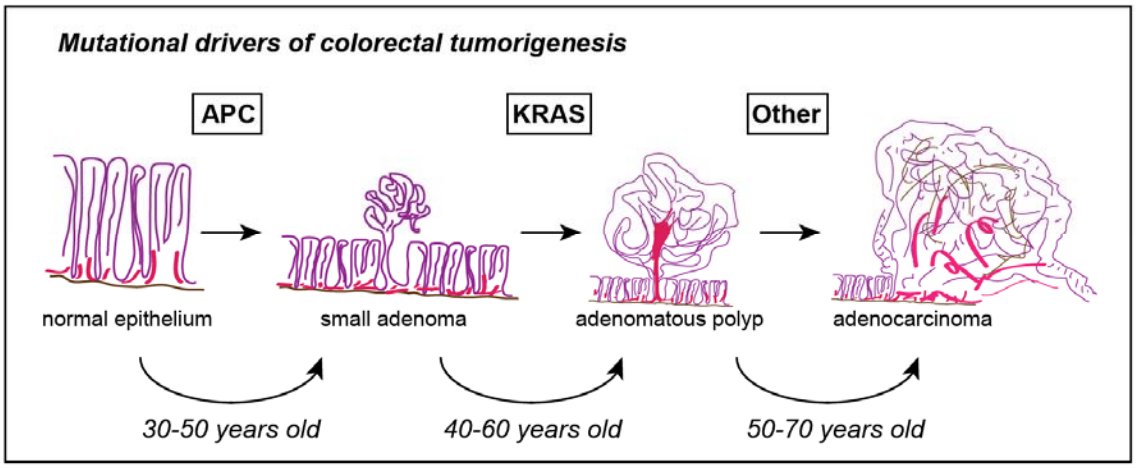

Figure 3. Mutational drivers of tumorigenesis. The process by which normal colonic epithelium transitions to invasive carcinoma through the acquisition of inactivating and activating mutations in tumor suppressors and oncogenes, respectively, over the lifetime of a patient. Adenomatous polyposis coli (APC) is a tumor suppressor that inhibits unwanted cell proliferation through the β-catenin pathway. KRAS, is a GTPase that promotes growth factor signaling. The age at which patients acquire each type of mutation is indicated at the bottom.

cells that cannot metastasize. In 1973, Dr. Isaiah Fidler overcame this challenge by applying *in vivo* selection to the study of metastasis[12]. In this model, cancer cells are injected into an immunocompromised mouse and allowed to disseminate, colonize and grow in distal organs until they form metastases[12] (Fig. 4). The resulting metastatic nodules are then harvested, expanded *in vitro* and injected into another mouse to repeat the selection process (Fig. 4). After multiple rounds of selection, the resulting cell line is tested to see if it forms metastases with greater efficacy than the parental cancer cell population from which it originated (Fig. 4)[13,14]. Once the increased metastatic ability of the derivative cell line is verified, the phenotypic, cell biologic, molecular and genetic differences between it and the parental line can be interrogated in order to understand the basis for its enhanced metastatic activity. A number of studies have successfully used this model to identify genes, transcriptional regulators, and post-transcriptional regulators that mediate cancer metastasis[13-18]. However, the question as to whether single base-pair mutations exist that act to specifically activate or inactive pro- or anti-metastatic genes, respectively, remains largely unanswered[5].

With the advent of next-generation sequencing, entire cancer genomes are now being sequenced on a daily basis[19]. This technology uses a quantitative "sequencing-by-synthesis" approach whereby fluorescently labeled dNTPs are imaged as they are incorporated into growing DNA strands that are complementary to fragments of the DNA being sequenced. By amplifying these fragments prior to sequencing, these platforms can produce over a billion reads

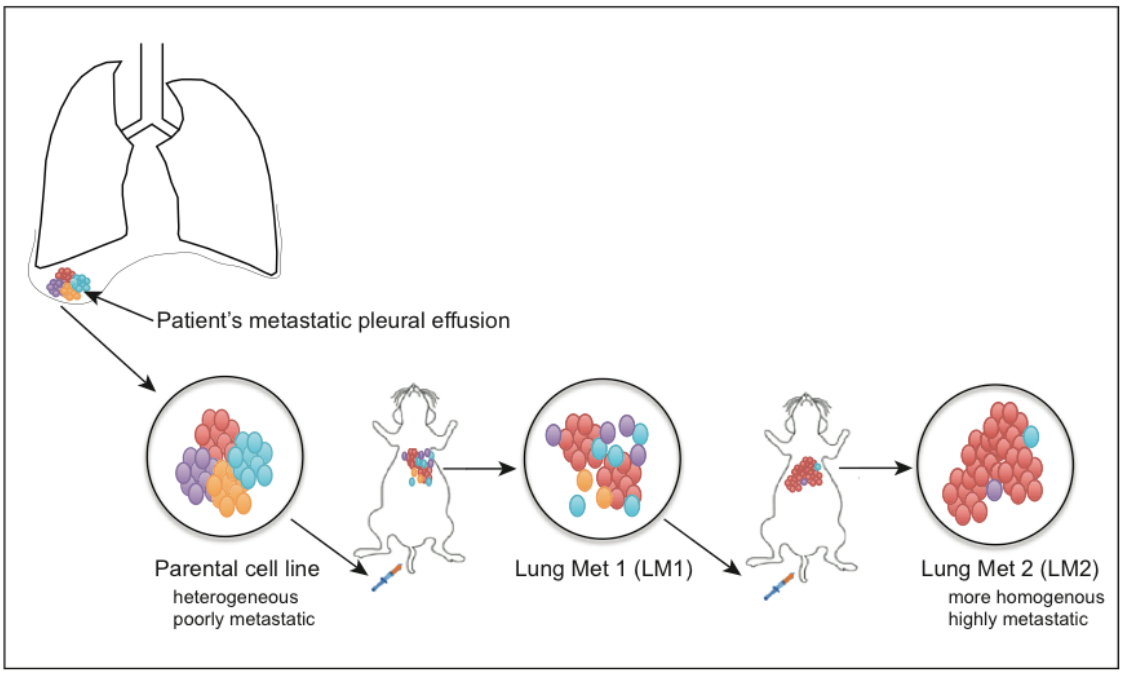

Figure 4. *In vivo* selection model of metastasis. The process by which highly metastatic sub-lines are generated from poorly metastatic cell populations harvested directly from the pleural effusions of breast cancer patients. Parental cell lines are expanded *in vitro*, injected into immunocompromised mice and allowed to disseminate and colonize target organs. Tumors from these mice are then extracted, cancer cells are expanded and injected into another mouse at lower cell numbers to promote the selection of highly metastatic cells. Successive waves of selection can be performed to generate more genetically homogenous highly aggressive derivative sub-lines, effectively isolating the genetic changes driving the metastatic process. Molecular and cellular differences between the parental and derivative lines can then be studied.

from 50-100 base pairs in length covering the genome many times over. These reads are then mapped to a reference genome using a computational program and analyzed by a bioinformatics framework specific for the desired application, such as the discovery of translocations, insertions/deletions (indels) or single nucleotide variants (SNVs)[19]. The application of this technology has also been tailored to provide both sequence and expression data from a cell's transcriptome. By quantifying the number of reads covering the transcriptome, RNA-sequencing (RNA-seq) can measure the expression of genes, non-coding RNAs, gene isoforms, splice variants as well as the frequencies of mutated alleles[20]. This technology is also optimal for the discovery of mutations in the protein-coding regions of only those genes that are expressed in a cell in a given biological context, such as metastasis.

To date, many studies have used next-generation sequencing to survey the integrity of cancer genomes and transcriptomes across a wide variety of cancer types[2]. As a result, the number of genes found mutated in cancer is increasing at a rate faster than ever before. However, there are a number of concerns raised by these studies. For one, the high cost of next-generation sequencing has forced many investigators to draw conclusions based on the sequencing of one biological sample, which can result in the discovery of rare or artifactual mutations. Second, while large collections of patient-matched primary and metastatic tumors would be the gold standard for identifying metastasis-promoting genetic changes, metastatic tumors are not routinely resected. This is because the prognosis for patients with metastatic disease is so poor that the risk

and morbidity of surgery vastly outweighs the benefit of removing a metastatic nodule originating from a tumor that has likely seeded many other sites in the organs of the patient. Another major problem with current cancer sequencing studies is that the vast majority of large-scale cancer sequencing studies neglect to validate the *in vivo* functionality of the identified mutations. Finally, studies looking for metastatic drivers often sequence the DNA or RNA of primary lesions where any mutations residing in small subclones are overlooked (Fig. 2). Recent reports estimate that the false negative rate of such sequencing studies approaches 37%[21]. This is thought to be due both the technological limitations of current sequencing platforms[5] and the contamination of cancer tissue with normal stromal tissue that effectively drowns out the low-frequency mutations residing in a relatively small number of tumor cells[22].

Based on the well-established role for non-synonomous mutations in causing the cellular phenotypes responsible for tumorigenesis, this study began with the hypothesis that there are functional non-synonomous single nucleotide variants (nSNVs) within malignant cells that contribute specifically to their metastatic capacity. Presented herein are the results of the design and implementation of an unbiased approach for the systematic discovery of low-frequency nSNVs that act as drivers of metastasis. This unique framework integrates next-generation RNA-sequencing with the *in vivo* selection of highly metastatic cells to overcome the current challenges of identifying low frequency cancer metastasis drivers and has led to the discovery of activating mutations in a large plasma membrane channel that drive metastasis. The characterization of

this mutation has provided insights into the molecular basis for metastatic cell survival during membrane stretch within the microvasculature.

CHAPTER II: THE SYSTEMATIC DISCOVERY OF RECURRENT NON-NEUTRAL nSNVs ENRICHED IN HIGHLY METASTATIC BREAST CANCER

To systematically identify mutations present in metastatic cells that may drive cancer progression, whole-transcriptomic RNA-seq was performed on the *in vivo*-selected[13,14] highly metastatic human breast cancer cell sub-lines, CN-LM1A and MDA-LM2, and the CN34 and MDA-MB-231 parental lines from which they were derived (Fig. 5 and Table 1). To minimize the false positive rate and allow for subsequent statistical analyses, biological replicates of each cell line were sequenced. The rationale for this approach was based on the hypothesis that allelic frequencies of mutations conferring enhanced metastatic capacity would likely be enriched in the transcriptomes of highly metastatic sub-lines relative to the transcriptomes of their less metastatic parental populations. To focus these efforts on the nSNVs most likely to promote metastasis, low-confidence variants were systematically excluded by removing known polymorphisms, low coverage (<10×) nSNVs, and any nSNV not detected in both biological RNA-seq replicates of each cell line. To identify nSNVs significantly enriched during metastatic selection, the differences in nSNV allelic frequencies between the highly metastatic sub-lines and their respective poorly metastatic parental lines were quantified[20]. The metastasis-enriched nSNVs that displayed an increase in allelic frequency over the four rounds of RNA-seq met the criteria for significance ($p < 0.05$, $q \leq 0.25$) by a one-tailed Student's *t*-test (Fig. 5 and Table 2). The computational tool PolyPhen-2[23] predicted, with high confidence (HumDiv score > 0.90), four of the recurrently enriched missense

variants to be non-neutral (Table 2). The genes bearing these nSNVs include the mitochondrial ribosome-binding factor *RBFA*, the transcription factor *REST*, the adherens junction regulatory factor *KRIT1* and the zinc-finger-containing gene *ZSWIM6*. A single nonsense variant, *PANX1 C268T*, was also significantly enriched in both sub-lines (Table 2). Sanger sequencing of cDNA independently confirmed the enrichment of these mutant alleles in metastatic breast cancer cells (Fig. 6). These alterations represent recurrently enriched mutations and candidate drivers of breast cancer metastasis.

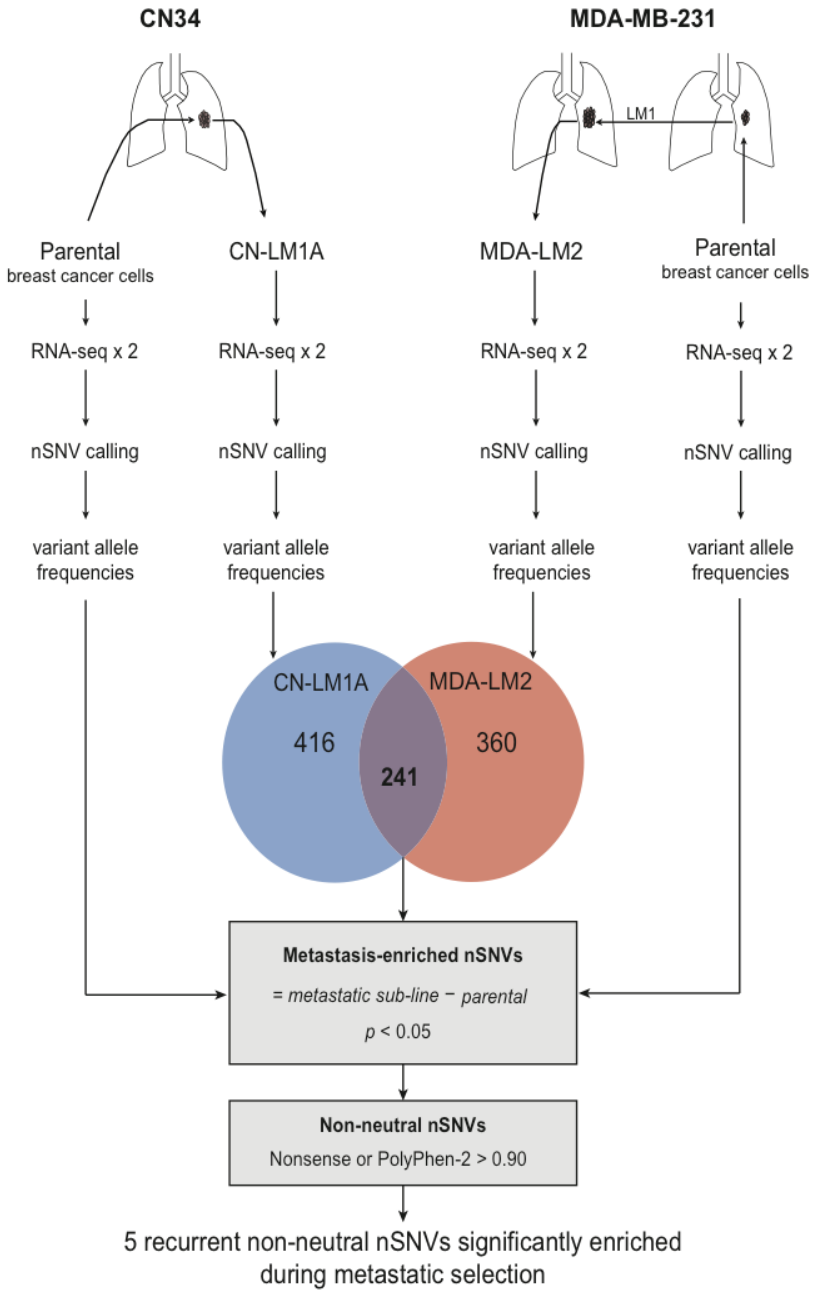

Figure 5. Framework for the systematic discovery of recurrent non-neutral nSNVs enriched in highly metastatic breast cancer. Schematic of the systematic discovery framework used to identify nSNVs enriched by allelic frequency in highly metastatic CN-LM1A and MDA-LM2 human breast cancer cells.

Table 1. RNA-seq summary

>9 unq reads	CN-LM1A_1	CN-LM1A_2	MDA-LM2_1	MDA-LM2_2
Parental total SNVs	46848	52384	50829	45752
LM total SNVs	45288	44579	53646	42851
Common total SNVs	30533	32277	39187	33931
Parental total SNPs	4849	5073	7345	6932
LM total SNPs	4341	4153	8361	7778
Common total SNPs	3513	3522	7012	6571
Parental total nSNVs	3266	3806	3667	3419
Parental MS nSNVs	3248	3786	3645	3402
Parental NS nSNVs	18	20	22	17
LM total nSNVs	3699	3837	4120	3467
LM MS nSNVs	3675	3820	4101	3453
LM NS nSNVs	14	17	19	14
Parental non-SNP total nSNVs	755	1099	1104	880
Parental non-SNP MS	746	1088	993	871
Parental non-SNP NS	9	10	11	9
LM non-SNP total nSNVs	1253	1423	1319	899
LM non-SNP MS	1239	1415	1308	892
LM non-SNP NS	14	8	11	7
LM-enriched nSNVs	614	708	378	399
LM nSNVs in seq replicates	416		360	
Recurrent	241			

Table 2. nSNVs recurrently enriched during breast cancer metastasis. Recurrent and non-neutral mutations identified to be significantly enriched in highly metastatic breast cancer cells by a one-tailed Student's *t*-test ($P < 0.05$); $n = 4$.

Gene	Genomic location	Base	Amino acid	fold-enrichment CN-LM1A	fold-enrichment MDA-LM2	*p*-value	Protein function	Mutated domain	PolyPhen 2 HumDiv
PANX1	11:93526390	**C268T**	**Q90***	**1.53** **1.46**	**1.48** **1.20**	**0.0023**	Plasma membrane megachannel	ECL1	**Nonsense**
RBFA	18:75906883	**G773T**	**G258V**	**1.70** **1.35**	**1.16** **1.44**	**0.0112**	Mitochondrial ribosome binding factor	GatB	**1.00**
REST	4:57492601	**G2821C**	**D941H**	**1.08** **1.28**	**1.23** **1.09**	**0.0372**	RE1-silencing transcription factor	C-terminal	**0.987**
KRIT1	7:91668596	**G1958A**	**S701N**	**1.47** **2.12**	**1.18** **1.28**	**0.0473**	Positive regulator of integrin-β1 signaling	Rap1a binding	**0.963**
ZSWIM6	5:60861703	**G1906A**	**V636M**	**1.22** **1.23**	**1.04** **1.19**	**0.0295**	Zinc finger SWIM-type 6	-	**0.906**

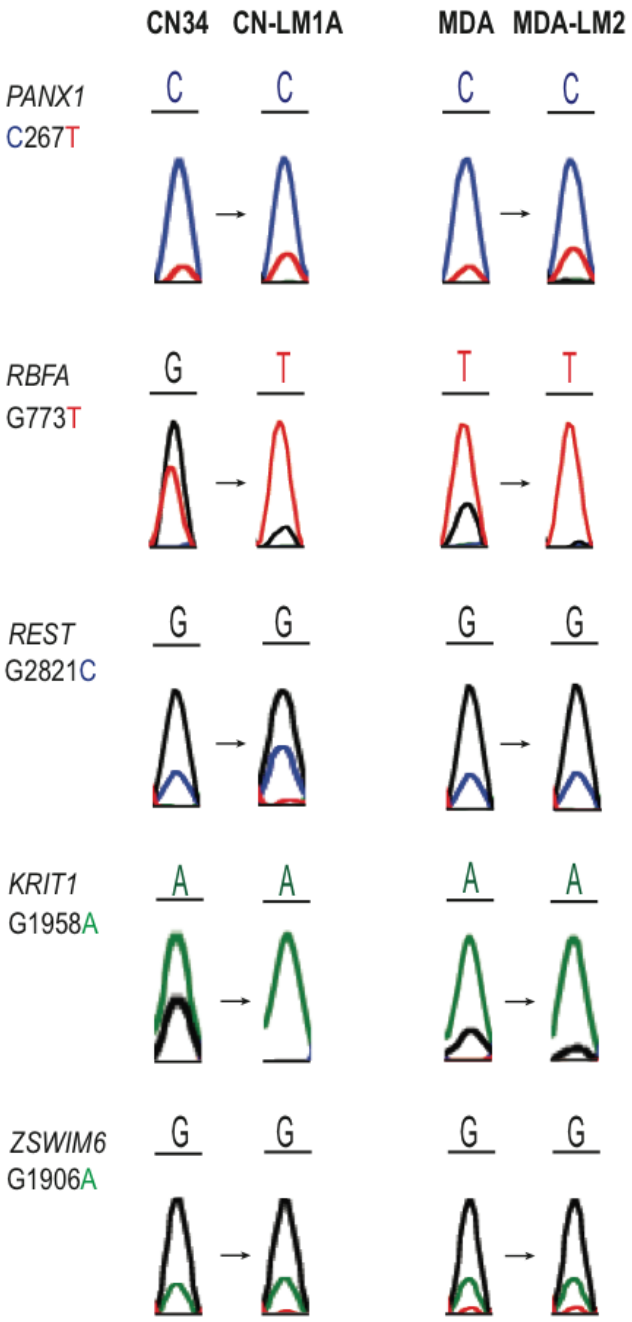

Figure 6. cDNA Sanger sequencing validation of recurrently enriched non-neutral nSNVs. Sanger sequencing traces from the cDNA of CN34, CN-LM1A, MDA-MB-231 and MDA-LM2 cells at the nSNV alleles predicted to result in non-neutral substitutions by PolyPhen-2.

CHAPTER III: A NONSENSE MUTATION IN THE MECHANOSENSITIVE PANX1 CHANNEL PROMOTES METASTATIC CELL SURVIVAL IN THE MICROVASCULATURE

Because the *PANX1 C268T* mutation results in an altered cell-surface channel protein, it was reasoned that, if functional, it might offer potential for therapeutic targeting. Allele-specific RNA-seq (Table 3) and Sanger sequencing of gDNA (Fig 7) validated the transcriptomic and genomic enrichment of the *PANX1 C268T* allele in the highly metastastatic derivative sub-lines, respectively. The *PANX1 C268T* nonsense mutation substitutes a premature termination codon for the glutamine codon at position 90 of the 426 amino acid PANX1 protein, leaving only the N-terminal fragment, $PANX1^{1-89}$, expressed (Fig 8). *PANX1* encodes the monomeric subunit of a heximeric plasma membrane channel that, when activated, mediates the release of ATP from cells into the extracellular space (Fig. 8)[24-29]—a well established autocrine/paracrine signaling pathway[30] recently implicated in intravascular signaling during metastasis[31]. The knowledge that PANX1 homo-oligomerizes to form functional channels (Fig. 8) and that metastatic cells express both wild-type and mutant PANX1, suggested that $PANX1^{1-89}$ may interact with full-length PANX1. In support of this, prominent co-localization of PANX1 and $PANX1^{1-89}$ was detected at the plasma membrane (Fig. 9). To directly test whether $PANX1^{1-89}$ interacts with full-length PANX1, reciprocal co-immunoprecipitation experiments were performed that revealed $PANX1^{1-89}$ to associate with full-length PANX1 (Fig 10). To further confirm this interaction and was not an artifact of non-specific binding *in vitro*, the question of

Table 3. Allele-specific RNA-seq of the *PANX1 C268T* allele. Allele-specific RNA-seq of the *PANX1 C268T* allele in biological triplicates of the CN34 and MDA-MB-231 parental breast cancer cells and their respective lung metastatic derivatives, CN-LM1A and MDA-LM2. Mean enrichment was quantified by measuring the increase in frequency of the *PANX1 C268T* allele in the metastatic sub-lines as compared to the corresponding parental lines; n = 3.

Allele-specific RNA-seq (biological triplicates)	CN-LM1A	MDA-LM2
Mean enrichment (%)	5.44	5.74
***P*-value**	0.02	0.01

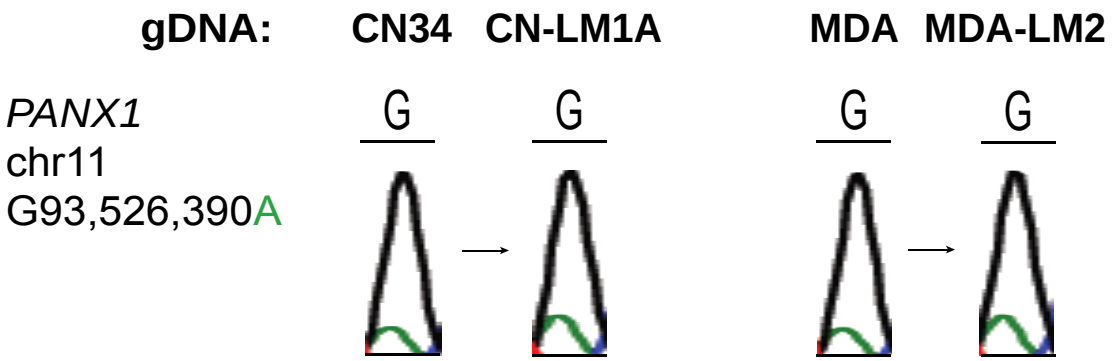

Figure 7. gDNA Sanger sequencing of the *PANX1 C268T* allele. Sanger sequencing of the *PANX1* mutant allele from genomic DNA of each parental and metastatic line.

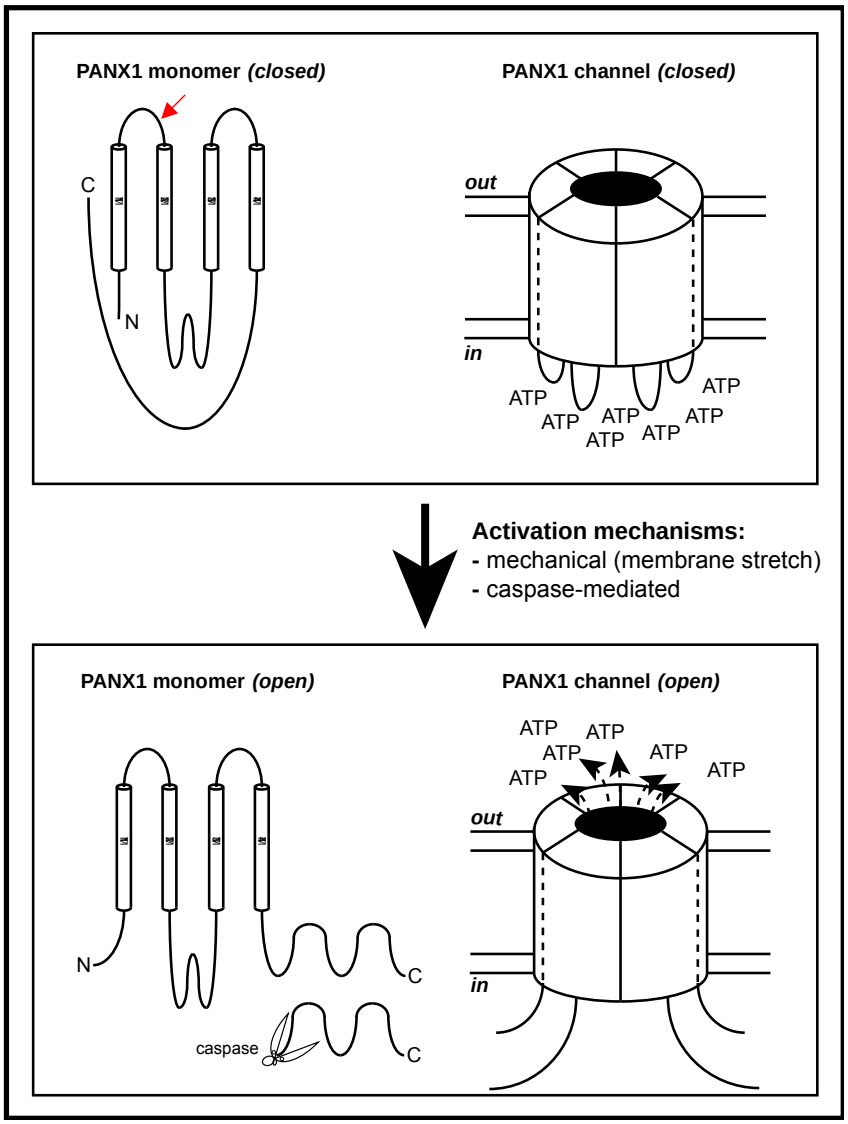

Figure 8. The PANX1 megachannel. The proposed confirmation of PANX1 monomers and homo-heximeric channels in the closed (top panel) and open (bottom panel) state. Association of the autoinhibitory C-terminus with the N-terminus pore-lining first transmembrane (TM1) domain is thought to impede the release of ATP through PANX1. Upon activation by membrane stretch the C-terminus is dislodged by conformational changes in the channel. During apoptosis, caspase cleavage of the PANX1 C-terminus releases ATP that functions to recruit immune cells to the site of cell death. Red arrow indicates position of PANX1 Q90* mutation.

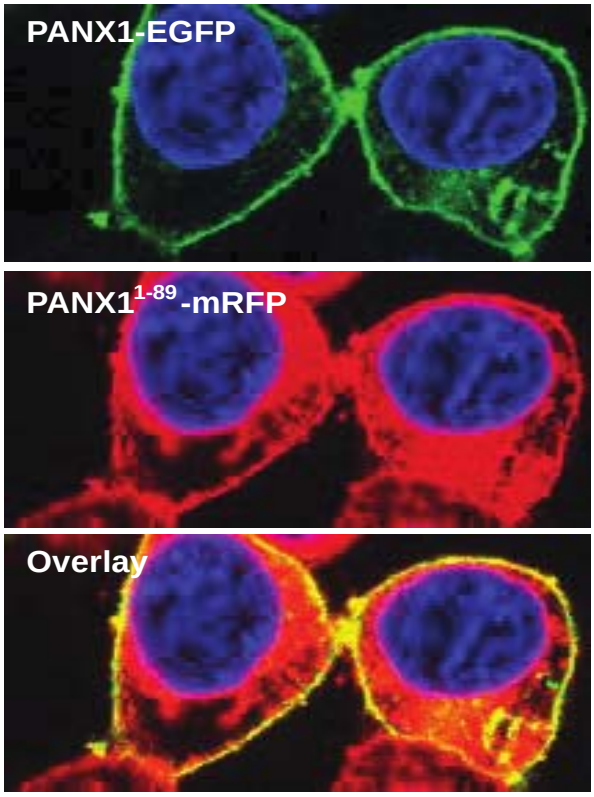

Figure 9. Cellular localization of wild-type PANX1 and mutant PANX1$^{1-89}$. Confocal microscopy images of HEK293T cells expressing PANX1-EGFP (green) and PANX1$^{1-89}$-mRFP (red). Co-localization at the plasma membrane is shown by channel overlay (yellow).

Figure 10. PANX1$^{1-89}$ associates with wild-type PANX1 to form heteromeric cellular complexes. **a**, Co-immunoprecipiation of Flag-tagged full-length PANX1$^{1-426}$ and endogenous PANX1$^{1-89}$ from CN-LM1A and MDA-LM2 cells. Anti-PANX1 N-terminal antibody detected a band similar in size to that of Flag-tagged PANX1$^{1-89}$ expressed in HEK293T cells. The presence of this band in the metastatic sub-lines suggests that endogenous PANX1$^{1-89}$ associates with Flag-tagged full-length PANX1$^{1-426}$. The multiple bands representing full-length PANX1 represent the previously described glycosylated forms of PANX1. **b,** Co-immunoprecipitation of PANX1$^{1-89}$-Flag from HEK293T cells co-transfected with full-length PANX1$^{1-426}$. Anti-PANX1 N-terminal antibody was used to detect the associated PANX1 species. The multiple full-length PANX1 bands represent the previously described glycosylated forms of PANX1. The input lysates were immunoblotted for PANX1. **c,** Increasing concentrations of DSP (dithiobis[succinimidyl propionate]) crosslinker were applied to HEK293T cells expressing Flag-tagged PANX1 prior to lysis. PANX1 complexes were detected using anti-FLAG M2 antibody. A complex of approximately 300 kDa represented the largest crosslinked PANX1 species, suggesting the ultimate formation of a heximeric PANX1 channel. **d**, Anti-PANX1 and anti-RFP immunoblotting of DSP crosslinked lysates from HEK293T cells expressing PANX1-EGFP, PANX1-EGFP and PANX1$^{1-89}$-mRFP or PANX1$^{1-89}$-mRFP. The heximeric PANX1-EGFP channel is predicted to be approximately 480 kDa. Molecular weights are indicated. **e**, Co-immunoprecipitation of PANX1$^{1-89}$-RFP from protein-crosslinked (2mM DSP) HEK293T cells expressing PANX1-EGFP, PANX1-EGFP and PANX1$^{1-89}$-mRFP, or PANX1$^{1-89}$-mRFP. Anti-GFP antibody was used to detect the wild-type PANX1 in complex with mutant PANX1$^{1-89}$. Molecular weights are indicated.

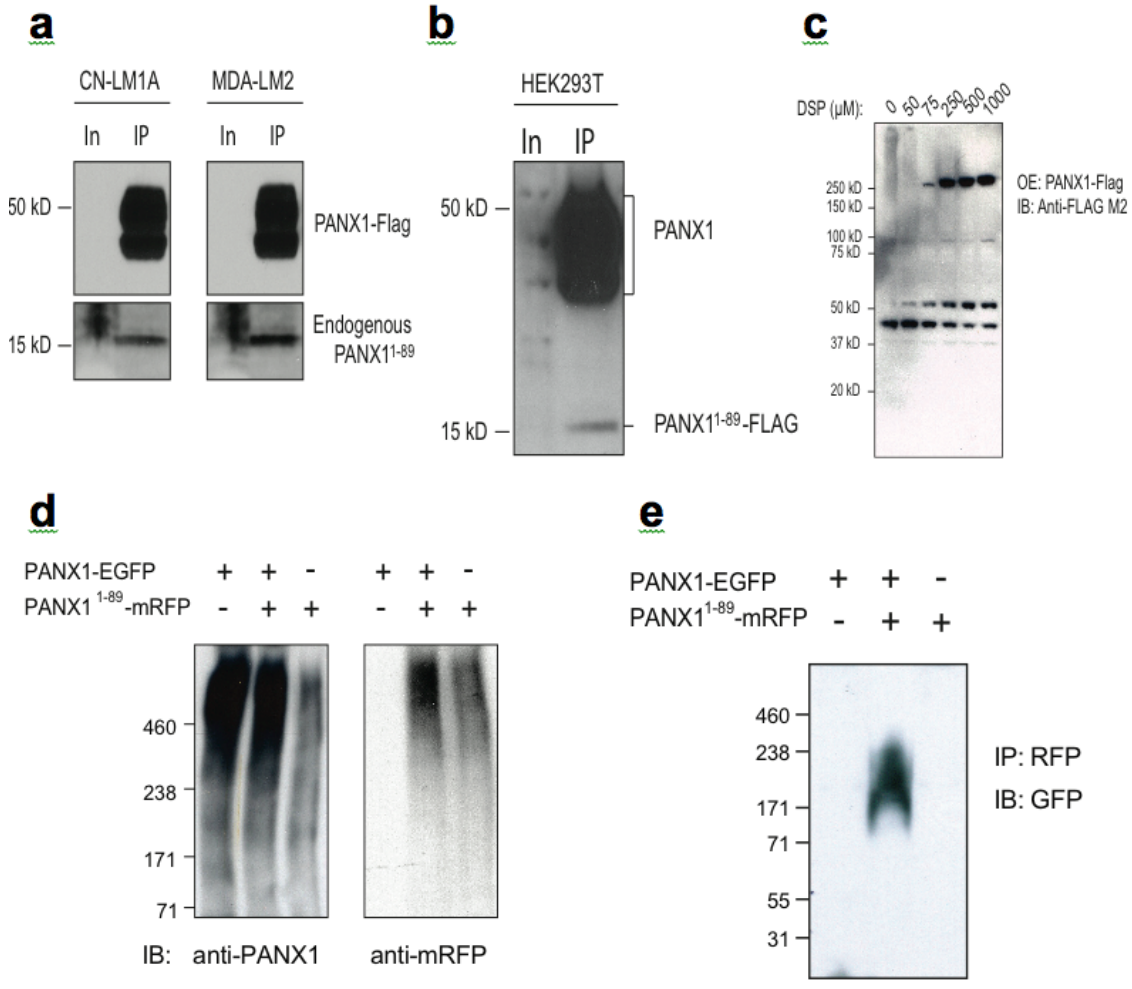
a
CN-LM1A
MDA-LM2
In
IP
In
IP
50 kD
15 kD
PANX1-Flag
Endogenous
PANX1^1-89
b
HEK293T
In
IP
50 kD
15 kD
PANX1
PANX1^1-89-FLAG
c
DSP (μM):
0
50
75
250
500
1000
250 kD
150 kD
100 kD
75 kD
50 kD
37 kD
20 kD
OE: PANX1-Flag
IB: Anti-FLAG M2
d
PANX1-EGFP
PANX1 1-89-mRFP
460
238
171
71
IB:
anti-PANX1
anti-mRFP
e
PANX1-EGFP
PANX1^1-89-mRFP
460
238
171
71
55
31
IP: RFP
IB: GFP

whether PANX1$^{1-89}$ complexes with full-length PANX1 in living cells was tested by performing crosslinking of cellular proteins in culture. Co-immunoprecipitation of PANX1$^{1-89}$ from protein-crosslinked cells revealed that mutant protein to be closely associated with wild-type PANX1 *in vivo* (Fig. 10). Based on the sum of these results, it was hypothesized that the interaction between PANX11-89 and full-length PANX1 results in altered PANX1 channel activity. To test this, ATP release was measured from cells overexpressing wild-type PANX1 alone, wild-type PANX1 and PANX1$^{1-89}$, or PANX1$^{1-89}$ alone. PANX1-mediated ATP release was quantified by measuring the reduction in extracellular ATP release (Fig. 11) in the presence of the PANX1 channel inhibitor carbenoxolone (Cbx)[28,32-34] (Fig. 12). Indeed, when co-expressed with full-length PANX1, truncated PANX1$^{1-89}$ significantly enhanced extracellular ATP release through PANX1 channels (Fig. 13a-b). ATP release was not enhanced when PANX1$^{1-89}$ was expressed alone in *PANX1*-deficient human cells (Fig. 13a) or *PANX1*-null mouse embryonic fibroblasts (MEFs) (Fig. 13c), suggesting that mutant PANX1$^{1-89}$ does not homo-oligomerize to form functional ATP release channels. Enhanced ATP release caused by PANX1$^{1-89}$ was independent of caspase signaling, a known activator of PANX1 in pre-apoptotic cells[28,35], as mutation of the caspase cleavage site in PANX1 did not impair the enhancement of ATP release (Fig. 14). Additionally, PANX1$^{1-89}$ lost the ability to augment ATP release when co-expressed with PANX1$^{1-297}$ (Fig. 15), a mutant lacking the intracellular C-terminus domain that has been shown to interact with the pore of the channel to impede ATP release[35] (Fig. 8), suggesting that this domain may be required for channel activation by

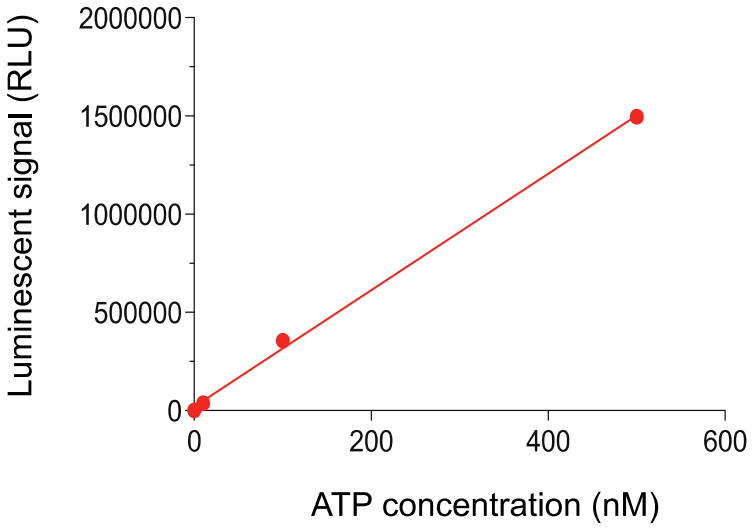

Figure 11. Luminescent standard curve for extracellular ATP concentration measurements. Increasing concentrations of ATP (0, 50, 100, 500 nM) were measured using the Cell-Titer Glo luciferase assay.

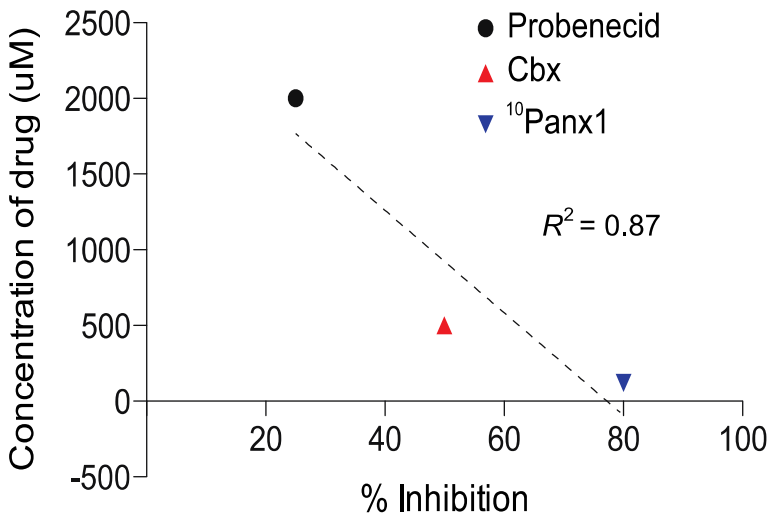

Figure 12. PANX1 channel inhibitor potencies. The % inhibition of extracellular ATP release from metastatic derivative sub-lines at one minute was measured in the presence of three independent PANX1 inhibitors (Probenecid, Cbx and ^{10}Panx1) at varying concentrations (2 mM, 500 μM and 100 μM, respectively).

Figure 13. PANX1$^{1-89}$ enhances PANX1-mediated ATP release. a, Quantification of PANX1-mediated ATP release from HEK293T cells transfected with 8 μg control vector, 8 μg wild-type PANX1, 5 μg wild-type PANX1 and 3 μg PANX1$^{1-89}$, or 8 μg PANX1$^{1-89}$, and pretreated for 10 min with 500 μM carbenoxolone (Cbx) or an equivalent volume of PBS; *n* = 4-8. **b**, Quantification of extracellular ATP release from *PANX1*-null mouse embryonic fibroblasts (*PANX1* KO MEFs) transfected with 5 μg human full-length PANX1 or 5 μg human full-length PANX1 and 2.5 μg human PANX1$^{1-89}$; *n* = 7. **c**, Quantification of extracellular ATP release from *PANX1* KO MEFs transfected with 5 μg human PANX1$^{1-89}$ or 5 μg vector control; *n* = 8. Error bars, s.e.m., *ns*, nonsignificant; *, $P < 0.05$; **, $P < 0.01$; ***, $P < 0.001$ by a one-tailed Student's *t*-test.

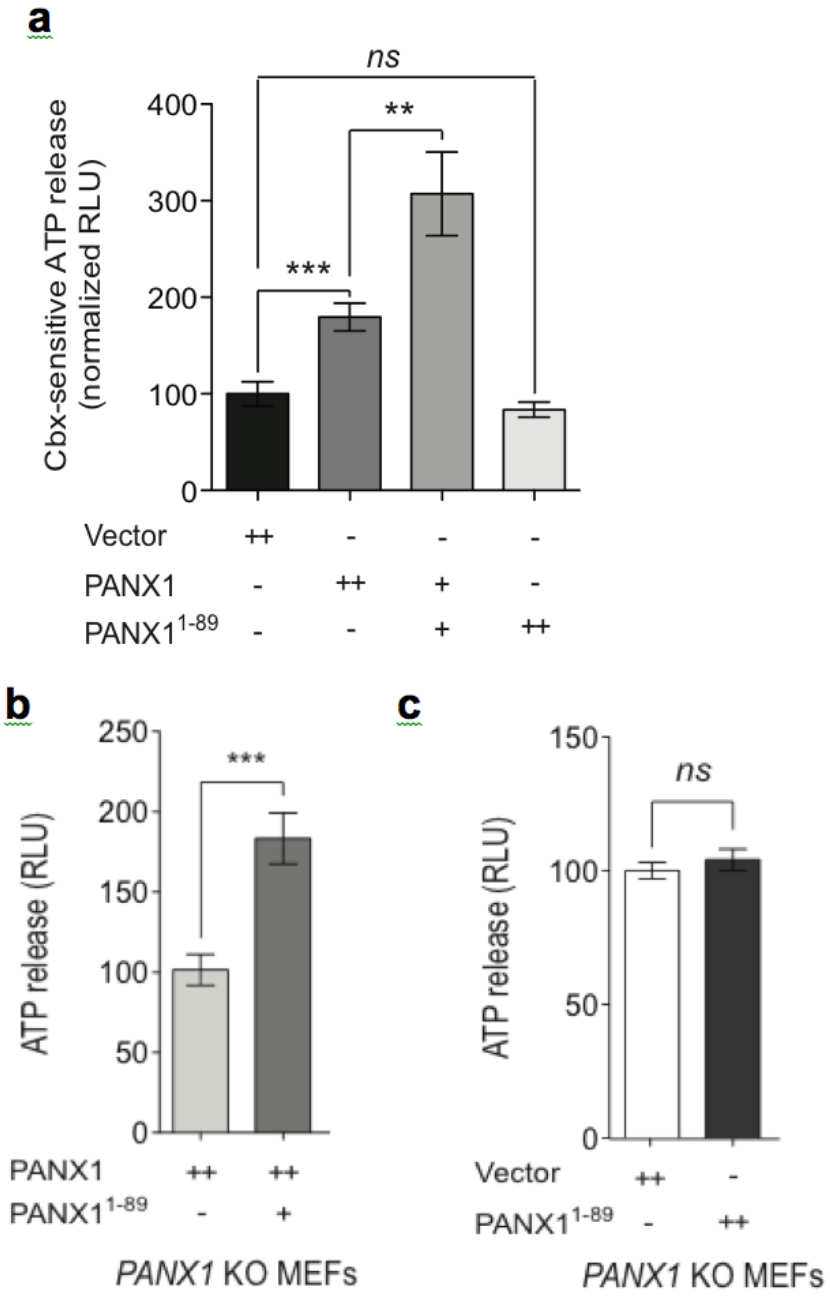
a
ns
**
***
Cbx-sensitive ATP release (normalized RLU)
400
300
200
100
0
Vector ++ - - -
PANX1 - ++ + -
PANX1 1-89 - - + ++
b
***
ATP release (RLU)
250
200
150
100
50
0
PANX1 ++ ++
PANX1 1-89 - +
PANX1 KO MEFs
c
ns
ATP release (RLU)
150
100
50
0
Vector ++ -
PANX1 1-89 - ++
PANX1 KO MEFs

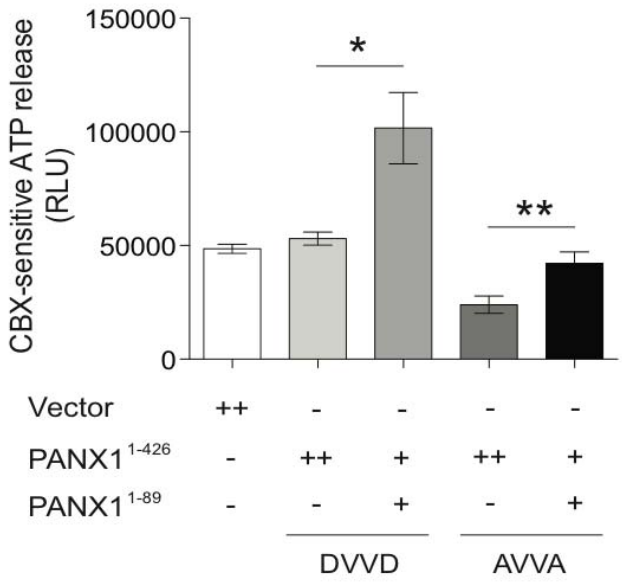

Figure 14. Augmentation of PANX1-mediated ATP release by PANX1$^{1-89}$ is independent of caspase activity. Quantification of PANX1-mediated ATP release from HEK293T cells transfected with 5 μg control vector, 5 μg wild-type PANX1 (DVVD), 2.5 μg wild-type PANX1 and 2.5 μg PANX1$^{1-89}$, 5 μg caspase resistant full-length PANX1 (AVVA), or 2.5 μg caspase resistant full-length PANX1 and 2.5 μg PANX1$^{1-89}$; n = 4. Error bars, s.e.m., *, $P < 0.05$; **, $P < 0.01$; ***, $P < 0.001$ by a one-tailed Student's t-test.

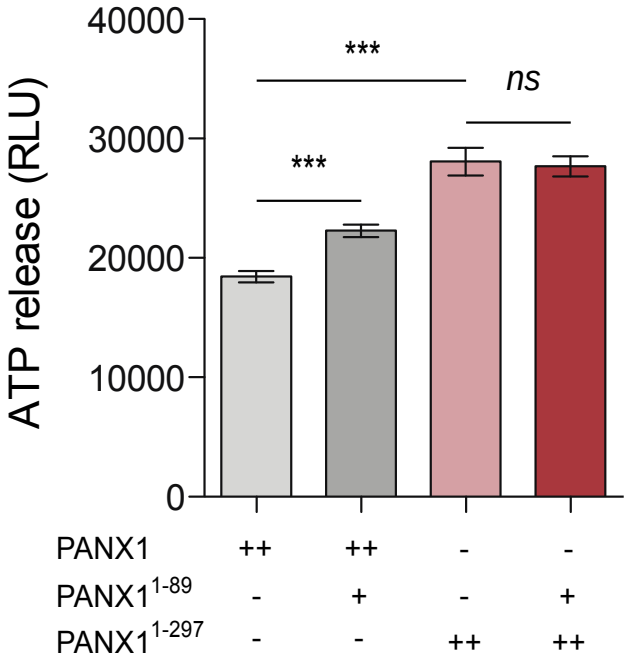

Figure 15. The C-terminus of wild-type PANX1 channels is required for PANX1$^{1-89}$ to enhance PANX1-mediated ATP release. Quantification of ATP release from HEK293T cells transfected with 5 µg wild-type PANX1, 5 µg wild-type PANX1 and 2.5 µg PANX1$^{1-89}$, 5 µg C-terminus-deleted PANX1$^{1-297}$ or 5 µg PANX1$^{1-297}$ and 2.5 µg PANX1$^{1-89}$; n = 8-12. Error bars, s.e.m., *ns*, nonsignificant; *, $P < 0.05$; **, $P < 0.01$; ***, $P < 0.001$ by a one-tailed Student's *t*-test.

PANX1$^{1-89}$. These findings reveal that PANX11-89 interacts with full-length PANX1 to augment ATP release through PANX1 channels.

These results prompted the question of whether metastatic breast cancer cells express active PANX1 channels. Treatment of CN-LM1A and MDA-LM2 cells with three established PANX1 inhibitors—probenecid (Prob)[34,36], Cbx, or the more potent mimetic peptide ^{10}Panx1[28,34,37] (Fig. 12)—significantly reduced extracellular ATP release (Fig. 16a), suggesting that highly metastatic cells mediate substantial ATP release through PANX1 channels. It was next asked whether the increased expression of PANX1$^{1-89}$ in metastatic breast cancer cells impacts PANX1 channel activity. CN-LM1A and MDA-LM2 sub-lines, which RNA-seq revealed to express roughly 1.5-fold more *PANX1 C268T* than their parental lines, secreted nearly 5-fold more PANX1-mediated ATP than their parental lines (Fig. 16b). This increase in channel activity can not be attributed to greater expression of *PANX1* in highly metastatic cells, as metastatic CN-LM1A and MDA-LM2 cells did not display increased total *PANX1* mRNA levels relative to their parental lines (Fig. 17). These data suggest that PANX1$^{1-89}$ may nonlinearly augments PANX1-mediated ATP release. Moreover, expressing PANX1$^{1-89}$ in BT549, MDA-MB-468 and HCC1806 cells—three distinct human breast cancer cell lines harboring wild-type endogenous PANX1—was sufficient to significantly enhance PANX1-mediated ATP release (Fig. 18). These findings reveal PANX1$^{1-89}$ to be an activator of PANX1 channels and implicate the N-terminal domain of PANX1 as a positive regulator of channel activation in metastatic breast cancer cells.

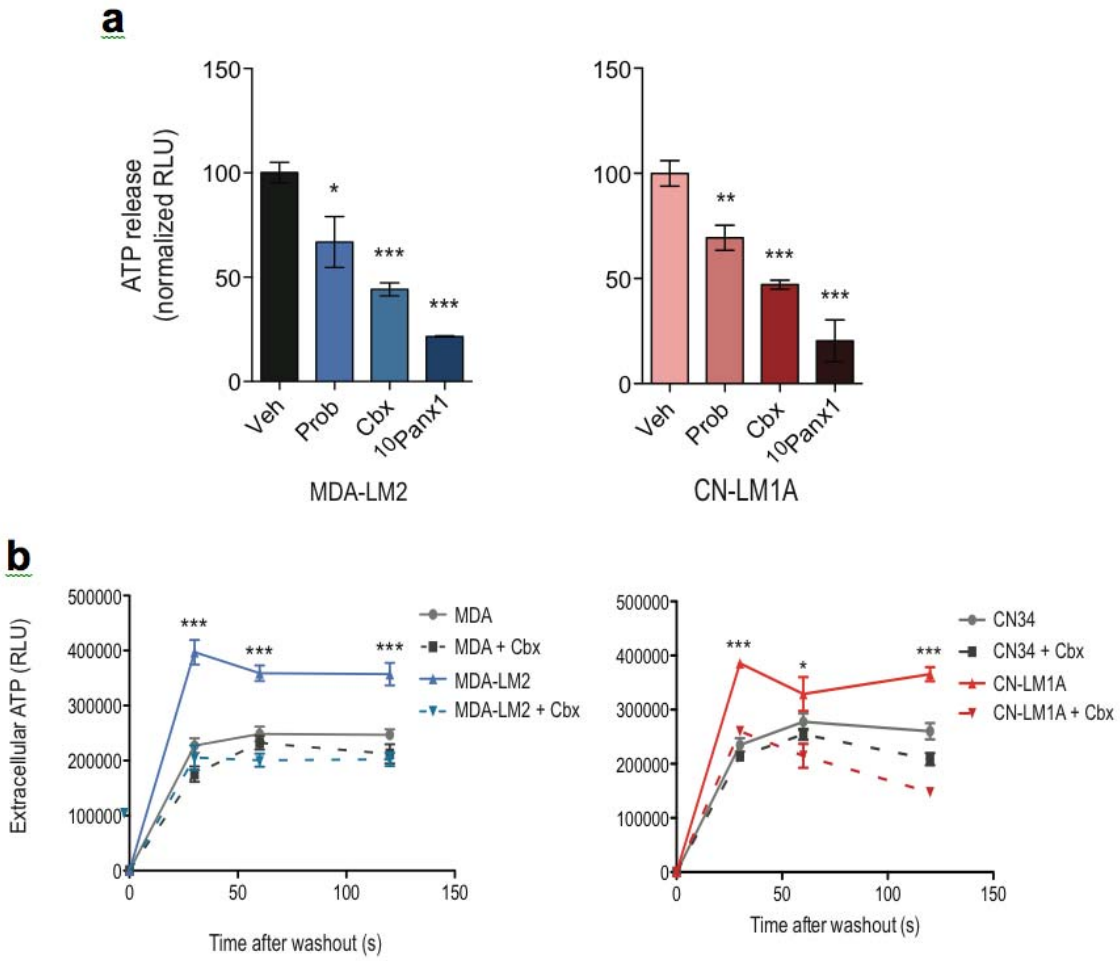

Figure 16. Highly metastatic breast cancer cells exhibit enhanced ATP release via PANX1 channels. a, Quantification of PANX1-mediated ATP release from MDA-LM2 (left panel) and CN-LM1A (right panel) sub-lines pretreated for 10 min with PBS, 2mM probenecid (Prob), 500 μM Cbx, or 100 μM ^{10}Panx1 peptide; *n* = 3-4. **b**, Time-course measurements of ATP release from MDA-MB-231 (left panel) and CN34 (right panel) parental cells and the MDA-LM2 and CN-LM1A metastatic derivatives sub-lines pretreated with Cbx (500 μM) or PBS for 10 min; *n* = 4. Error bars, s.e.m., *, $P < 0.05$; **, $P < 0.01$; ***, $P < 0.001$ by a one-tailed Student's *t*-test.

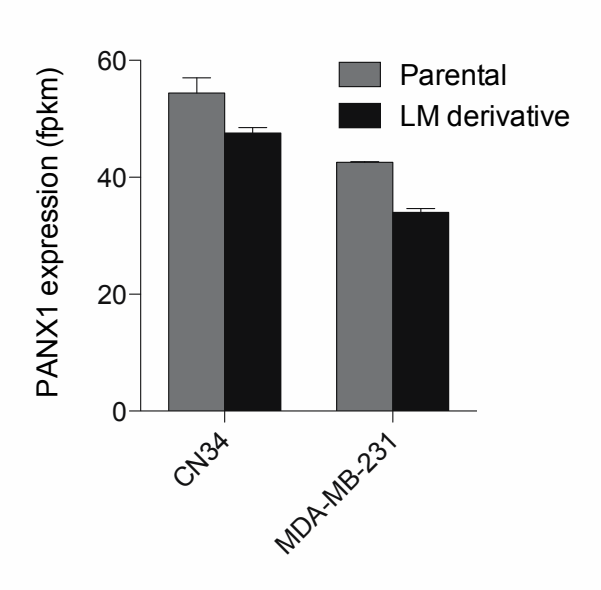

Figure 17. Total PANX1 expression in *in vivo* selected metastatic breast cancer cells. CN34, CN-LM1A, MDA-MB-231 and MDA-LM2 total PANX1 mRNA expression quantified by RNA-seq; FPKM values averaged over two rounds of RNA-seq for each cell line. Error bars, s.e.m.

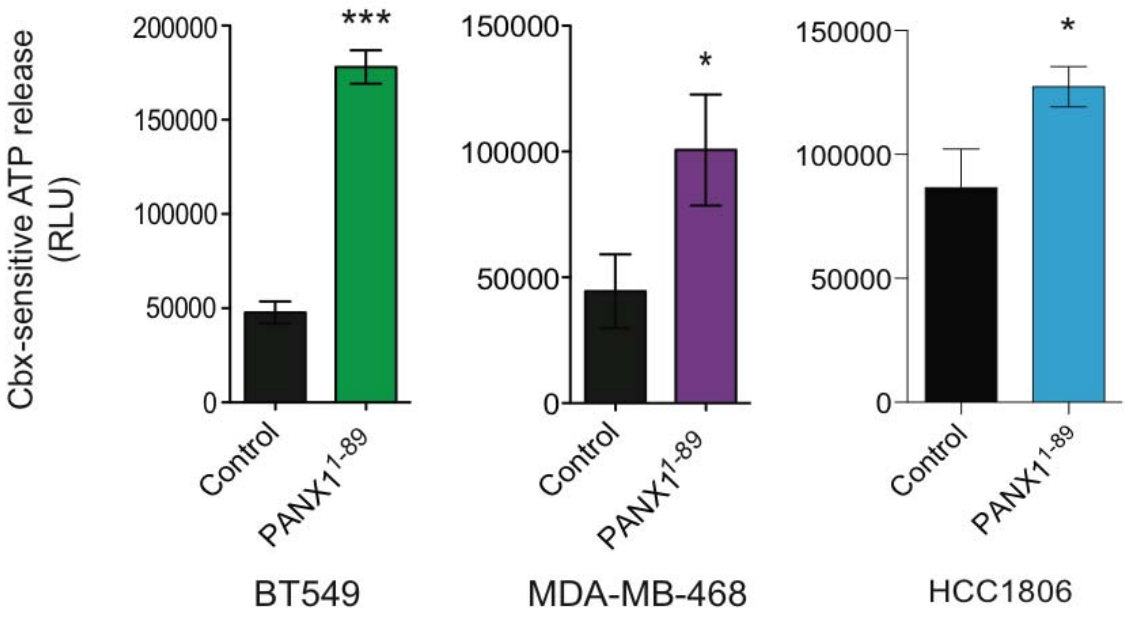

Figure 18. PANX1$^{1-89}$ enhances PANX1 activity in metastatic breast cancer cells. Quantification of Cbx-sensitive ATP release from BT549, MDA-MB-468 and HCC1806 metastatic breast cancer cells expressing PANX1$^{1-89}$ or a control vector; n = 4. Error bars, s.e.m., *, $P < 0.05$; **, $P < 0.01$; ***, $P < 0.001$ by a one-tailed Student's *t*-test.

The role of PANX1 activation in metastatic progression was subsequently examined. It was first asked whether PANX1 channels are activated *in vivo*. To address this, MDA-LM2 cells expressing plasma membrane-anchored extracellular luciferase were treated with Cbx or vehicle, injected into the tail-veins of mice, and the extracellular ATP release from cancer cells in the lung was quantified through bioluminescence imaging of the lungs. Consistent with PANX1-mediated ATP release *in vivo*, cancer cells entering the lung vasculature were found to release extracellular ATP that was attenuated upon pharmacological inhibition of PANX1 (Fig. 19). To determine if the early activation of PANX1 in the blood vessels of the lung is necessary for efficient metastasis, PANX1 channels were acutely blocked by preincubating CN-LM1A and MDA-LM2 cells with the ^{10}Panx1 inhibitory peptide or its corresponding scrambled peptide and their metastatic activity was assessed through tail-vein lung colonization assays. This acute (30 min) inhibition of PANX1 significantly inhibited metastasis as evidenced by reductions in metastasis at early time-points that persisted at 6-week endpoints (Fig. 20). PANX1$^{1-89}$ expression was also sufficient to promote metastasis in cancer cells expressing endogenous wild-type PANX1, as expressing the truncated mutant in MDA-MB-468 and HCC1806 cells led to a significant increase in metastatic dissemination in orthotopic (Fig. 21) and tail-vein (Fig. 22) metastasis assays. These experiments also revealed the non-organ-specific pro-metastatic effect of PANX1$^{1-89}$, as cells expressing the mutation exhibited an enhanced capacity to spread systemically and colonize distant organs such as the lung, liver and bone (Fig. 22). Consistent

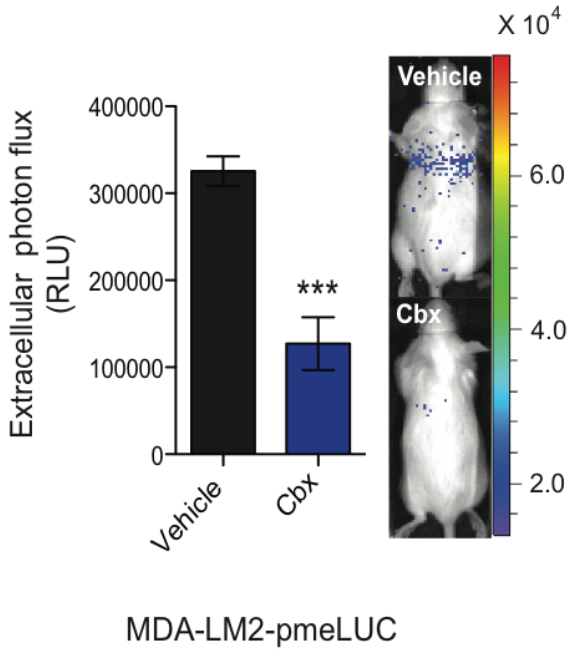

Figure 19. Breast cancer cell PANX1 channels are active soon after entry into the lung vasculature. Quantitative bioluminescence imaging of extracellular ATP release by cancer cells in the lung vasculature 5 min after tail-vein injection of 1 × 10^5 MDA-LM2 cells expressing plasma membrane-anchored extracellular luciferase (MDA-LM2-pmeLUC). MDA-LM2-pmeLUC cells were pretreated for 10 min with either Cbx (500 μM) or PBS prior to injection into FVB/NJ mice; *n* = 5-7. Error bars, s.e.m., *, $P < 0.05$; **, $P < 0.01$; ***, $P < 0.001$ by a one-tailed Student's *t*-test.

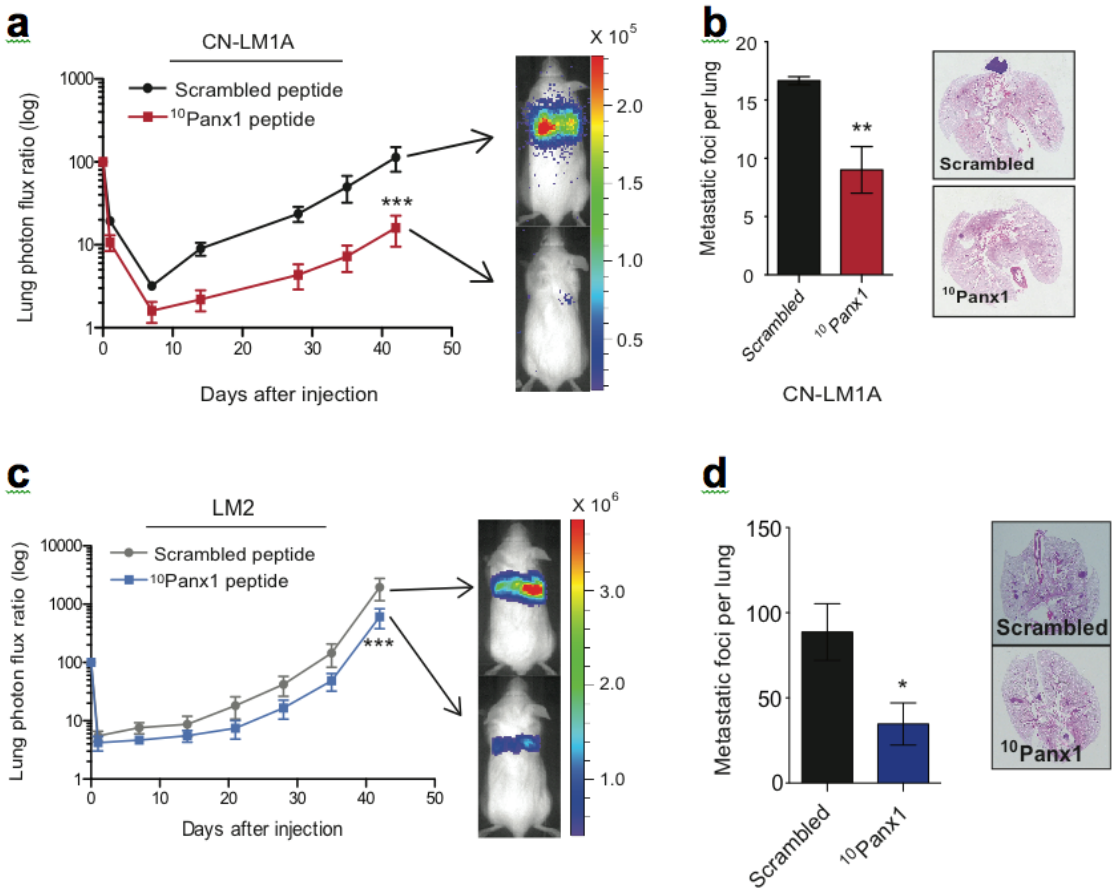

Figure 20. PANX1 activity promotes metastatic lung colonization. **a**, Quantitative bioluminescence imaging of lung metastasis after the injection of 1 × 10^5 highly metastatic CN-LM1A breast cancer cells pretreated with 100 μM ^{10}Panx1 or scrambled peptide, into NOD scid (NS) mice; *n* = 6-7. **b**, Day 42 quantification of metastatic foci (left) and representative lung images (right) from H&E stained lungs of mice injected with CN-LM1A cells pretreated with ^{10}Panx1 or scrambled peptide; *n* = 3. **c**, Quantitative bioluminescence imaging of lung metastasis after the injection of 4 × 10^4 MDA-LM2 (right panel) breast cancer cells pretreated with 100 μM ^{10}Panx1 or scrambled peptide, into NOD scid (NS) mice; *n* = 5. **d**, Day 42 quantification of metastatic foci (left) and representative lung images (right) from H&E stained lungs of mice injected with MDA-LM2 cells pretreated with ^{10}Panx1 or scrambled peptide. Error bars, s.e.m., *, $P < 0.05$; **, $P < 0.01$; ***, $P < 0.001$ by a one-tailed Student's *t*-test.

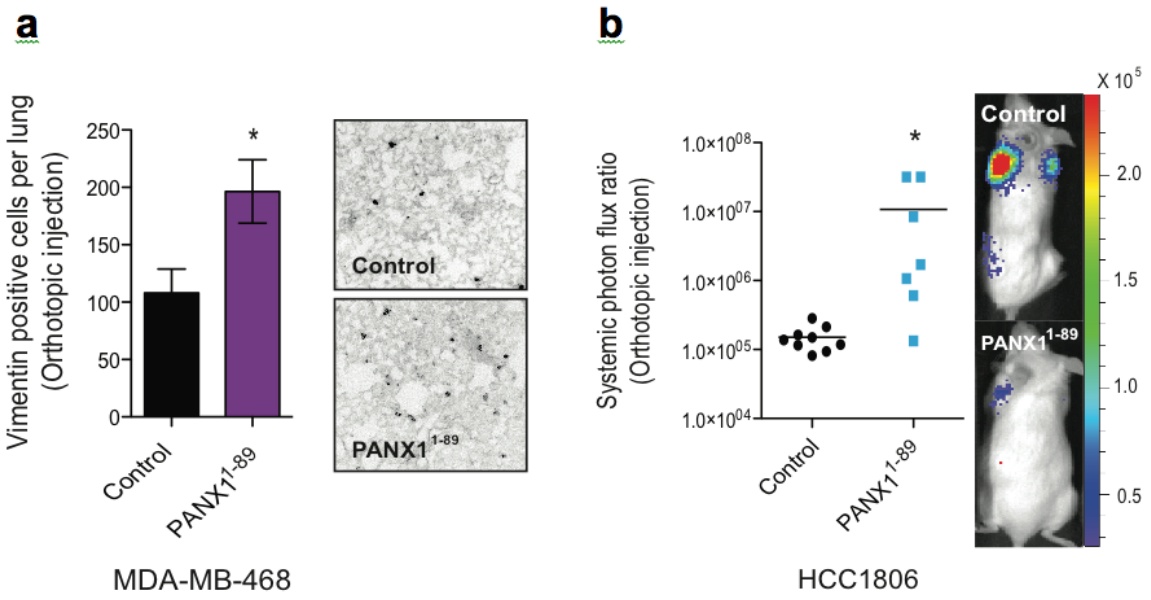

Figure 21. PANX1$^{1-89}$ promotes spontaneous metastatic dissemination and colonization. a, The numbers of vimentin positive breast cancer cells in the lung were counted one week after the extraction of size-matched mammary fat pad primary tumours generated by the orthotopic injection of 2.5× 10^5 MDA-MB-468 cells expressing PANX1$^{1-89}$ or control vector into NOD scid gamma (NSG) mice; *n* = 3-5. **b**, Quantitative bioluminescence imaging of systemic metastasis one week after the extraction of size-matched mammary fat pad tumours generated by the orthotopic injection of 5 × 10^5 HCC1806 breast cancer cells expressing PANX1$^{1-89}$ or control vector into NSG mice; *n* = 7-9. Error bars, s.e.m., *, $P < 0.05$; **, $P < 0.01$; ***, $P < 0.001$ by a one-tailed Student's *t*-test.

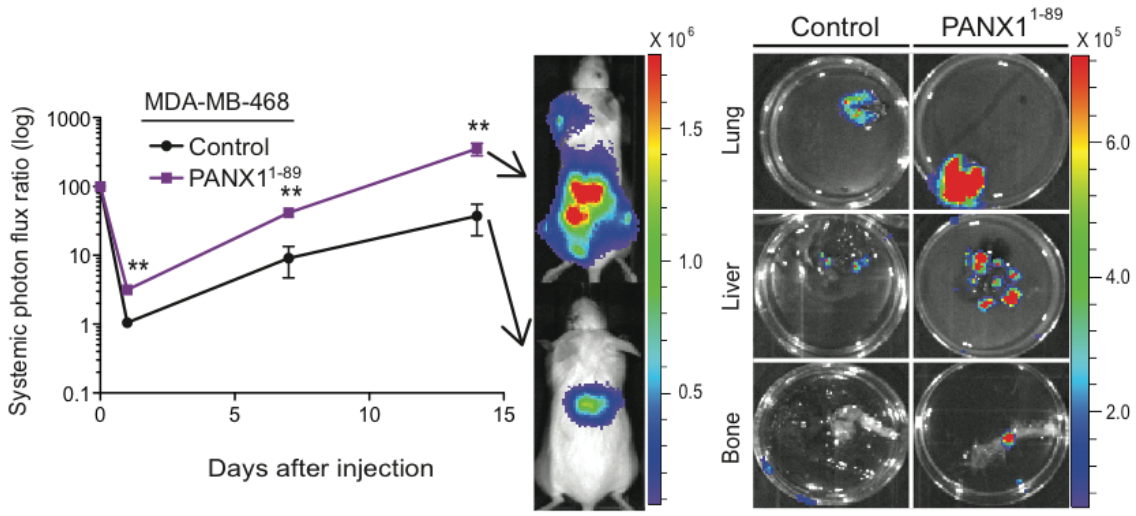

Figure 22. The pro-metastatic effect of PANX1$^{1-89}$ is non-organ-specific. Quantitative bioluminescence imaging of systemic metastasis after the tail-vein injection of 1 × 10^6 MDA-MB-468 breast cancer cells, expressing PANX1$^{1-89}$ or control vector, into NSG mice (left). *Ex vivo* bioluminescence imaging of metastatic target organs (lung, liver and bone) 14 days after tain-vein injection of MDA-MB-468 cells (right). Error bars, s.e.m., *, $P < 0.05$; **, $P < 0.01$; ***, $P < 0.001$ by a one-tailed Student's *t*-test.

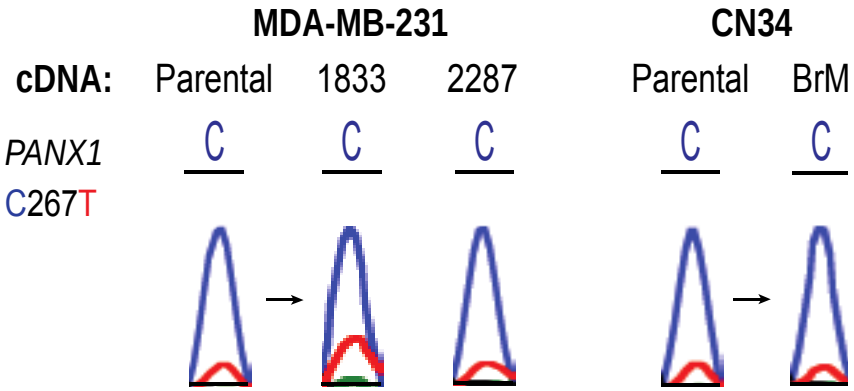

Figure 23. *PANX1 C268T* is detected in metastatic breast cancers tropic for bone and brain. Sanger sequencing traces from the cDNA of MDA-MB-231 and CN34 parental cell lines as well as the MDA-MB-231 bone-tropic sub-line 1833, the MDA-MB-231 brain-tropic sub-line 2287 and the CN34 brain-tropic sub-line BrM.

with this, the *PANX1 C268T* mutation was detected in MDA-MB-231 sub-lines tropic for bone and brain as well as a CN34 sub-line tropic for brain (Fig. 23).

Because purinergic signaling at the plasma membrane plays a role in many cellular processes[30], it was hypothesized that augmented ATP release through mutant PANX1 channels could be responsible for the metastasis-enhancing effect of $PANX1^{1-89}$. To address this, CD39, a plasma membrane-anchored extracellular ATP hydrolase, was expressed in CN-LM1A cells. The ability for these cells to metastasize to the lungs was then tested. CD39 expression, which effectively depleted the levels of extracellular ATP (Fig. 24), significantly reduced the metastatic lung signal at early (Fig. 25c) and late (Fig. 25a) time-points, and substantially reduced the number of metastatic foci in the lungs (Fig. 25b).

Because the metastatic effects of PANX1 inhibition, $PANX1^{1-89}$ expression and extracellular ATP depletion were consistently significant within 24 hrs of cancer cells being tail-vein injected, the role of PANX1 channels within this time frame was tested. To confirm that PANX1 channel inhibition blunts early metastatic dissemination, tail-vein injections of CN-LM1A and MDA-LM2 metastatic cells pretreated with ^{10}Panx1 were performed and lung bioluminescence was quantified daily, over three days. Consistent with PANX1 channels functioning to promote early metastatic dissemination, inhibition of PANX1 led to a significant (2-fold) decrease in lung bioluminescence as early as day one (Fig. 26a), as well as a reduction in the number of disseminated breast cancer cells detected histologically at day three (Fig. 26b).

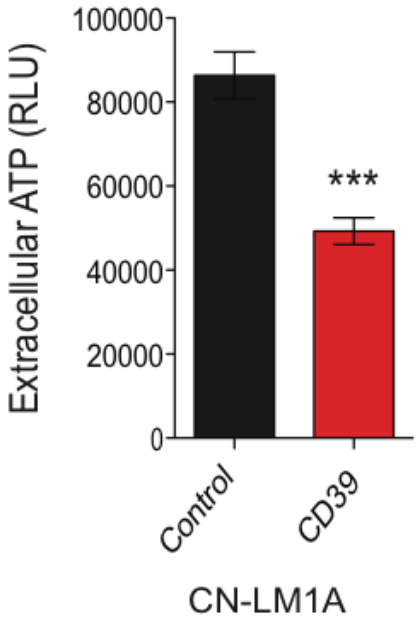

Figure 24. CD39 effectively depletes extracellular ATP. Quantification of extracellular ATP release from CN-LM1A cells expressing the extracellular ATP hydrolase CD39 or control vector; n = 8. Error bars, s.e.m., ***, $P < 0.001$ by a one-tailed Student's t-test. Error bars, s.e.m., *, $P < 0.05$; **, $P < 0.01$; ***, $P < 0.001$ by a one-tailed Student's t-test.

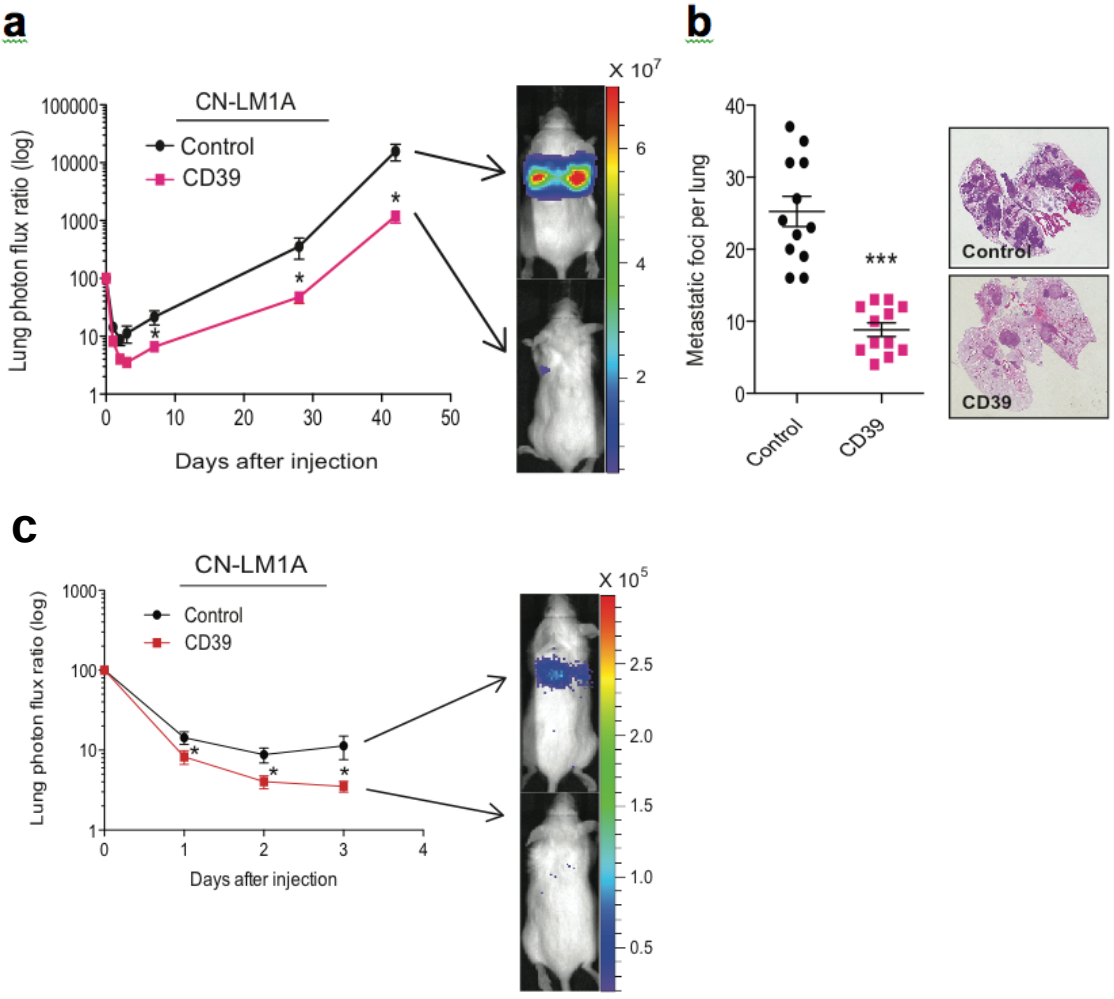

Figure 25. Extracellular ATP promotes breast cancer metastasis to the lung. **a**. Quantitative bioluminescence imaging of lung metastasis after tail-vein injection of 1 × 10^6 metastatic CN-LM1A cells, expressing CD39 or control vector, into NS mice; *n* = 5-6. **b**, Lungs from day 42 were extracted, H&E stained, and the numbers of metastatic foci were quantified; *n* = 10-12. **c**, Daily quantitative imaging of lung bioluminescence for three days subsequent to the injection of 1 × 10^5 CN-LM1A breast cancer cells expressing CD39 or control vector, into NS mice; *n* = 5-6. Error bars, s.e.m., *, $P < 0.05$; **, $P < 0.01$; ***, $P < 0.001$ by a one-tailed Student's *t*-test.

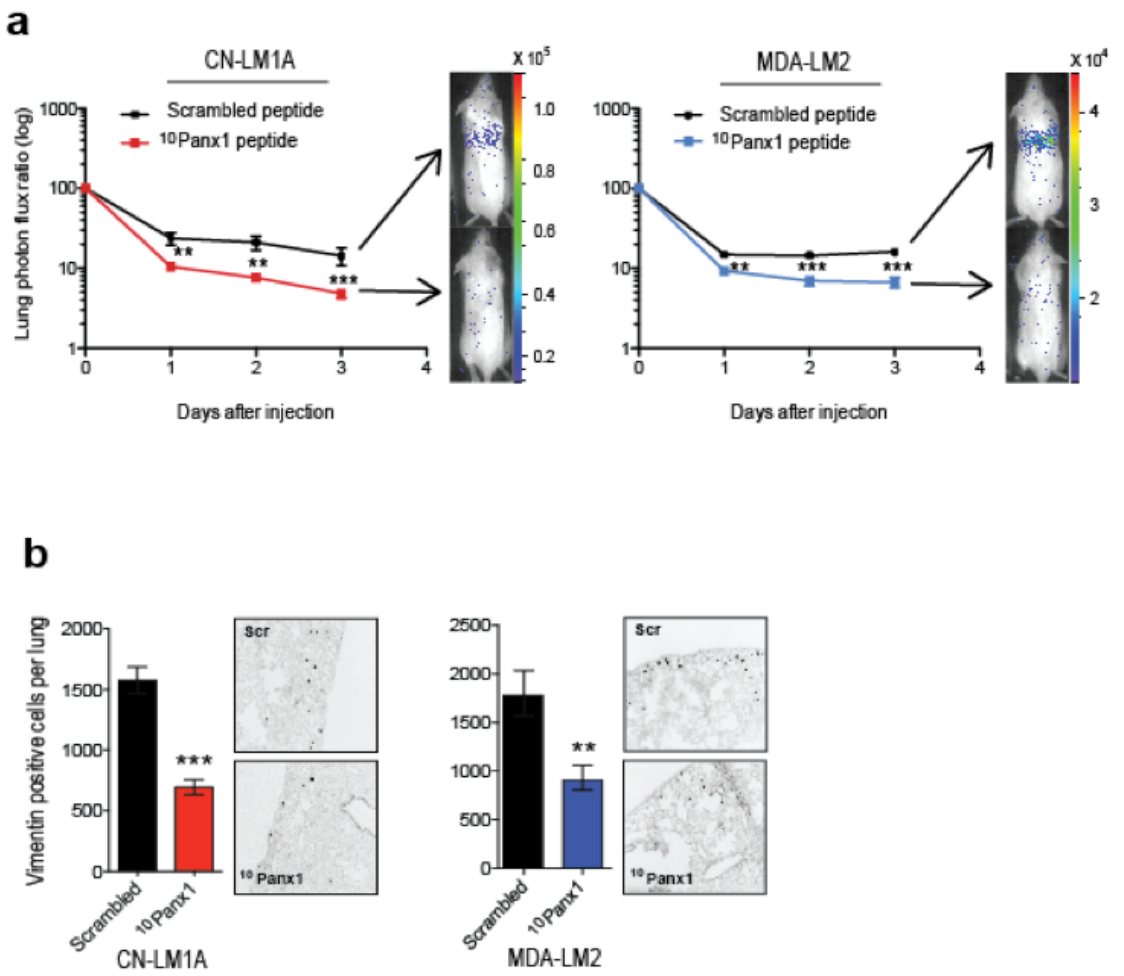

Figure 26. PANX1 channel activity promotes metastatic dissemination within days of cancer cell entry into the blood stream. a, Daily quantitative imaging plot of lung bioluminescence subsequent to the injection of 1 × 10^5 metastatic CN-LM1A (left panel) or 4 × 10^4 MDA-LM2 (right panel) breast cancer cells pre-treated (30 min) with 100 μM ^{10}Panx1 or scrambled peptides, into NS mice; *n* = 7. **b**, Lungs from mice were extracted at day 3, sectioned and stained for vimentin and the numbers of vimentin-positive cancer cells were quantified; *n* = 7. Error bars, s.e.m., *, $P < 0.05$; **, $P < 0.01$; ***, $P < 0.001$ by a one-tailed Student's *t*-test.

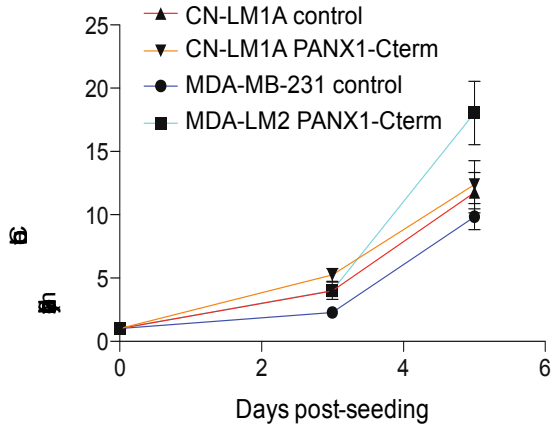

Figure 27. Molecular PANX1 inhibition does not suppress breast cancer cell proliferation. Quantification of proliferation over 5 days for CN-LM1A and MDA-LM2 cells over-expressing the autoinhibitory C-terminal domain of PANX1 or control vector; *n* = 4. Error bars, s.e.m.

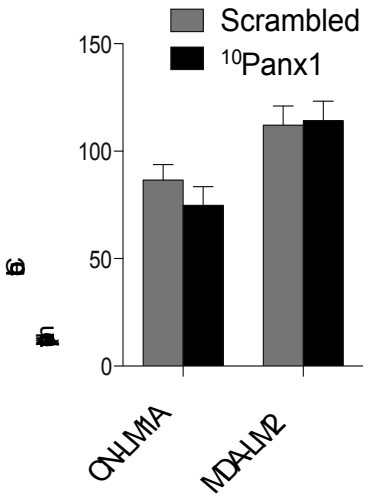

Figure 28. Peptidergic PANX1 inhibition has no effect on early proliferation. Quantification of 24 hour cell survival for CN-LM1A and MDA-LM2 cells pretreated for 15 min with 100μM ^{10}Panx1 or scrambled peptide; *n* = 7-8. Error bars, s.e.m.

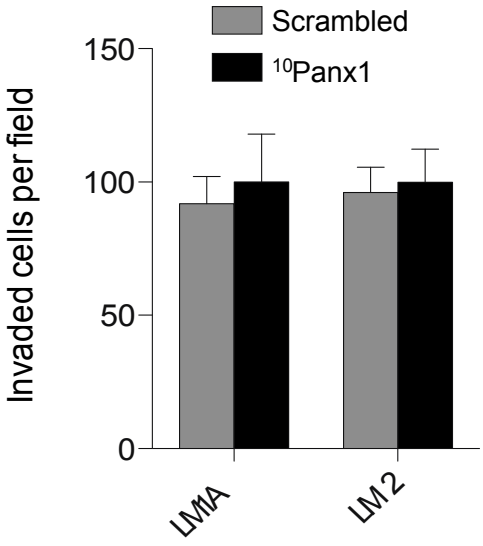

Figure 29. PANX1 activity is not required for invasion. Quantification of 24 hour invasion for CN-LM1A and MDA-LM2 cells in the presence of 100μM ^{10}Panx1 or scrambled peptide; *n* = 4. Error bars, s.e.m.

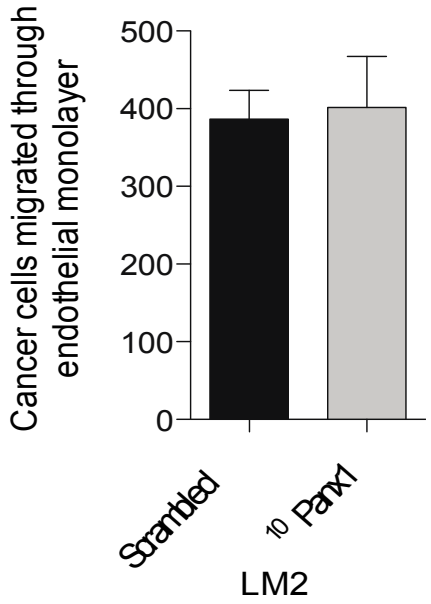

Figure 30. PANX1 activity is not required for transendothelial migration. Quantification of 24 hour trans-endothelial migration for MDA-LM2 cells in the presence of 100 μM ^{10}Panx1 or scrambled peptide; *n* = 4. Error bars, s.e.m.

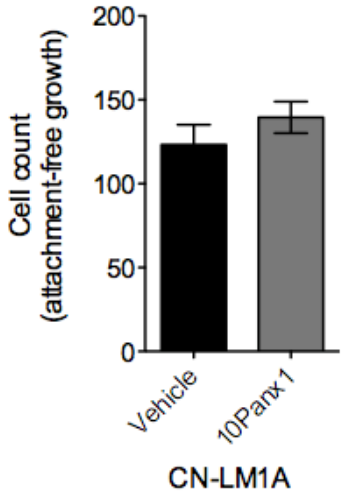

Figure 31. PANX1 activity is not required for anchorage-independent cell survival. Quantification of 36 hour anchorage-independent cancer cell survival for CN-LM1A cells in the presence of 100 μM ^{10}Panx1 or scrambled peptide; *n* = 4. Error bars, s.e.m.

The acute impact of PANX1 channel inhibition on cancer-cell lung bioluminescence at 24 hrs suggested a block in metastatic progression while cells were in the vasculature. In support of this, PANX1 blockade did not inhibit proliferation, invasion, transendothelial migration or anchorage-independent cell survival capacity (Figs. 27-31). To assess cancer-cell fate in the lung vasculature, CN-LM1A and MDA-LM2 metastatic cells preincubated with ^{10}Panx1 or scrambled peptides were injected into the tail-vein of mice and *in vivo* caspase activity was quantified using a luciferase-based reporter. In support of enhanced intravascular cell death, *in vivo* caspase activity was significantly augmented upon PANX1 inhibition at early time-points (3 and 6 hrs) post-injection (Fig. 32)—well before monocyte recruitment (24 hrs)[38] or extravasation (48 hrs)[18,38]. The function of PANX1$^{1-89}$ in intravascular metastatic cell survival was then tested. Expression of PANX1$^{1-89}$ in BT549 and MDA-MB-468 cells led to significant (2-3 fold) increases in cancer-cell lung bioluminescence 18 hrs after injection (Fig. 33a) and significant decreases in *in vivo* caspase activity 3 hrs and 6 hrs after injection (Fig. 33b). These data establish a role for PANX1$^{1-89}$ in the suppression of intravascular cell death through its enhancement of PANX1 channel activity and reveal PANX1 as a driver of metastatic breast cancer cell dissemination.

Confocal microscopy revealed that, at the time when PANX1 activity was found to mediate survival (3 hrs post-injection), cancer cells were confined within the pulmonary vasculature and many had become morphologically elongated in small blood vessels (Fig. 34). Consistent with the quantitative *in vivo* caspase

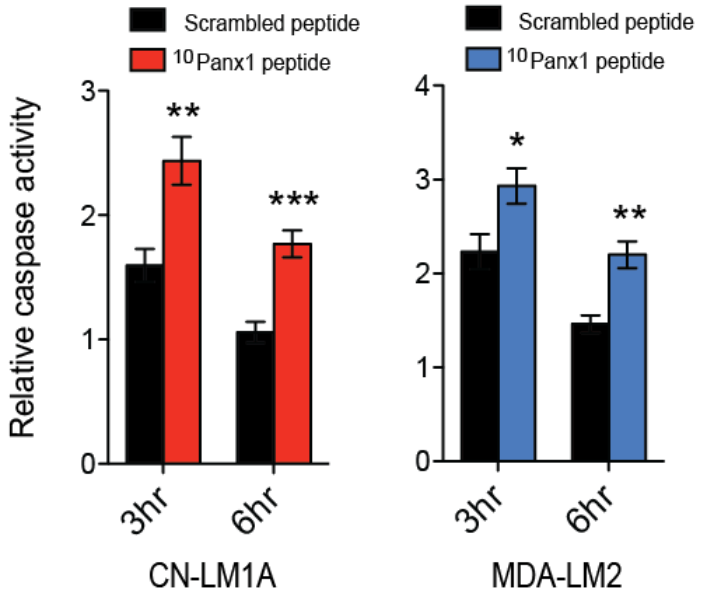

Figure 32. PANX1 channel inhibition increases caspase-mediated intravascular cancer cell death. *In vivo* quantification of luciferase-based caspase-3/7 activity at 3 hr and 6 hr after tail-vein injection of 1×10^5 CN-LM1A (left panel) or 4×10^4 MDA-LM2 (right panel) breast cancer cells, pre-treated with 100 μM ^{10}Panx1 or scrambled peptide, into NS mice; $n = 5$. Error bars, s.e.m., *, $P < 0.05$; **, $P < 0.01$; ***, $P < 0.001$ by a one-tailed Student's *t*-test.

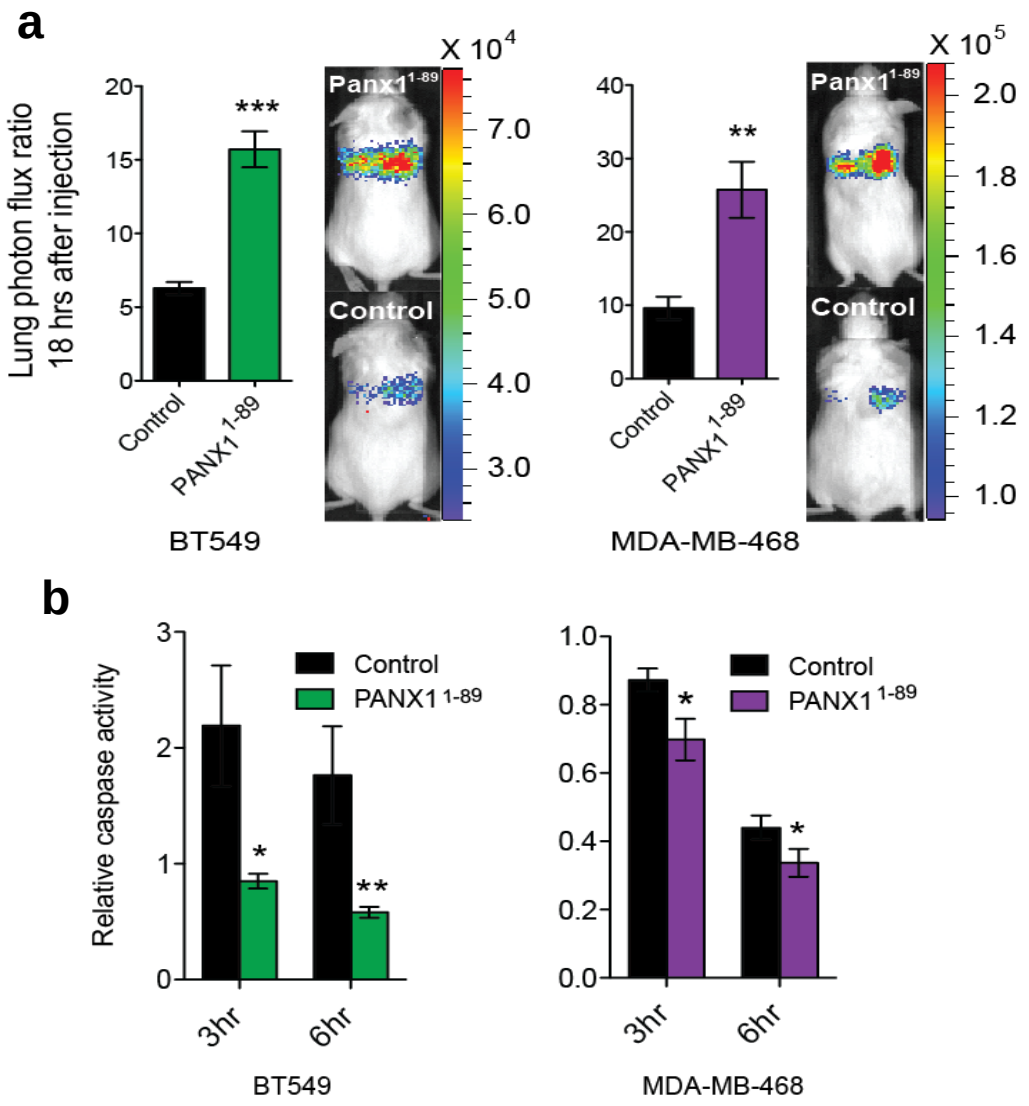

Figure 33. PANX1$^{1-89}$ promotes the intravascular survival of breast cancer cells. a, Quantitative imaging of lung bioluminescence 18 hrs post tail-vein injection of 1 × 10^6 BT549 (left panel) and 1 × 10^6 MDA-MB-468 (right panel) breast cancer cells, expressing PANX1$^{1-89}$ or a control vector, into NSG mice; *n* = 6. **b**, *In vivo* quantification of luciferase-based caspase-3/7 activity at 3 hr and 6 hr post tail-vein injection of 1 × 10^6 BT549 (left panel) or 1 × 10^6 MDA-MB-468 (right panel) breast cancer cells, expressing either PANX1$^{1-89}$ or a control vector, into NS mice; *n* = 4−5. Error bars, s.e.m., *, $P < 0.05$; **, $P < 0.01$; ***, $P < 0.001$ by a one-tailed Student's *t*-test.

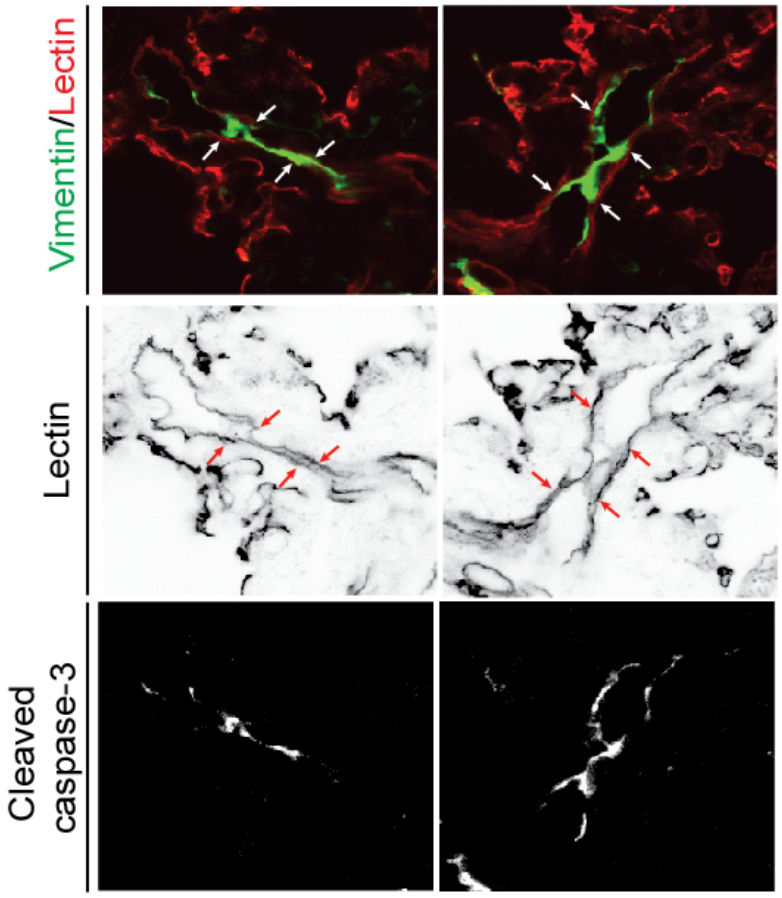

Figure 34. Confocal microscopy of cancer cells in the lung microvasculature. Representative images of mouse lungs stained for cancer cells and blood vessels (green and red, respectively, top panel), blood vessels (black, middle panel) or cleaved caspase-3 (white, bottom panel) 3 hrs after tail-vein injection of 1 × 10^5 CN-LM1A cells pre-treated with 100 μM ^{10}Panx1. Arrows indicate endothelium.

measurements, a number of these intravascular cancer cells displayed activated caspase immunoreactivity (Fig. 34). Of the many mechanisms responsible for the inefficiency of metastasis, intravascular death is responsible for the loss of up to >90% of the cancer cells entering the microvasculature of a secondary organ[39-42]. Because PANX1 is a mechanosensitive channel that opens during plasma membrane stretch[24-27] and caspase-positive breast cancer cells were often elongated in the small lung vessels soon after injection (Fig. 34), it was hypothesized that PANX1 activation during cancer cell deformation in the vasculature might underlie its observed role in early cancer-cell survival. To test this, it was first asked whether PANX1 channels could be mechanically activated in metastatic breast cancer cells. Hypotonic cell swelling—an established perturbation that imparts plasma membrane stretch in a well-controlled manner[25-27,43,44]—significantly increased the amplitude of PANX1-mediated ATP release in CN-LM1A and MDA-LM2 breast cancer cells (Fig. 35). To test the role of PANX1 activity in promoting survival during membrane stretch, CN-LM1A and MDA-LM2 cells were hypotonically stretched in the presence of ^{10}Panx1 or scrambled peptides. The number of viable cancer cells remaining after incubation in hypotonic solution was significantly reduced when cells were subjected to PANX1 channel inhibition (Fig. 36). Importantly, cell viability was fully rescued in the PANX1-inhibited cells through the addition of extracellular ATP (Fig. 36), suggesting that ATP signaling at the cell surface mediates the observed survival phenotype. Furthermore, CN-LM1A and MDA-LM2 cell viability was dramatically decreased upon exposure to hypotonic solution supplemented with suramin (Fig.

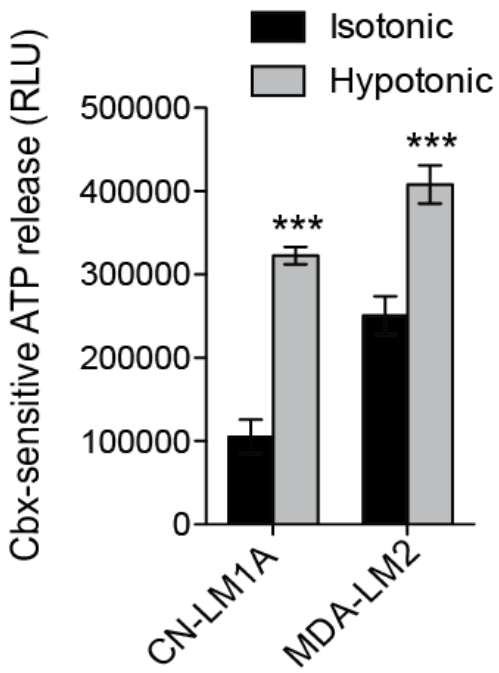

Figure 35. Plasma membrane stretch activates mechanosensitive PANX1 channels in metastatic breast cancer cells. Quantification of PANX1-mediated Cbx-sensitive ATP release from CN-LM1A and MDA-LM2 cells during 5 min exposure to isotonic (100% PBS) or hypotonic (70% PBS) solution; n = 3−4. Error bars, s.e.m., *, $P < 0.05$; **, $P < 0.01$; ***, $P < 0.001$ by a one-tailed Student's t-test.

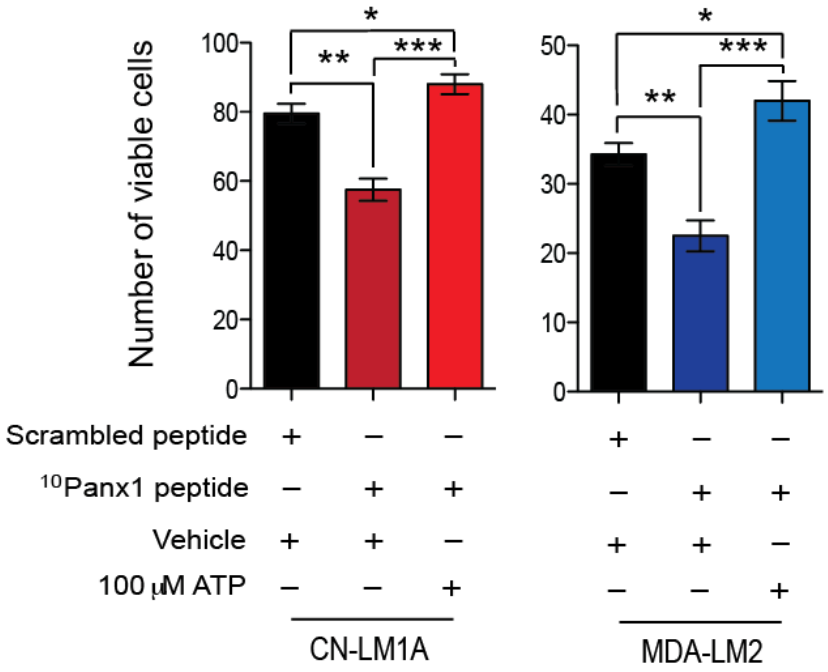

Figure 36. ATP-release from PANX1 channels promotes cell survival during plasma membrane stretch. Quantification of viable, trypan blue-negative, CN-LM1A (left panel) and MDA-LM2 (right panel) cells after 1 hr incubation in extremely hypotonic (12.5% PBS) solution in the presence of scrambled peptide (100 μM), ^{10}Panx1 peptide (100 μM) or ^{10}Panx1 peptide (100 μM) and 100 μM ATP; n = 4. Error bars, s.e.m., *, $P < 0.05$; **, $P < 0.01$; ***, $P < 0.001$ by a one-tailed Student's *t*-test.

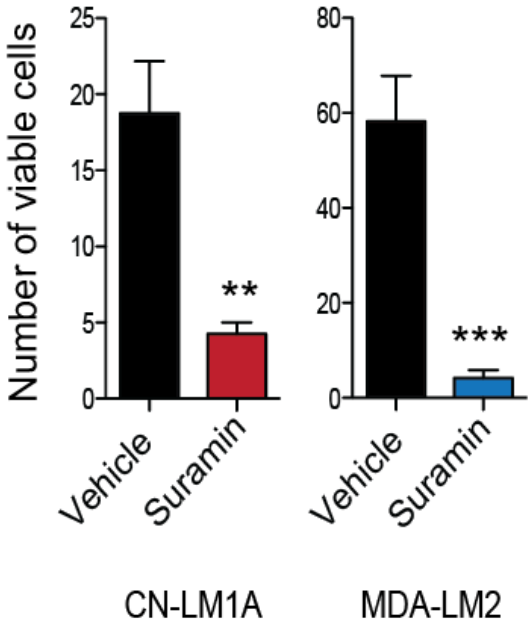

Figure 37. Purinergic signaling via P2y receptors promotes cell survival during plasma membrane stretch. Quantification of viable, trypan blue-negative, CN-LM1A (left panel) and MDA-LM2 (right panel) cells after 15 min incubation in extremely hypotonic (12.5% PBS) solution in the presence of suramin (50 μM) or water vehicle; n = 4. Error bars, s.e.m., *, $P < 0.05$; **, $P < 0.01$; ***, $P < 0.001$ by a one-tailed Student's *t*-test.

37)—a broad-spectrum antagonist of ATP-binding P2y purinergic receptors (P2yRs)[45]. These data suggest that ATP release stimulated by plasma membrane stretch activates P2yRs that signal to protect cancer cells from lethal mechanical injury. Consistent with ATP being necessary for cancer cell survival in the vasculature, CN-LM1A and MDA-LM2 lung bioluminescence was significantly reduced 6 hrs after tail-vein co-injection of cells with apyrase, a potent extracellular ATP hydrolase (Fig. 38)[28,46]. These data reveal a role for extracellular ATP release through mechanosensitive PANX1 channels as a cancer-cell-autonomous survival signal during critical deformation of the plasma membrane.

PANX1$^{1-89}$ expression was also found to promote cancer-cell survival during membrane stretch. CN-LM1A and MDA-LM2 sub-lines, in which display greater PANX1$^{1-89}$ expression and PANX1 activity relative to their parental lines, were significantly more resistant to lethal hypotonic stretch than their parental lines (Fig. 39). Moreover, expressing PANX1$^{1-89}$ in BT549 and MDA-MB-468 cells significantly enhanced the survival of these lines during hypotonic stretch (Fig. 3l). The addition of apyrase to PANX1$^{1-89}$-expressing cells in hypotonic solution completely abrogated the survival advantage afforded by PANX1$^{1-89}$ expression (Fig. 40), suggesting that extracellular ATP is responsible for this effect. These data reveal that PANX1$^{1-89}$−induced PANX1 channel activity enhances the efficiency of metastasis by promoting metastatic breast cancer cell survival during physical deformation.

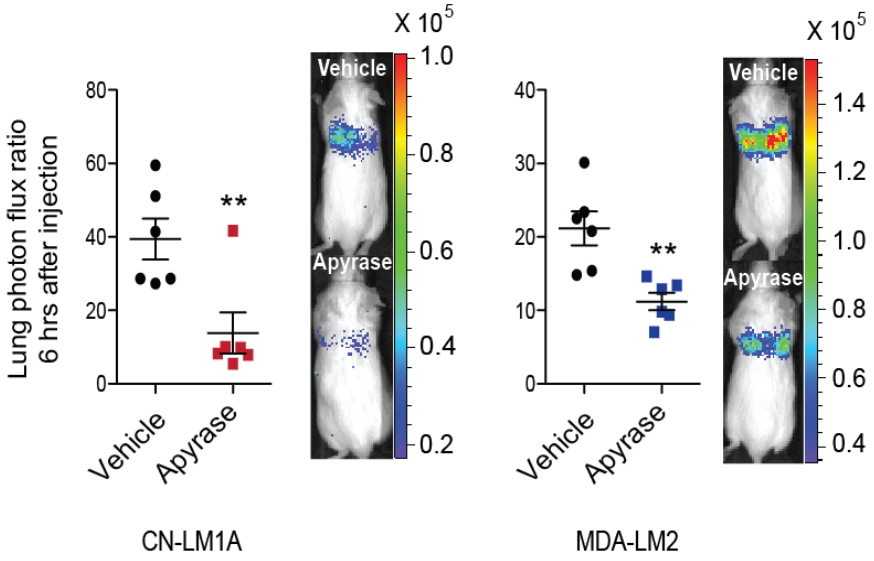

Figure 38. Extracellular ATP is required for early cancer cell survival in the lung vasculature. a, Quantitative imaging of lung bioluminescence at 6 hrs post tail-vein injection of 1 × 10^5 CN-LM1A (left panel) or 4 × 10^4 MDA-LM2 (right panel) breast cancer cells pre-treated (30 min) and co-injected with apyrase (2U/ml) into FVB/NJ mice; n = 6. Error bars, s.e.m., *, $P < 0.05$; **, $P < 0.01$; ***, $P < 0.001$ by a one-tailed Student's t-test.

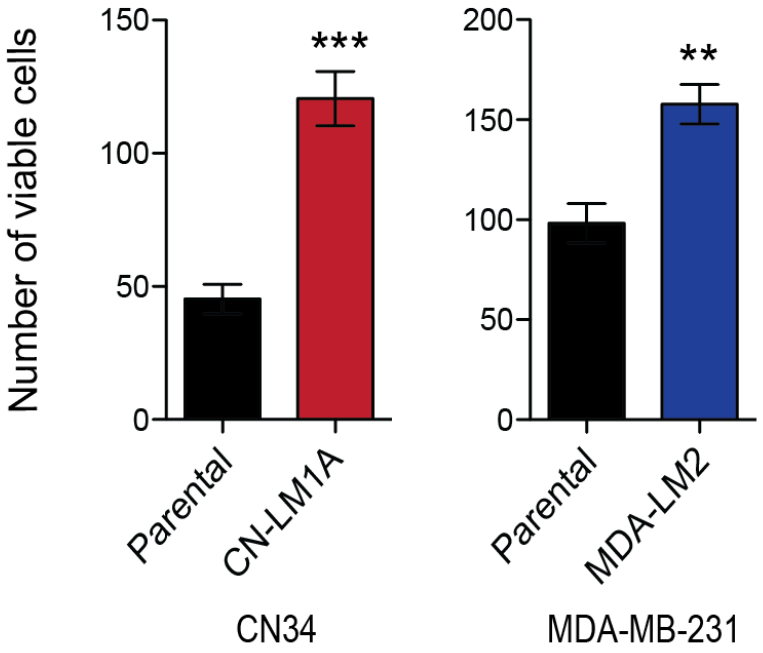

Figure 39. Highly metastatic breast cancer sub-lines exhibit increased resistance to stretch-induced cell death. Quantification of viable, trypan blue-negative, CN34, CN-LM1A, MDA-MB-231 and MDA-LM2 cells after 1 hr extreme hypotonic (12.5% PBS) stretch; $n = 4$. Error bars, s.e.m., *, $P < 0.05$; **, $P < 0.01$; ***, $P < 0.001$ by a one-tailed Student's *t*-test.

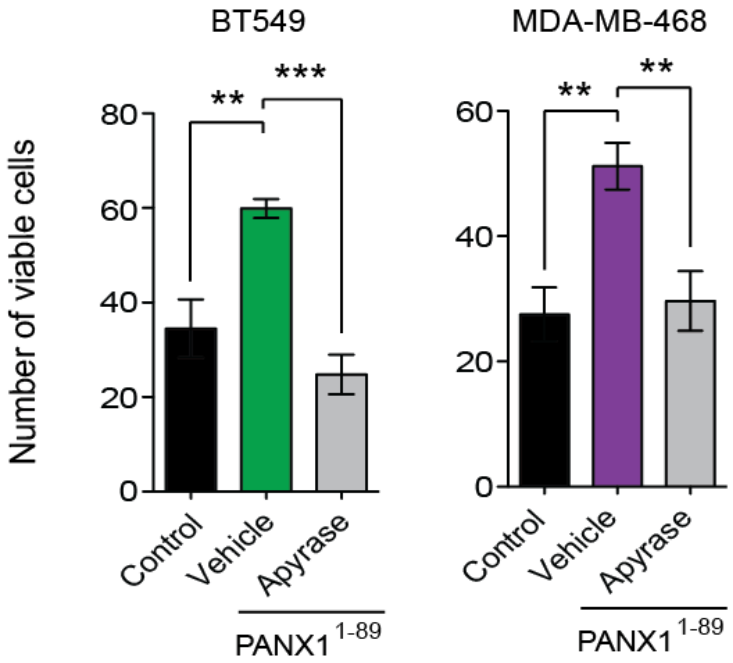

Figure 40. Augmented PANX1-mediated ATP release by PANX1$^{1-89}$ promotes cell survival during plasma membrane stretch. Quantification of viable, trypan blue-negative BT549 (left panel) and MDA-MDA-468 (right panel) cells expressing PANX1$^{1-89}$ or a control vector after 1 hr extreme hypotonic (12.5% PBS) stretch in the presence of succinate buffer or apyrase (2U/ml); n = 4. Error bars, s.e.m., *, $P < 0.05$; **, $P < 0.01$; ***, $P < 0.001$ by a one-tailed Student's t-test.

CHAPTER IV: THE CLINICAL SIGNIFICANCE OF ACTIVATED PANX1 CHANNELS IN METASTASIS

To determine if PANX1 mutations are relevant to human cancer progression, publically available cancer-sequencing datasets were analyzed (see methods). This search uncovered six additional PANX1-truncating mutations in cancers of the colon, lung and brain (Fig. 41 and Table 4). In addition to the truncating mutations, an in-frame deletion of lysine 91 was detected in a breast carcinoma, while missense mutations were found in eleven lung carcinomas, five colon carcinomas, two liver carcinomas, two endometrial carcinomas, as well as cancers of the breast, bladder, pancreas, esophagus, larynx, kidney and prostate (Table 4). Four of the PANX1 missense mutations predicted by PolyPhen-2 to be non-neutral were then tested for their effects on PANX1-mediated ATP release. Consistent with channel-activating functional roles, each of the four missense mutations significantly augmented PANX1-mediated ATP release relative to wild-type PANX1 (Fig. 42). To determine if mutant PANX1 could promote metastasis by an epithelial cancer type other than breast cancer, PANX1 L47fs*18—a truncating mutation detected in a metastatic colon adenocarcinoma (Fig. 41)—was expressed in WiDR and sw480 human colon cancer cell lines harboring wild-type endogenous PANX1. The expression of L47fs*18 in both of these lines significantly enhanced PANX1-mediated ATP release (Fig. 43), hepatic dissemination at early time-points (Fig. 44), liver metastatic colonization upon portal-circulation injection of cancer cells (Fig. 45), as well as survival during membrane stretch (Fig. 46). PANX1 L47fs*18 also co-localized with full-length

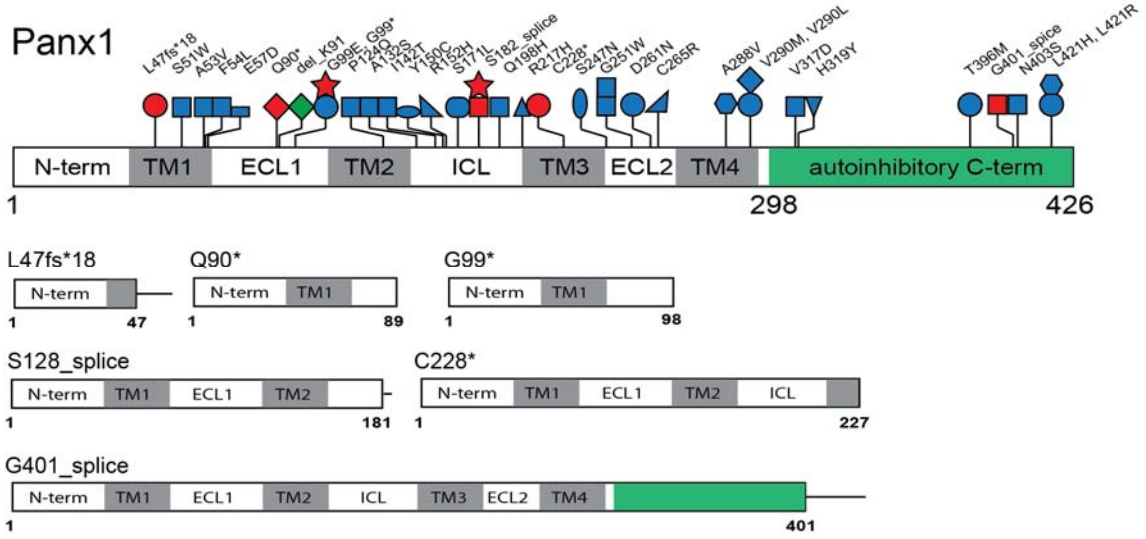

Figure 41. The distribution of PANX1 mutations detected in patients' primary tumors. Top panel, the distribution of PANX1 mutations detected in clinical tumours. Red: truncation; green: deletion; blue: substitution. ⬭ , bladder; ☆ , brain; ◇ , breast; ○ , colon; ⬡ , endometrium; ⬯ , kidney; ◿ , larynx; ▭ , liver; □ , lung; ◺ , oesophagus; ▽ , pancreas; and △ , prostate. Bottom panel, schematics of the PANX1 domain fragments predicted to be generated by truncating mutations identified in cancers of the colon (L47fs*18 and C228*), lung (S182_splice and G401_splice), brain (G99* and S182_splice) and the recurrently enriched nonsense mutation in metastatic breast cancer cells (Q90*). Error bars, s.e.m., *, $P < 0.05$; **, $P < 0.01$; ***, $P < 0.001$ by a one-tailed Student's *t*-test.

Table 4. Frequencies of PANX1 mutations in patients' primary tumors.

Primary Tissue	Histology	Unique mutated samples (NS/MS)	Total samples	Mutation frequency (%)
Larynx	Squamous cell Ca	1	17	**5.88**
Liver	Hepatocellular Ca	2	72	**2.78**
Lung	Squamous cell Ca	4	179	**2.23**
Lung	Adenocarcinoma	9	596	**1.51**
Breast (TCGA)	HER2-enriched	1	58	**1.72**
Breast (TCGA)	Basal-like	1	98	**1.02**
Colon	Adenocarcinoma	7	498	**1.40**
Bladder	Carcinoma	1	103	**0.97**
Endometrium	Endometrioid Carcinom	2	258	**0.78**
Pancreas	Ductal Ca	1	137	**0.73**
Esophagus	Adenocarcinoma	1	161	**0.62**
Brain	Neuroblastoma	2	362	**0.55**
Kidney	Clear Cell Carcinoma	1	359	**0.28**
Prostate	Carcinoma	1	319	**0.31**

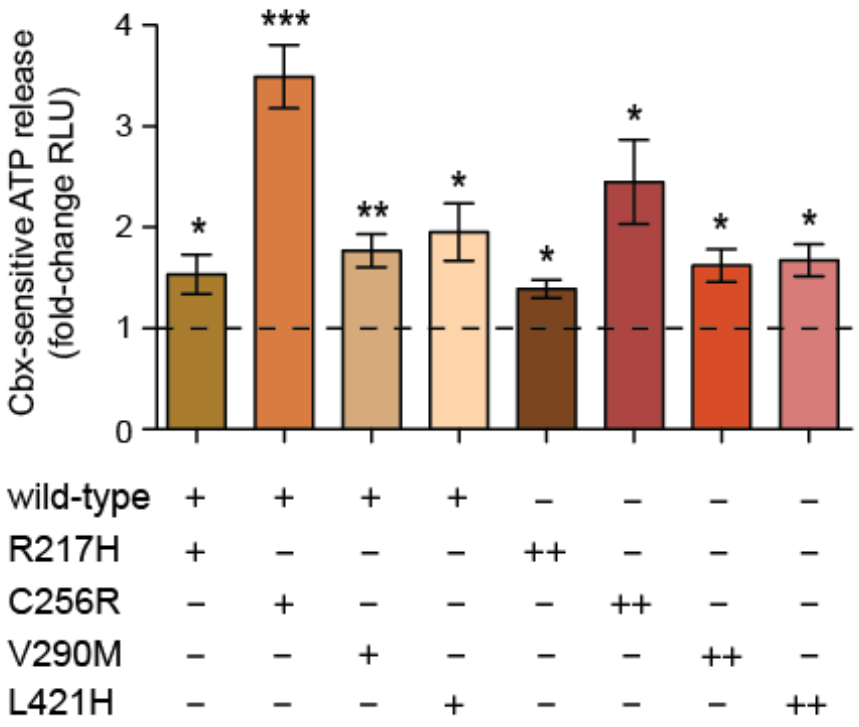

Figure 42. The effect of clinically identified non-neutral missense mutations on PANX1-mediated ATP release. Quantification of Cbx-sensitive ATP release from HEK293T cells transfected with 5 μg wild-type PANX1 (dotted line), 2.5 μg wild-type PANX1 and 2.5 μg mutant PANX1, or 5 μg mutant PANX1; n = 3−4. **c**, Quantification of Cbx-sensitive ATP release from WiDR colon cancer cells expressing PANX1-L47fs18* or a control vector; n = 8. Error bars, s.e.m., *, P < 0.05; **, P < 0.01; ***, P < 0.001 by a one-tailed Student's t-test.

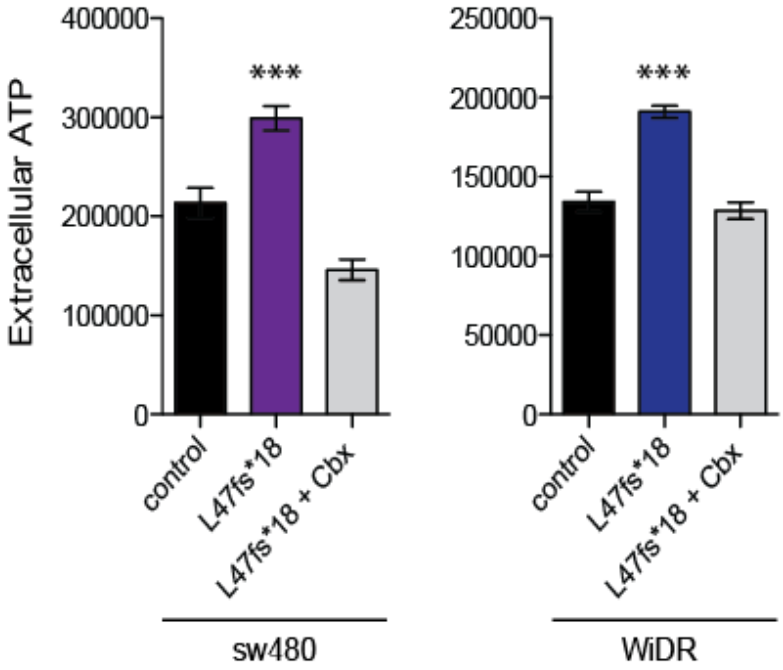

Figure 43. PANX1 L47fs*18 enhances PANX1-mediated ATP release from metastatic colon cancer cells. Quantification of Cbx-sensitive ATP release from sw480 (left panel) or WiDR (right panel) colon cancer cells expressing PANX1-L47fs18* or a control vector; *n* = 8. b, Error bars, s.e.m., *, $P < 0.05$; **, $P < 0.01$; ***, $P < 0.001$ by a one-tailed Student's *t*-test.

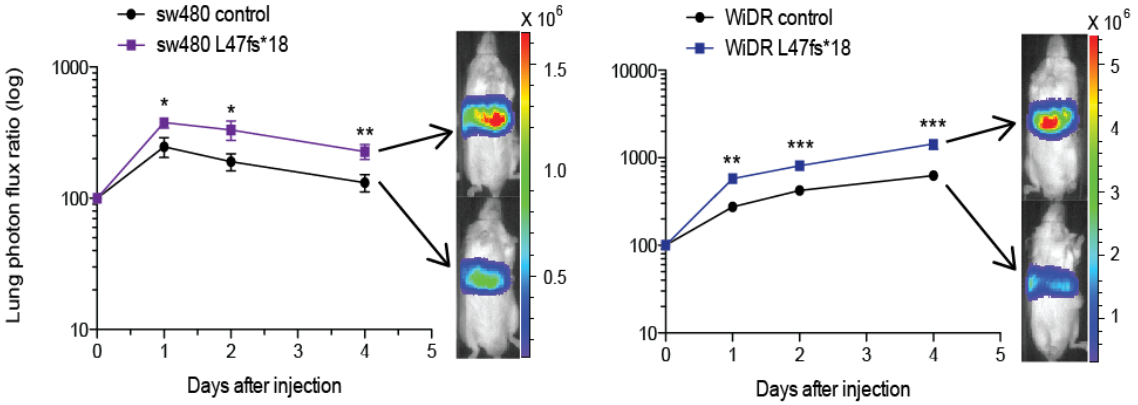

Figure 44. PANX1 L47fs*18 promotes the early hepatic dissemination of cancer cells. Quantitative imaging of liver bioluminescence at one, two and four days after the intrasplenic injection of 5 × 10^5 sw480 (left panel) or WiDR (right panel) colon cancer cells, expressing PANX1 L47fs18* or a control vector, into NSG mice; *n* = 5. Error bars, s.e.m., *, $P < 0.05$; **, $P < 0.01$; ***, $P < 0.001$ by a one-tailed Student's *t*-test.

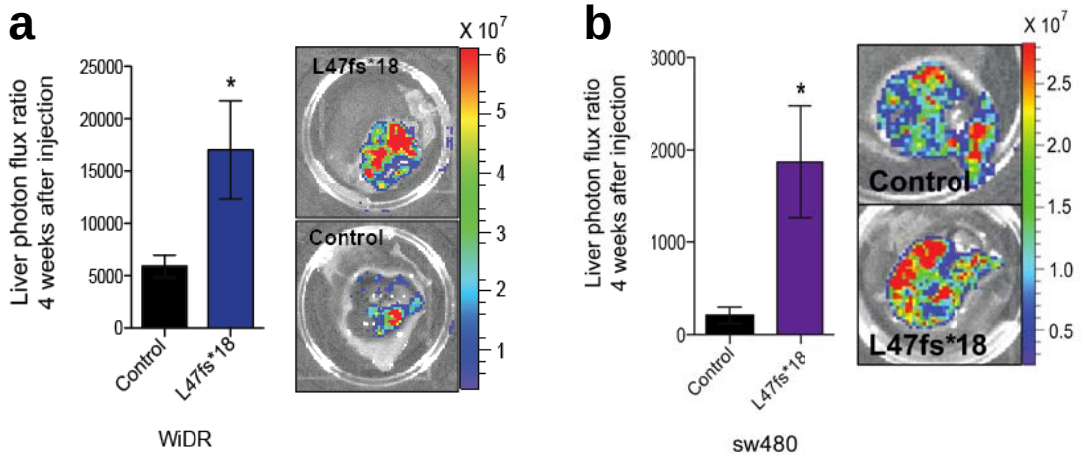

Figure 45. PANX1 L47fs*18 promotes metastatic liver colonization by colon cancer cells. a, Quantitative *in vivo* (left panel**)** and representative *ex vivo* (right panel) bioluminescence imaging of day 28 liver colonization after the intrasplenic injection of 5 × 10^5 WiDR colon cancer cells, expressing PANX1 L47fs18* or a control vector, into NSG mice; *n* = 5. **b**, Quantitative *in vivo* (left panel) and *ex vivo* (right panel) bioluminescence imaging of day 28 liver colonization after the intrasplenic injection of 5 × 10^5 sw480 colon cancer cells, expressing PANX1 L47fs18* or a control vector, into NSG mice; *n* = 5. Error bars, s.e.m., *, $P < 0.05$; **, $P < 0.01$; ***, $P < 0.001$ by a one-tailed Student's *t*-test.

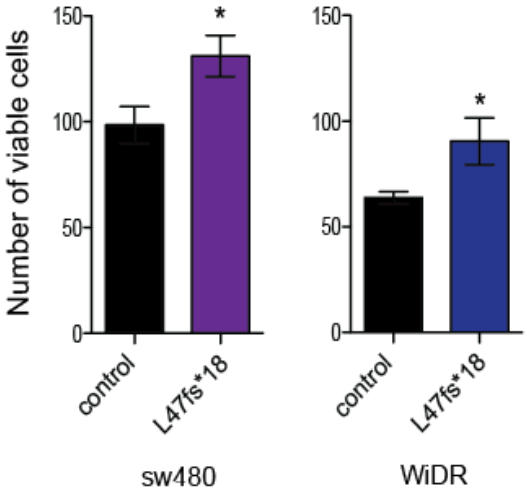

Figure 46. PANX1 L47fs*18 promotes cell survival during plasma membrane stretch. Quantification of viable, trypan blue-negative sw480 (left panel) and WiDR (right panel) colon cancer cells cells, expressing PANX1$^{1-89}$ or a control vector, after 2 hr extreme hypotonic (12.5% PBS) stretch; n = 4. Error bars, s.e.m., *, $P < 0.05$; **, $P < 0.01$; ***, $P < 0.001$ by a one-tailed Student's t-test.

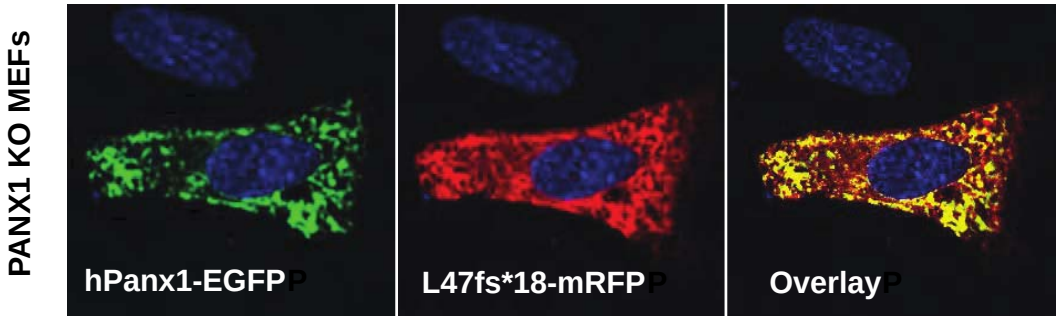

Figure 47. PANX1 L47fs*18 colocalizes with full-length PANX1. Confocal microscopy images of PANX1 KO MEFs expressing human PANX1-EGFP (green) and PANX1-L47fs*18-mRFP (red). Colocalization is shown by channel overlay (yellow).

PANX1 (Fig. 47), suggesting that this mutation, like PANX1$^{1-89}$, may also augment ATP release through interactions with full-length PANX1. These findings, as a whole, reveal a role for mutationally activated PANX1 channels in the survival and progression of multiple cancer types.

The discovery that PANX1 channel-activating mutations could promote metastasis led to the question of whether patients' cancers might also augment their ability to release ATP by upregulating *PANX1* expression as they progress. In support of this possibility, *PANX1* expression was significantly increased in high-grade breast cancers (Fig. 48), and patients whose primary breast, colon or lung tumors exhibited high *PANX1* expression had significantly worse metastasis-free survival (Fig. 49). These data suggest that many cancers use increasing *PANX1* expression in addition to mutational PANX1 activation to achieve the levels of ATP release optimal for metastasis.

Finally, the effect of pharmacologically inhibiting open PANX1 channels in metastatic cells during metastatic progression was tested. CN-LM1A cells pretreated with Cbx, a PANX1 channel inhibitor approved for the treatment of gastroesophogeal reflux disease (GERD) in the UK, showed a 100-fold reduction in their ability to metastasize to the lungs (Fig. 50). To better assess the clinical potential of this therapy, mice were treated with two different Cbx regimens prior to introducing metastatic breast cancer cells into the circulation (Fig. 51). Seven days of Cbx treatment significantly inhibited (3-fold) the ability for MDA-LM2 cells to colonize the lungs (Fig. 52a-b). Importantly, this treatment was well tolerated

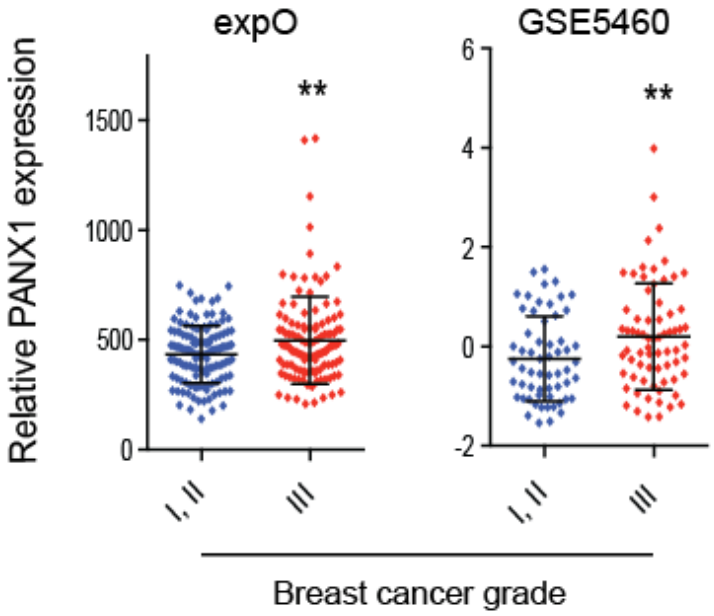

Figure 48. PANX1 expression in low- and high-grade breast cancer tumors. *PANX1* transcript expression in Bloom-Richardson low- (I, II) and high-grade (III) breast cancer tumours from the expO (n = 252) and GSE5460 (n = 129) datasets. Error bars, s.e.m., *, $P < 0.05$; **, $P < 0.01$; ***, $P < 0.001$ by a one-tailed Student's t-test.

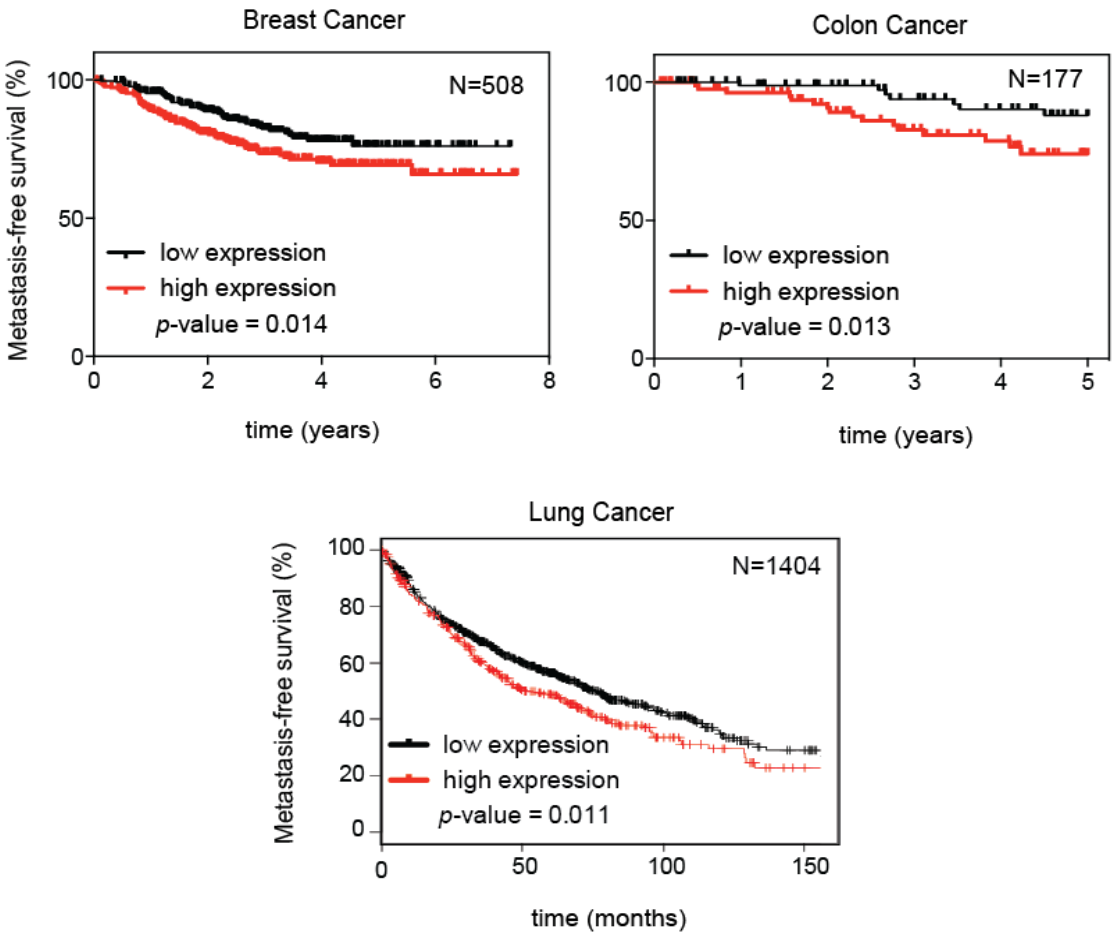

Figure 49. Correlation of metastasis-free survival and PANX1 expression levels in primary tumors from breast, colon and lung cancer patients. Kaplan–Meier curves for breast cancer[47] (*n* = 508), colon cancer GSE17536 (*n* = 177) and lung cancer[47] (*n* = 1404) datasets depicting metastasis-free survival of patients as a function of their primary tumours' PANX1 expression status. An expression greater or lower than the mean for the entire population was classified as high or low PANX1 expression, respectively. *P* values are based on a Mantel–Cox log-rank test. Error bars, s.e.m., *, $P < 0.05$; **, $P < 0.01$; ***, $P < 0.001$ by a one-tailed Student's *t*-test.

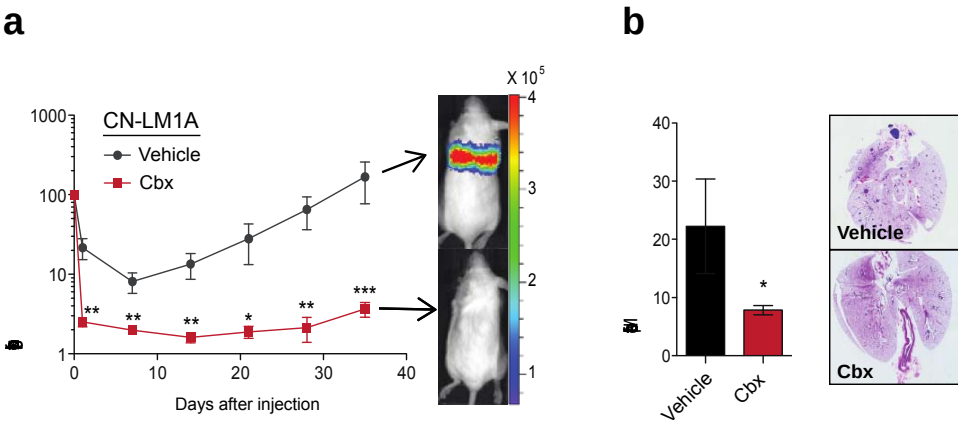

Figure 50. Pharmacological inhibition of PANX1 reduces lung metastasis. a, Quantitative bioluminescence imaging of lung metastasis after tail-vein injection of 1 × 10^5 CN-LM1A breast cancer cells pretreated for 30 min with Cbx (500 μM) or PBS vehicle into NS mice; *n* = 4-6. **b**, Day 35 quantification of metastatic foci (left) and representative lung images (right) from H&E stained lungs of mice injected with CN-LM1A cells pretreated with Cbx or PBS vehicle; *n* = 4-6. Error bars, s.e.m., *, $P < 0.05$; **, $P < 0.01$; ***, $P < 0.001$ by a one-tailed Student's *t*-test.

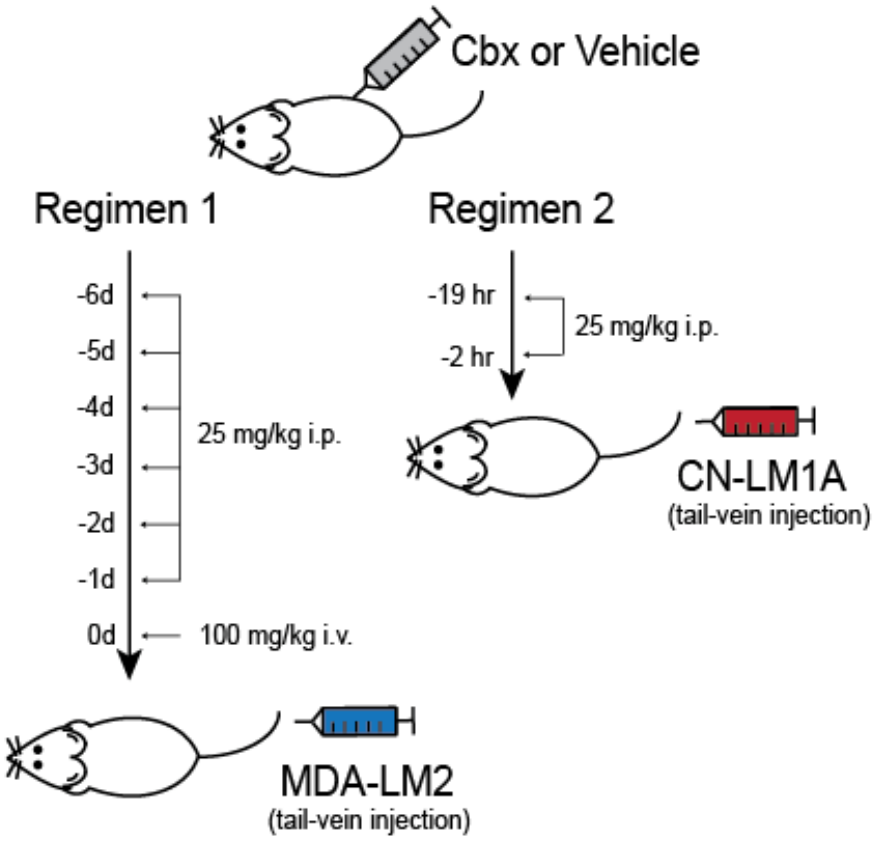

Figure 51. Therapeutic Cbx regimens tested in the study. Schematic depicting the two *in vivo* Cbx therapy regimens tested for pharmacological effect on breast cancer metastasis to the lung.

Figure 52. *In vivo* therapeutic inhibition of PANX1 channels with Cbx inhibits metastatic dissemination and lung colonization. a, Quantitative bioluminescence imaging of lung metastasis after tail-vein injection of 5×10^4 MDA-LM2 breast cancer cells into NS mice pretreated daily with 25 mg/kg i.p. Cbx or an equivalent volume of PBS for six days and with 100 mg/kg i.v. Cbx or an equivalent volume of PBS 30 min prior to cancer cell injection; *n* = 4-6. **b**, Lungs were extracted at day 14, H&E stained, and the number of metastatic foci were quantified; n = 4. **c**, Quantitative bioluminescence imaging of breast cancer cells in the lung 24 hrs after tail-vein injection of 1×10^5 CN-LM1A breast cancer cells into NS mice pretreated with 25 mg/kg i.p. Cbx or an equivalent volume of PBS 19 and 2 hours prior to cancer cell injection; *n* = 10. **d**, Lungs were extracted at 24 hrs, sectioned and stained for vimentin and the number of vimentin-positive cancer cells were quantified; *n* = 7-8. **e**, Quantitative bioluminescence imaging of the lungs at 4 weeks after tail-vein injection of 1×10^5 CN-LM1A breast cancer cells into NS mice pretreated with 25 mg/kg i.p. Cbx or an equivalent volume of PBS 19 and 2 hours prior to cancer cell injection; *n* = 9-10. **f**, Lungs were extracted at week 4, H&E stained, and the numbers of metastatic foci were quantified; *n* = 9-10. Error bars, s.e.m., *, $P < 0.05$; **, $P < 0.01$; ***, $P < 0.001$ by a one-tailed Student's *t*-test.

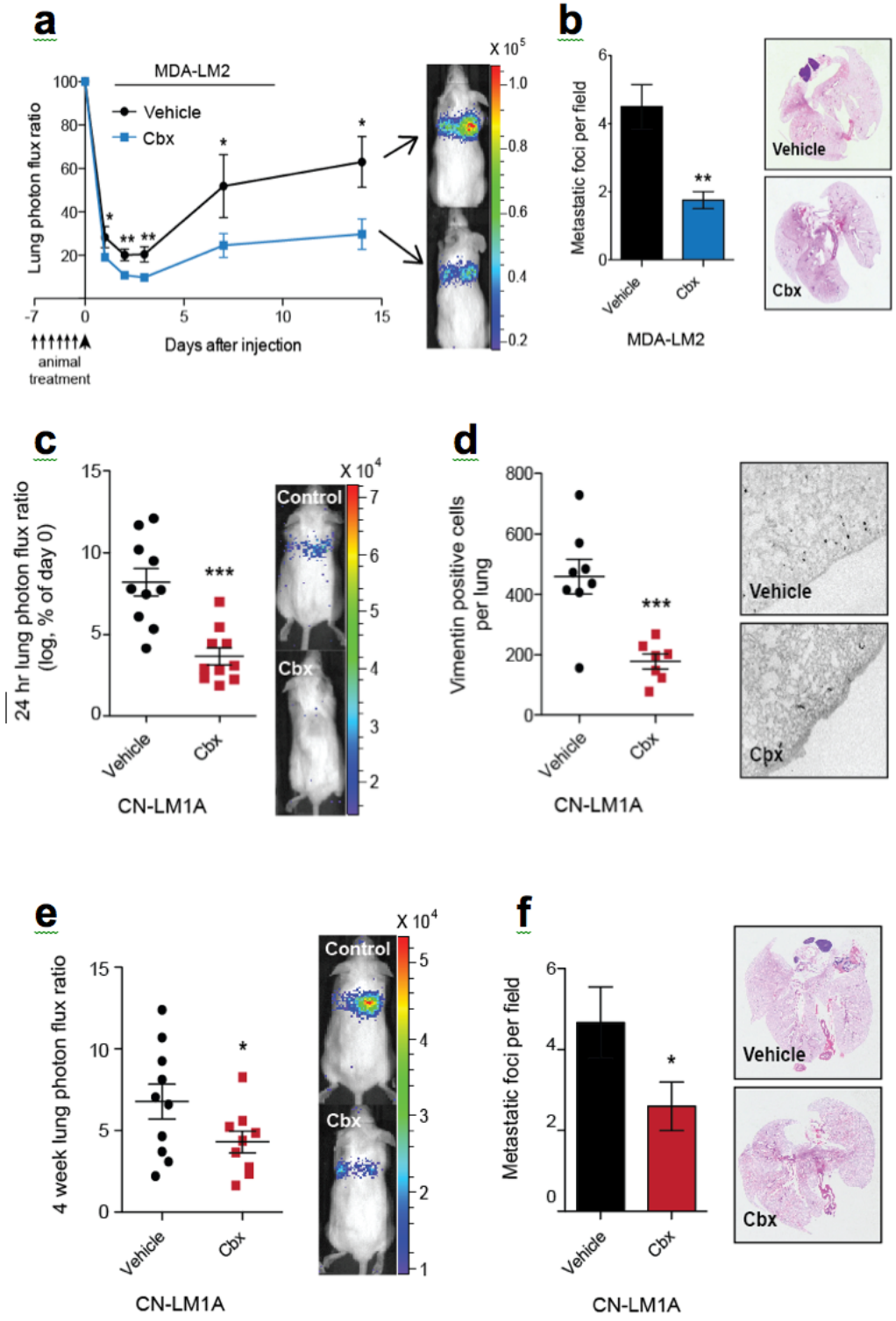
a
MDA-LM2
Vehicle
Cbx
Lung photon flux ratio
Days after injection
animal treatment
X 10^5
b
Metastatic foci per field
Vehicle
Cbx
MDA-LM2
c
24 hr lung photon flux ratio (log, % of day 0)
X 10^4
Control
Cbx
CN-LM1A
d
Vimentin positive cells per lung
CN-LM1A
e
4 week lung photon flux ratio
X 10^4
Control
Cbx
CN-LM1A
f
Metastatic foci per field
CN-LM1A

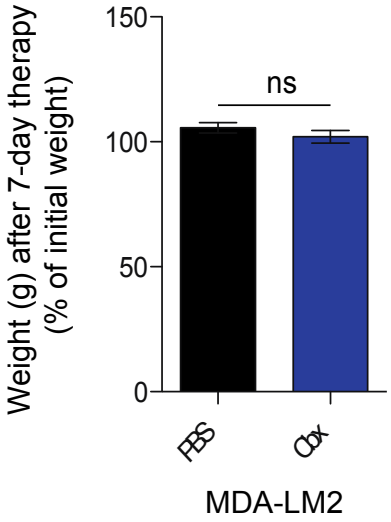

Figure 53. *In vivo* Cbx therapy does not affect mouse body weight. Mouse body weight before and after daily i.p. injections of Cbx (25 mg/kg) or an equivalent volume of PBS vehicle for seven days; n = 4-6. Error bars, s.e.m., ns, nonsignificant by a one-tailed Student's *t*-test.

and did not impact body weight (Fig. 53). Strikingly, reducing this treatment to two doses of Cbx within 24 hrs of cancer cell injection significantly reduced the number of CN-LM1A cells in the lungs at as early as 24 hrs (Fig. 52c-d) as well as lung metastatic colonization at four weeks (Fig. 50e-f).

CHAPTER V: SUMMARY

This work identifies *PANX1* mutations in multiple cancers as activators of PANX1 channel activity and drivers of metastasis in epithelial cancers such as breast and colon carcinomas. A working model is proposed whereby the mutational augmentation of ATP release via mechanosensitive PANX1 channels cell-autonomously promotes cancer cell survival in the setting of microvascular-induced physical stress—an important barrier to metastatic progression (Fig. 54). The data presented suggest that ATP exerts this effect through purinergic receptors on the cell surface, which have been previously implicated in survival signaling during mechanical stress[46]. The integrated approach to identifying and functionally testing putative metastasis-promoting genetic variants developed and employed in this study also identified PANX1 as a potential therapeutic target whose inhibition may reduce the development of metastasis. In the future, follow up studies investigating the specific molecular and structural mechanisms by which nonsense and missense mutations in PANX1 cause enhanced ATP release through activated PANX1 channels as well as studies testing the feasibility of targeting active PANX1 channels for the prevention of metastasis in humans, should be performed.

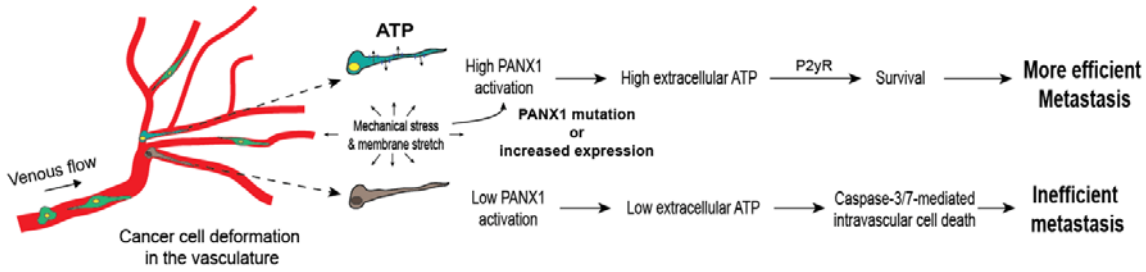

Figure 54. The working model: increased PANX1 channel activity enables intravascular metastatic cell survival. Proposed working model in which ATP released from stretch-activated PANX1 channels acts to suppress cancer cell death during mechanical stress in the microvasculature. The increased levels of PANX1 channel activity necessary for optimal metastatic efficiency may be achieved through mutational activation or enhanced gene expression.

CHAPTER VI: DISCUSSION

The potential underestimation of PANX1-mutation frequency in cancer—The identification of a recurrent mutation that promotes metastasis independent from cell proliferation raises questions about the rationale behind focusing the efforts of current cancer sequencing studies on uncovering those mutations that are most frequently detected in bulk tumors. Molecular blockade of PANX1 ATP-release channels in MDA-LM2 cells resulted in accelerated cell proliferation (Fig. 27), suggesting that mutations increasing the activity of these channels, while promoting the ability for a cell to survive vascular dissemination, might be selected against and as such result in only a small fraction of cells in the primary tumor harboring such mutations. The proliferative disadvantage of such PANX1-mutant subclones would then allow the other, less metastatic, subclones to comprise the majority of a tumor. With our current next-generation tumor sequencing technologies—recently estimated to miss up to 37% of lower frequency mutations[5,21]—the frequencies at which such metastatic driver mutations are detected by the sequencing of bulk tumors are likely to be low. Further contributing to this problem is the contamination of tumor tissue with neighboring and intermingled non-cancerous stroma[22]. Until tumor preparation and sequencing technologies improve, *in vivo* selection can provide utility in allowing for the isolation and detection of low frequency mutations that specifically function to drive metastasis.

The molecular mechanisms of mutational PANX1 activation—Taken together, the results of this study show that, when expressed with full-length PANX1, a truncated version of the PANX1 protein consisting of only the first 89 amino acids of the 426 amino acid protein ($PANX1^{1-89}$) (Fig. 8), interacts with full-length PANX1 (Fig. 10) and increases the release of ATP mediated though PANX1 channels (Fig. 13). In metastatic breast cancer cells, this channel is mechanically activated by membrane stretch (Fig. 35). This increase in PANX1-mediated extracellular ATP release was found to promote the survival of metastatic cells in the vasculature of the lung (Figs. 32 and 33) at a time when they have become physically deformed (Fig. 34). An interesting question that arises from these results is how, in molecular and structural terms, can an 89-amino acid channel fragment cause increased activity of ATP-release channels?

While the most definitive answers to this question will require future crystolographic experimentation, evidence from this study provides some direction. Confocoal microscopy showed distinct co-localization of wild-type PANX1 and mutant $PANX1^{1-89}$ at the plasma membrane (Fig. 9), suggesting that 1) despite truncation, $PANX1^{1-89}$ can effectively colocalize to the plasma membrane when co-expressed with wild-type PANX1 and, 2) interactions formed between $PANX1^{1-89}$ and wild-type PANX1 channels do occur at the cell surface. By crosslinking proteins in cultured cells before lysing them, the immunoprecipitation of $PANX1^{1-89}$ showed that mutant and wild-type PANX1 form a multimeric complex (Fig. 10). This crosslinked complex migrated at a molecular weight higher than would be expected if only one protein of each form were in

complex, suggesting that mutant PANX1$^{1-89}$ is integrated into a hetero-multimeric complex with PANX1. ATP-release studies indicated that the C-terminus of full-length PANX1 is required for the PANX1$^{1-89}$-mediated enhancement of channel activity (Fig. 15). This observation suggests that the association between PANX1$^{1-89}$ and wild-type PANX1 may cause a conformational change in the structure of the PANX1 channel that relaxes the steric impedance of the pore by the autoinhibitory tail[35].

There are two possible models that may explain how PANX1$^{1-89}$ functions (Fig. 55). In the first model, PANX1$^{1-89}$ interacts with the normal PANX1 channel formed by six wild-type PANX1 subunits. PANX1$^{1-89}$ could either be anchored to the plasma membrane via its transmembrane domain (TM1) in proximity to the channel or it could remain completely cytoplasmic. (Fig. 55) Anchored to the membrane or not, it is likely that the mutant, resembling the N-terminal pore-forming domain of the PANX1 channel[48], functions as a decoy for the auto-inhibitory C-terminus that normally interacts with TM1 to block the pore[35]. In the second model, PANX1$^{1-89}$ substitutes for one or more of the full-length PANX1 subunits forming the channel (Fig 55). The observed increase in ATP-release might then be explained by a change in either the size of the pore or the mechanical gating of the channel. If this model holds true, then a mutant channel, with new molecular and physical properties, would emerge. To gain insight into which model is correct, one could test PANX1-mediated ATP release in the presence of increasing concentrations of the ^{10}Panx1 peptide. If the PANX1$^{1-89}$

fragment replaces wild-type PANX1 to form a new channel, the response to the inhibitory peptide mimetic would be expected to be altered.

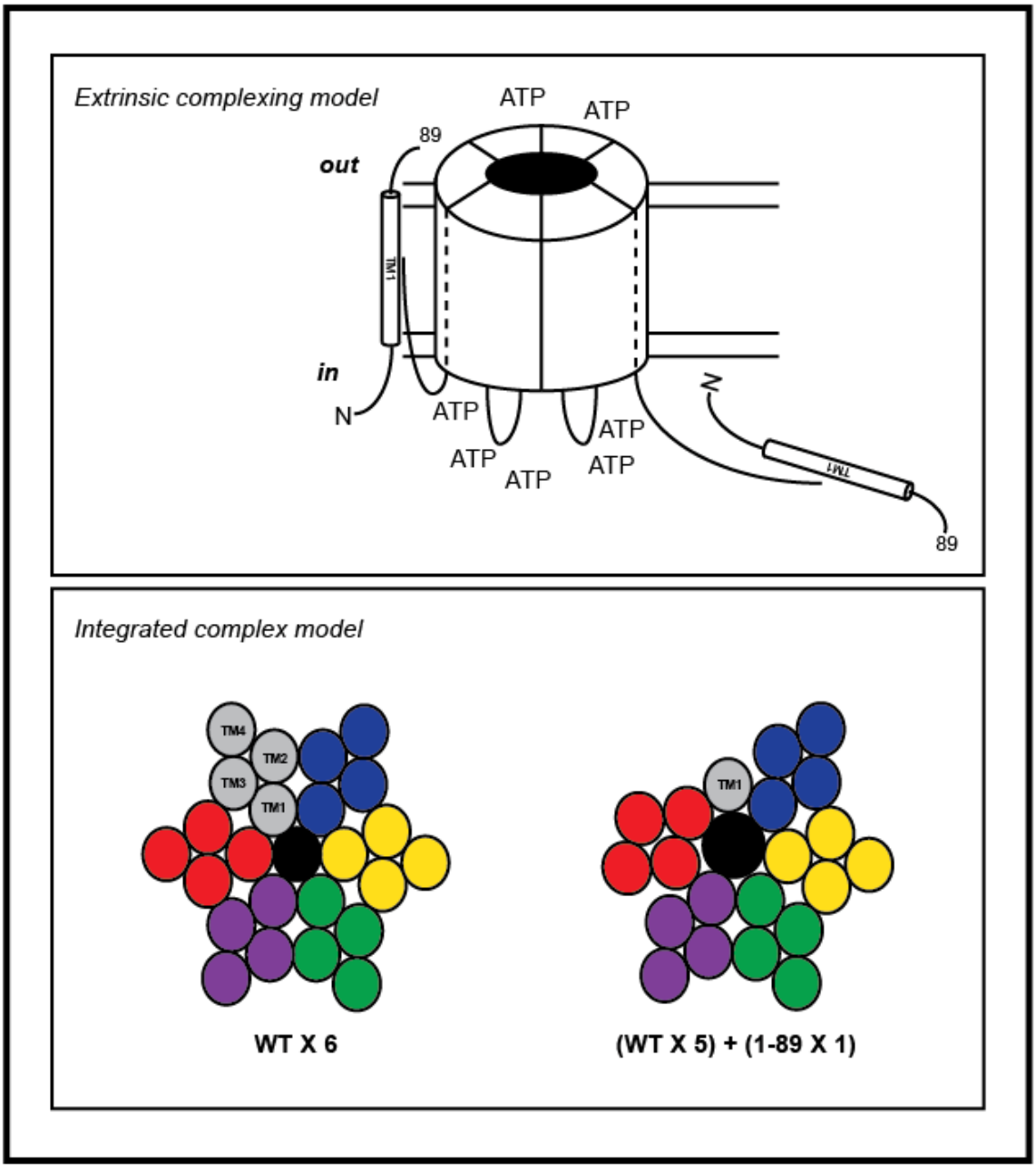

Figure 55. Hypothetical models of PANX1$^{1-89}$-mediated augmentation of PANX1 channel activity. See text for discussion.

Solving the question of how PANX1$^{1-89}$ mediates enhancement of ATP release through PANX1 channels should be of interest to many seemingly unrelated fields. Channel structural biologists and electrophysiologists may gain insight into the gating mechanisms of mechanosensitive channels in human cells—a largely unresolved area of research. Those in the field of membrane biophysics may benefit from a deeper understanding of the mechanisms bridging mechanical stress on the cell membrane and the pathways that translate these forces into molecular signals. And cancer biologists may begin to look for more specific molecules that can inhibit these mutant channels for the prevention of metastatic dissemination and may also be motivated to look for other molecular mediators of cellular deformation.

The physical properties of metastatic cells—Observations that a large fraction of cancer cells perish upon arriving in the microvasculature of a secondary organ were first made over two decades ago[39]. While a bottleneck to metastatic colonization of this magnitude would seem to be of great interest to cancer biologists, relatively little effort has been given to furthering our understanding of the mechanisms that allow one cell to survive microvascular deformation when many others do not. An unbiased screen for mutations that promote metastasis has highlighted the importance of microvascular cell death as an impediment to metastatic colonization and has revealed the first molecular basis for cancer survival during lethal stretch. Investigations into other molecular regulators of survival during physical stress should be vigorously pursued.

A number of experiments could be performed to search for additional regulators of survival during deformation. One method would be to inject cancer cells into the vasculature of mice, harvest the blood and lungs shortly after (on the order of hours), collect and expand the surviving cancer cells, and continue repeating the process until highly deformable metastatic cancer cells have been selected. One could then compare the abilities of the parental cells and the resulting highly deformable sub-lines to stretch *in vivo* and *in vitro*. If these sub-lines prove to be more metastatic, any genetic changes (transcriptional, mutational, epigenetic, or otherwise) recurrently present in the deformable sub-lines could be investigated. To improve the chance of identifying important regulators of cell survival during deformation, *in vitro* selection of deformable cells could be performed in parallel. Current methods for stretching cells *in vitro* include placing cells in hypotonic solution, running cells through a microfluidics device or applying physical force with a mechanical cell-stretching device. Looking for genetic alterations found by both *in vivo* and *in vitro* stretch selection methods should allow investigators to filter out many nonfunctional passenger genetic changes. To improve even further on the methods for identifying regulators of deformation that promote metastasis, the genetic changes identified by stretch selection could be compared to the genetic changes seen upon *in vivo* metastatic selection, as any important mediators of deformation that function to improve metastatic efficiency should be enriched under both selective processes.

Identifying additional molecular regulators of survival during microvascular metastatic cell deformation may implicate new signaling pathways that could then

be targeted for the prevention of metastatic dissemination. Furthermore, a more detailed understanding of the physical characteristics of highly deformable cells may lead to the development of devices that could be surgically implanted into the vasculature of patients diagnosed with an aggressive primary tumor to specifically destroy cancer cells without disrupting erythrocytes, megakaryocytes, immune cells or other vital circulating factors.

The therapeutic role for targeting cancer dissemination—The discovery of activating mutations in PANX1, a plasma membrane channel that promotes the efficiency of metastatic dissemination, has revealed a potential therapeutic target for the prevention of metastasis. *In vivo* inhibition of this channel through the treatment of mice with carbenoxolone (Cbx), a drug approved in the UK for the treatment of gastroesophageal reflux disease (GERD), was shown to significantly decrease both metastatic dissemination at 24 hrs and metastatic lung colonization (Fig. 52). These data suggest that inhibiting PANX1 channels with Cbx therapy in patients diagnosed with primary tumors of known or unknown metastatic capabilities may hold potential for reducing metastatic burden. However, before implementing clinical trials testing the efficacy of Cbx therapy in such patients, it must be determined whether PANX1 inhibition effects the proliferation of cancer cells. Because the molecular inhibition of PANX1 channels in MDA-LM2 cells led to their accelerated proliferation, *in vivo* experiments whereby mice with established tumors are treated with Cbx and evaluated for tumor growth must be performed. If the results of these experiments show

unaltered, or even reduced, tumor growth, then serious consideration to initiating the design and implementation of clinical trials should be given.

If clinical trails do proceed and are shown to be effective, the future of targeting PANX1 may lie in resolving the structure of the open channel. Understanding the architecture of the pore and surrounding extracellular domains of PANX1 may suggest optimal targeting sites for the design of more specific and effective inhibitors.

Other nSNVs enriched during breast cancer metastasis to the lung—This study identified five recurrent nSNVs significantly enriched during breast cancer metastasis to the lung that were predicted to cause non-neutral alterations in the proteins they encode (Table 2). Four of these mutations were missense substitutions and one was a nonsense truncation. This study revealed the nonsense mutation, *PANX1 C268T*, to be a promoter of microvascular cancer cell survival during metastatic dissemination. It will be important for future investigations to test whether any of the four missense mutations also function to promote metastasis. The genes bearing the missense mutations included the mitochondrial ribosome-binding factor *RBFA*, the transcription factor *REST*, the adherens junction regulatory factor *KRIT1* and the zinc-finger-containing gene *ZSWIM6*. The potential functions of these mutations are discussed below.

RBFA encodes ribosome binding factor A, a largely uncharacterized human protein that has been suggested to regulate and promote the late maturation of the 28S small ribosomal subunit (SSU) in the mitochondria[49,50].

Inferences made by looking at 1) RbfA, the more thoroughly studied bacterial RBFA homologue, 2) the position of the *RBFA G773T* mutation in the RBFA protein (G258V), and 3) the function of mitochondrial proteins in general, suggest a possible role for this mutation in promoting metastasis. In bacteria, RbfA binds the SSU and plays a role in processing of the 16S rRNA precursor component of the SSU during late ribosome biosynthesis[50,51]. The release of RbfA from this subunit by the GTPase RsgA is required for the assembly of the bacterial ribosome[50]. Defects in RbfA release lead to growth defects that can be reversed by gain-of-function mutations in RbfA that result in the spontaneous release of RbfA from the SSU[50]. The location of the G258V mutation in the RBFA protein also provides a clue into its potential function. Glycine 258 is a highly conserved RBFA glycine that lies in the center of the GatB domain near the C-terminus of the RBFA. In the GatB protein, this domain interacts with tRNAs to transamidate Glu-tRNA to Gln-tRNA. Futhermore, structural studies have shown that RbfA binding to the SSU displaces a portion of the 16S rRNA involved in mRNA decoding and tRNA interactions[51]. It is possible that the GatB domain in human RBFA is responsible for interacting with rRNA during 28S SSU maturation and that a mutation in this domain might act to interfere with ribosomal maturation.

The relationship between mitochondria biology and cancer is also quite well established. For many years it has been known that cancer cells exhibit increased aerobic glycolysis—a phenomenon known as “the Warburg effect”—that makes the contribution of mitochondrial oxidative phosphorylation to total cellular energy production less significant[52]. Additionally, mitochondrial protein

alterations have also been implicated in promoting tumor cell metastasis through the generation of reactive oxygen species[53]. Based on this information, a putative model for the enhancement of metastasis by RBFA G258V can be proposed. If functional, the RBFA G258V mutation would likely interfere with mitochondrial protein translation. A mutation causing RBFA to resist removal from the SSU would result in reduced expression of those genes translated in the mitochondria, the majority of which are members of the protein complexes that comprise the electron transport chain[54]. Faulty ribosome assembly caused by RBFA G258V mutations that instead promote the premature spontaneous release of RBFA from the SSU would also be likely to result in improper ribosome maturation with resultant defects in mitochondrial protein translation. Though there is much evidence linking metabolic defects to cancer progression, the specific effect of RBFA G258V on metastasis would require further focused investigation.

Krev Interaction Trapped Protein 1 (KRIT1) functions in the regulation of cell-to-cell junctions between endothelial cells lining the blood vessel lumen[55]. The importance of normal KRIT1 function in maintaining stable endothelial junctions in humans has been validated by multiple studies identifying KRIT1 mutations as the cause of cerebral cavernous malformations[56-65]. Additionally, deletion of *KRIT1* in zebrafish led to the development of multiple vascular phenotypes, such as vessel dilation and thinning of vessel walls[66]. More recently, KRIT1 was shown to be a negative regulator of β-catenin signaling required for the stabilization of interactions between epithelial cells[67]. The junction-stabilizing

effects of KRIT1 are mediated by the binding of KRIT1 by the Rap1a GTPase[68]. The loss of KRIT1 at cell junctions results in increased β-catenin nuclear localization and transcriptional activity[67]. The KRIT1 S701N mutation resides in a highly conserved serine residue within the C-terminal KRIT1 band 4.1/Ezrin/Radixin/Moesin (FERM) domain, that regulates KRIT1's interaction with Rap1a as well as its localization to VE-cadherin-based adherens junctions[55]. This evidence suggests that a mutation in the KRIT1 FERM domain of metastatic cells could result in decreased cell adhesion and upregulated β-catenin signaling, both of which have been strongly implicated in promoting cancer metastasis[69,70]. To test this hypothesis, one could overexpress wild-type or mutant KRIT1 in the context of endogenous KRIT1 knockdown in metastatic cells and test their ability to metastasize *in vivo*. If these studies show that the expression of wild-type KRIT1 suppresses metastasis relative to KRIT1 S701N, investigations into the mutation's effect on Rap1a binding and β-catenin signaling should naturally follow.

RE1-silencing transcription factor (REST) functions as a repressor of neuron-specific genes in non-neural tissues and immature neurons[71]. REST has been shown to act as both a suppressor and promoter of tumor formation[72,73]. In breast cancer patients specifically, the loss of REST expression has been shown to result in a significantly worse prognosis and earlier disease recurrence[74]. The REST D941H mutation lies at the C-terminus of the REST protein. Interestingly, this mutation is positioned near a C-terminal zinc-finger domain known to bind to the co-repressor CoREST[75] and to be sufficient for repressing neuronal

transcription [76]. Based on this evidence, the REST D941H mutation could interfere with the interaction between REST and its C-terminal-binding co-repressors to induce the expression of a certain set of neuronal genes that promote the de-differentiation and metastatic capability of epithelial breast cancer cells. This mutation should be investigated through *in vivo* metastasis assays in a manner similar to that described above for the testing of the KRIT1 mutation. If this mutation proves to be functional in metastasis, it would be interesting to then look at the gene signatures induced by REST D941H expression relative to wild-type REST expression.

ZSWIM6 is an uncharacterized zinc-finger-containing protein of 1215 amino acids with no identifiable conserved domains. The ZSWIM6 V636M mutation lies near the center of this protein. By studying the role of wild-type ZSWIM6 and ZSWIM6 V636M in metastasis, important insight into its normal function could also be acquired.

Studying putative metastasis mutations in the future—The recent development of new technologies for the study of nucleotide substitutions in human genes will certainly benefit those interested in testing putative metastasis-promoting mutations. While overexpression and knockdown studies have become the mainstay of studying the function of protein coding mutations, they are not without significant drawbacks. Unless the function of a missense mutation is very simplistic, the overexpression of wild-type and mutant proteins to supraphysiological levels has the propensity to either create artificial phenotypes

or mask real effects. Similarly, the knockdown of genes using shRNA or siRNA can result in ineffective protein reduction. To overcome these challenges, those studying cancer genetics will likely adopt genome-editing techniques that significantly increase the efficiency of targeted gene modifications historically performed by homologous recombination.

Zinc-finger nucleases (ZNFs), transcription activator-like effector nucleases (TALENs) are rapidly advancing systems increasingly utilized for targeted genomic editing in many cell types. The general mechanism by which these systems act to modify specific sequences in the genome is by recognizing and cleaving a desired endogenous DNA site to form double strand breaks (DSBs) that induce high frequency homology-directed repair (HDR)[77]. By simultaneously providing a plasmid of donor DNA containing the desired genomic alteration sequence flanked by DNA homologous to the site of the DSB, the desired edits can be incorporated into the native genome through HDR. These systems differ in the way they recognize target DNA sequences and, by extension, in which sequences they can be used to edit. While zinc-finger proteins can theoretically target any desired sequence, the DNA recognition sequences of TALENs are most efficient when they start with a thymine (T) nucleotide[77].

The clustered regularly interspaced short palindromic repeats (CRISPR) system is the most recent genome-editing method to emerge and is currently the most constrained in the sequences it can be used to edit[78]. The CRISPER system acts as a site-specific DNA endonuclease that is used to perform RNA-

guided genome editing in human cells[77,78]. While it shows much promise, fairly strict target sequence requirements of the CRISPER/Cas system make it the most constrained of the three systems. However, since it is the most affordable method available for targeted genome editing, CRISPER will likely become rapidly more versatile in time.

By adding or removing a potentially functional mutation from the genome of cancer cells, these molecular tools will overcome the drawbacks of overexpression and knockdown highlighted above. As the efficiency of editing improves over time, these systems will likely become the gold standard for testing the roles of putative mutations in many diseases—perhaps most predominantly those implicated in cancer initiation and metastasis. As our understanding of the mutational drivers of cancer progression advances, more effective targeted therapies can be developed.

CHAPTER VII: MATERIALS AND METHODS

Cell culture—BT549 and MDA-MB-468 cells were a generous gift from S. Chandarlapaty (Human Oncology & Pathogenesis Program, Memorial Sloan-Kettering Cancer Center). CN34, MDA-MB-231 cells and their respective sub-lines, LM1A and LM2, were propagated as previously described[13,14,16]. HEK293T, *PANX1*-null MEFs, MDA-MB-468 and WiDR cells were cultured in DMEM-based media supplemented with 10% FBS, glutamine, pyruvate, penicillin, streptomycin and fungizone. BT549 and HCC1806 lines were cultured in RPMI-based media supplemented with 10% FBS, glutamine, pyruvate, penicillin, streptomycin and fungizone. Sw480 cells were cultured in McCoy's media supplemented with 10% FBS, glutamine, pyruvate, penicillin, streptomycin and fungizone. HUVEC cells were cultured as previously described[15,16]. All transfections were performed using Lipofectamine 2000 (Life Technologies).

RNA sequencing, read alignment, allele frequency quantification and SNV calling—Total RNA was extracted using the MiRvana kit (Ambion) and reverse transcribed using the cDNA First-Strand Synthesis kit (Life Technologies). For whole-transcriptome sequencing, cDNA libraries were generated using the mRNA Sequencing Sample Preparation Kit (Illumina, 2009) according to the manufacturer's instructions and sequencing-by-synthesis was performed using the GAIIx sequencer (Illumina). For read alignment, the quality of the reads generated by high-throughput sequencing was first examined using the FASTX toolkit (http://hannonlab.cshl.edu/fastx_toolkit/). The reads were then trimmed

and filtered by quality and aligned against the human genome (release hg18) using the TopHat aligner[79], which builds exon models *de novo* from the RNA-seq data and aligns reads across splice junctions. PCR duplicates that might interfere with SNV calling were removed. A statistical framework was then implemented to identify SNVs from the read alignments based on the assumption that biological variations will be found in a significant number of reads, while non-biological variations will not. A Poisson-Binomial distribution[80] was used to calculate the p-values of significance, taking into account the total number of reads at each genomic position, number of reads with mismatches, as well as the error rate at each sequencing cycle (e.g. typically the sequencing error is higher during later stages of sequencing). *P*-values were corrected for multiple hypotheses using the Benjamini-Hochberg method[81] and the false discovery rate was controlled to 1%. SNVs identified in less than 10 unique reads were removed from further analysis. The SNVs were also filtered to remove known single nucleotide polymorphisms (SNPs) reported in dbSNP (v130) and annotated with in-house programs (Elemento Laboratory, W.C.M.C., in preparation). Two additional computational algorithms (SNVmix[82] and VarScan[83]) independently validated these methods. SNV allelic ratios were calculated by dividing the number of unique reads containing a given variant by the total number of unique reads at each position[20]. Amino acid substitutions resulting from the nSNVs were ranked by the likelihood of being non-neutral using the computational tool PolyPhen-2 (http://genetics.bwh.harvard.edu/pph2/)[23].

Allele-specific RNA-seq—Two-step PCR reactions of the *PANX1 C268T* allele in biological triplicates of each cell line were performed using the barcoded primers listed in Table 5. PCR amplicons were then sequenced using the HiSeq2000 (Illumina) platform. Position specific quantification of each allele was performed and used to calculate the *PANX1 C268T* allelic frequency of each cell line replicate.

Sanger sequencing— Sanger sequencing was performed by GENEWIZ. Sequencing primers are listed in Table 5.

Sequence Database Search—Clinical PANX1 mutations across human cancers were identified by searching the annotated variants provided by the Catalogue of Somatic Mutations in Cancer (COSMIC) and previous next-generation sequencing studies[84-88].

Animal studies— All animal work was conducted in accordance with protocols approved by the Institutional Animal Care and Use Committee at The Rockefeller University. Seven- to eight-week-old age-matched female NOD/SCID mice were used for breast cancer tail-vein lung colonization- and systemic-metastatic colonization assays[14,16]. Eight-week-old age-matched male NOD/SCID gamma mice were used for colon cancer liver metastatic colonization assays (through intrasplenic injection)[16]. *PANX1*-null mice (Shestopalov lab, University of Miami) were bred for the generation *PANX1*-null MEFs at embryonic

day 14 (E14). For the *in vitro* PANX1 inhibition metastasis assays, 1×10^5 LM1A or 4×10^4 LM2 cells in100 µl were incubated for 30 min with either 100 µM ^{10}Panx1 (Tocris), 100 µM scrambled peptide (Tocris), 500 µM Cbx (Sigma-Aldrich) or an equivalent volume of PBS vehicle and injected intravenously into the lateral tail-vein. For the *in vivo* therapeutic PANX1 inhibition metastasis assays, mice were weighed, treated with Cbx or an equivalent volume of PBS by intraperitoneal injections at the indicated times and doses, and then tail-vein injected with 1×10^5 LM1A or 4×10^4 LM2 cells. For the PANX1 extracellular ATP release assays, 1×10^5 MDA-LM2 cells expressing plasma membrane-anchored luciferase[89] (LM2-pmeLUC) were preincubated with Cbx (500 µM) or an equivalent volume of PBS vehicle and injected into seven-week-old age-matched female FVB/NJ mice. For orthotopic metastasis assays, two primary tumors per NSG mouse were generated through bilateral injections of 2.5×10^5 MDA-MB-468 or 5.0×10^5 HCC1806 breast cancer cells into the lower mammary fat pads. The resulting tumors were measured every three days, size-matched, extracted at 100 mm^3 and metastatic cell dissemination and colonization was noninvasively assayed through bioluminescence imaging as previously described[14]. For the long-term metastasis assays involving extracellular ATP depletion, 1×10^6 CN-LM1A cells expressing the plasma membrane-anchored extracellular ATP hydrolase CD39 or control vector, were injected into the lateral tail-vein of NS mice. For the acute extracellular ATP depletion assays, cells were preincubated with apyrase (2U/ml; NEB) or an equivalent volume of succinate buffer control and injected into seven-week-old age-matched female FVB/NJ

mice. For the truncated PANX1 *in vivo* metastasis assays, 5×10^5 cells (MDA-MB-468, BT549, sw480 or WiDR) per 100 µl PBS were introduced intravenously through tail-vein (MDA-MB-468 and BT549) or intrasplenic (sw480 and WiDR) injections. Caspse activity was measured *in vivo* through retro-orbital injection of 0.75 mg of VivoGlo™ Caspase 3/7 Substrate (Z-DEVD-Aminoluciferine Sodium Salt) (Promega)[90] per mouse.

Generation of PANX1-null MEFs—MEFs from E14 *PANX1*-null embryos were generated as previously described[91].

Generation of retrovirus and stable overexpression cells—Generation of retroviral-overexpressing cells was performed as previously described[14-16]. Primers used to generate overexpression constructs are listed in Table 5. C-terminus fluorescent protein-tagged PANX1, PANX1$^{1-89}$ and PANX1-L47fs*18 were cloned into the respective pcDNA3-EGFP and pcDNA3-mRFP1 vectors with a GRPLE linker. Plasma-membrane anchored extracellular luciferase was cloned as previously described[89]. CD39 (clone 5762493, Open Biosystems) was stably expressed using the lentiviral pLenti vector system. For bioluminescent tracking of MDA-MB-468, BT549, HCC1806, sw480 and WiDR cancer lines, cells were labeled with a triple-fusion protein reporter construct as previously described[5].

Analysis of mRNA expression—Expression of mRNA was quantified as described previously[14]. Primers can be found in Table 5.

Immunofluorecence and confocal microscopy—Cells expressing fluorescently tagged proteins were fixed in 4% paraformaldehyde, stained with DAPI (Roche), mounted using ProLong Gold Antifade reagent (Life Technologies), and imaged using the Leica TCS SP5 II system.

Immunoprecipitation and immunoblotting—Cellular lysates were prepared by lysing cells (10-40 million) overnight in ice-cold RIPA buffer containing protease and phosphatase inhibitors (Roche). The next day, cellular debris was removed by centrifugation (12,000 rpm) for 20 min at 4 °C. A 50 µL slurry of Anti-FLAG M2 Magnetic Beads (Sigma-Aldrich) was added to the supernatant and rocked for 4 hrs at 4 °C. The beads were then washed three times with ice-cold lysis buffer. The immunoprecipitated proteins were eluted by denaturation in Laemmli buffer at 95 °C for 5 min, separated using SDS–PAGE, transferred to a PVDF membrane (Pierce), blocked and probed using a primary antibody to the N-terminal of PANX1 (1:1,000; ZMD.695 from Life Technologies). Bound antibodies were chemi-luminescently detected using horseradish peroxidase–conjugated secondary antibodies (1:10,000), ECL Western Blotting Substrate (Pierce) and the SRX-101A (Konica Minolta) developer, according to the manufacturer's instructions.

Protein crosslinking immunoprecipitation and immunoblotting— Dithiobis[succinimidyl propionate] (DSP) was dissolved in anhydrous DMSO, diluted in PBS to formulate crosslinking solutions at the concentrations indicated, and used to crosslink cells in culture according to the manufacturer's instructions (Pierce). Crosslinked cells were then washed twice in PBS and lysed using ice-cold RIPA buffer supplemented with protease and phosphatase inhibitors (Roche). Lysates were collected by cell scraping, sonicated and rotated at 4 °C for 4-12 hrs. Cellular debris was removed by centrifugation (12,000 rpm) for 20 min at 4 °C. Protein concentrations were measured using the BCA protein assay (Pierce). For immunoprecipitation of crosslinked proteins, a 50 µL slurry of Anti-RFP Magnetic Beads (MBL International) was added to 200 µg protein lysates diluted in 750 µL Co-IP lysis buffer (Thermo Scientific) and rocked for 4 hrs at 4 °C. The beads were then washed three times in Co-IP lysis buffer, resuspended in Non-Reducing Lane Marker Sample Buffer (Thermo Scientific), boiled at 95 °C for 5 min, and separated using SDS-PAGE on a Novex 3-8% Tris-Acetate gel (Life Technologies). For crosslinked PANX1 complex immunoblotting, primary antibodies to PANX1 (1:1000; Life Technologies), GFP (1:1000, ab290 from Abcam) and RFP (1:1000; biotin conjugated ab34771 from Abcam) were used. Bound antibodies were chemi-luminescently detected using horseradish peroxidase–conjugated secondary antibodies, ECL Western Blotting Substrate (Pierce) and the SRX-101A (Konica Minolta) developer, according to the manufacturer's instructions.

ATP release assays —Cells were seeded in quadruplicate at 100,000-200,000 cells per well in 24-well plates and grown overnight. Each well was then washed with 200 µl PBS. For PANX1 inhibition, cells were incubated at room temperature for 10 min in PBS supplemented with one of the following reagents: Cbx (500 µM), PB (2 mM; Life Technologies), ^{10}Panx1 (100 µM) or an equivalent dose of the appropriate vehicle control (100% PBS or scrambled peptide). The wash or pretreatment solution was then aspirated, replaced with 200 µM fresh 100% PBS or 70% PBS (hypotonic stretch assays) for the indicated times, harvested and transferred to microcentrifuge tubes, and then spun at 1,000 rpm for 2 min at room temperature. Supernatants were transferred to 96-well plates and ATP was measured using the CellTiter-Glo Luminescent Cell Viability Assay (Promega) according to the manufacturer's instructions. For hypotonic stretch assays, the numbers of viable cells remaining post-stretch were counted for each treatment condition to rule out the contribution of cell lysis to extracellular ATP levels.

Histology—For histological quantification of single breast cancer cells, mice lungs were extracted at one and three days post cancer cell injection. By administering solutions through the heart and trachea, lungs were perfused and fixed with PBS and 4% paraformaldehyde, respectively. Frozen lung sections (10 microns thick) were stained with an antibody raised against human vimentin (1:40, Vector Laboratories) and DAPI. Alexa Fluor 488 Dye (1:200, Life Technologies) was used to detect vimentin. Slices were mounted using ProLong

Gold Antifade Reagent (Life Technologies). For histological quantification of metastatic foci, mice lungs were extracted at the indicated time-points, perfused and fixed as above, and sent out for sectioning and H&E staining (Histoserv). Quantification of cells and metastatic foci in histological step-sections was performed in a blinded manner. For endothelial labeling, 100 mg of biotinlyated lectin dissolved in PBS was injected retro-orbitally and allowed to circulate for 5 min prior to fixation. Mice were subsequently sacrificed, and their lungs were extracted without perfusion and fixed in 4% paraformaldehyde overnight. Frozen lung sections (10 microns thick) were stained with antibodies against human vimentin (1:40, Vector Laboratories) and cleaved caspase-3 (1:2000, Cell Signaling Technology). Primary antibodies were detected using Alexa-fluor dye-conjugated secondary antibodies (1:200, Life Technologies.) Stained sections were mounted using ProLong Gold Antifade Reagent (Life Technologies). Images were obtained using Zeiss scanning laser confocal microscope (LSM 510).

Hypotonic deformation cell viability assays—Cells were seeded in quadruplicate at 100,000 cells per well in 24-well plates and grown overnight. When comparing wild-type and mutant PANX1-expressing cells, replicate plates of cells were counted at the time of the assay for normalization. Each well was then washed once with 200 µl 100% PBS. For PANX1 inhibition, cells were incubated with 100 µM ^{10}Panx1 or scrambled peptides for 10 min in 100% PBS. The wash or pretreatment solution was then aspirated, and the cells were

stretched in 200 µl hypotonic solution (12.5% PBS) supplemented with the indicated reagents or vehicle controls for the times indicated. For ATP rescue experiments, 100 µM ATP (NEB) was added to the ^{10}Panx1 hypotonic solution, and an equivalent volume of water was added to the control hypotonic solution. For pan-P2yR inhibition experiments, suramin (50 µM; Sigma-Aldrich) or water vehicle control was added to the pretreatment solution. For ATP depletion experiments, apyrase (2 U/ml) or an equivalent volume of succinate buffer control was added to the hypotonic solution. After deformation, the cells were gently washed twice with 100% PBS, trypsinized, stained with trypan blue (Sigma-Aldrich) and the remaining viable cells were quantified.

Cancer cell proliferation—For molecular PANX1 inhibition assays, 5×10^3 cancer cells overexpressing either the autoinhibitory C-terminal domain or control vector were seeded in quadruplicate in a 96 well plate in a 100 µl volume of DMEM-based containing 10% FBS. At days 0, 3, and 5, cells were trypsinized and viable cells were counted using a hemocytometer. Proliferation counts were normalized to day 0. For peptide inhibition proliferation assays, cancer cells were pretreated with 100 µM ^{10}Panx1 peptide or vehicle for 15 min and seeded into 24 well plates (25,000 cells/well) under the same conditions as pretreatment. After 24 hrs, cancer cells were trypsinized and viable cells were counted using a hemocytometer.

Invasion assays—Invasion assays were performed as previously described[16]. Briefly, serum starved sub-lines were pretreated for 15 min with 100 μM of ^{10}Panx1 peptide or scrambled peptide in 0.2% FBS DMEM-based media, seeded onto Trans-well invasion chambers (BD Biosciences) under the same treatment conditions and incubated for 18-20 hrs. Cells that had invaded the inserts were counted in five fields per insert and then quantified using ImageJ.

Transendothelial migration assays—Transendothelial migration assays were performed as previously described[16]. Briefly, serum starved Cell Tracker Green CMFDA-labeled (Life Technologies) MDA-LM2 cells were pretreated for 15 min with 100 μM of ^{10}Panx1 peptide or scrambled peptide in 0.2% FBS DMEM-based media, seeded on a monolayer of HUVEC cells under the same treatment conditions (50,000 cells/well) and incubated for 18 hrs. Migrated cells were counted in five fields per insert and then quantified using ImageJ.

Anchorage-independent survival—Cancer cells (5,000 cells/well) were seeded in quadruplicate on 96-well Ultra-Low Attachment Surface plates (Corning) in the presence of 100 μM of ^{10}Panx1 peptide or scrambled peptide in 10% FBS DMEM-based media and incubated for 36 hours. Cell suspensions were then transferred to microcentrifuge tubes, isolated by centrifugation (1,000 rpm) for 5 min, trypsinized and counted using a hemocytometer.

Statistical analysis and clinical validation of PANX1 expression—To determine the association between *PANX1* gene expression and tumor grade, we used two independent datasets (expO and GSE5460) to stratify tumors based on BR-grades (high versus low) and employed one-tailed unpaired t-test to calculate the associated p-values. For Kaplan-Meier curves depicting associations between public datasets of breast[47], lung[47] and colon (GSE17536) tumor PANX1 expression and metastasis-free survival, an expression score greater or lower than the mean of the entire population was classified as high or low PANX1 expression, respectively. P-values are based on a Mantel-Cox log-rank test.

Table 5. List of primers used in this study.

Cloning primers	Sequence
PANX1-F-EcoRI	CGGAATTCATGGCCATCGCTCAACTG
PANX1-R-SalI	ACGCGTCGACTCAGCAAGAAGAATCCAGAAGTC
PANX1(1-89)-R-SalI	ACGCGTCGACCTACTGAACAGCCGCCCAGCAATA
PANX1-FLG-R_SalI	ACGCGTCGACTCACTTGTCATCGTCGTCCTTGTAGTCGCAAGAAGAATCCAGAAGTC
(1-89)-FLG_R_sall	ACGCGTCGACTCACTTGTCATCGTCGTCCTTGTAGTCCTGAACAGCCGCCCAGCAATA
PANX1(Ct)-Fwd	CGGAATTCatgCCATTCCGACAGAAGACAGAT
PANX1_Fluoro_F	CGGGATCCATGGCCATCGCTCAACTG
PANX1_WT-GFP_R	GCGGCCGCCCGCAAGAAGAATCCAGAAGTC
PANX1_Q90-RFP_R	GCGGCCGCCCCTGAACAGCCGCCCAGCAATA
Px1_L47fs-RFP_R	GCGGCCGCCCTCTGTGTACCAATCGAGATC
CD39_F	GGATCCATGGAAAGTGAAGAGTTGGCAGA
CD39_R	GAATTCCTATACCATATCTTTCCAGAA
PANX1-delCt-R	ACGCGTCGACCTAAACAAACAGCGTGTAGACAACCA
Sequencing primers	**Sequence**
PANX1_C268-F	GCCATGGCCATCGCTCAACT
PANX1_C268-R	GGCTTTCAGATACCTCCCACAA
PANX1_gDNA-F	CTGTTGGGAGGTTTGCAGTCGTG
PANX1_gDNA-R	AGATACAGCACTGGTTGGCTACAA
KRIT1-F	GAAAAACAGATTGAAGACCCACTA
KRIT1-R	ACCACGAGACCAGCCTGTTTTGTA
RBFA-F	CCTGAGGAATGTGCCACCGATAGT
RBFA-R	TCCTCTGTTCTGCCACCTCCTCTC
REST-F	AGAGCCTCCCCTTCACA
REST-R	CGAGCCCCATGCAATCCAGA
ZSWIM6-F	AGCCACTTGCAGCACATTATCAGC
ZSWIM6-R	CAGCGAGGGTAGCGGTTGG
PANX1-seg-1-F	GCGCCCGGCCGGTGACTGG
PANX1-seg-1-R	AACTTGGGCTCCGTGGGCTCCTTC
PANX1-seg-2-F	CCGGCCGGTGACTGGGTGAAGG
PANX1-seg-2-R	GCGAAGGCCAGCGAGATGAGCA
PANX1-seg-3-F	GAGCCCACGGAGCCCAAGTTCAAG
PANX1-seg-3-R	TCGCAAAGAGCAGCAGGATGTAGG
Allele Specific Primers	
asC268T-F	TCCCTACACGACGCTCTTCCGATCTATTACGCGCTTTGTGGATTCATATTGC
asC268T-R	GTTCAGACGTGTGCTCTTCCGATCTGGGAGGTTTCCAGACTCG
Illumina_C268T-F	AATGATACGGCGACCACCGAGATCTACACTCTTTCCCTACACGACGCTCTTCCGATCT
Illumina_C268T-R	CAAGCAGAAGACGGCATACGAGATCGTGATGTGACTGGAGTTCAGACGTGTGCTCTTCCGATCT
Quickchange Primers	
PANX1-136delC_QC-F	GGACAAGATGGTCACGTGCATTGCGGTGGGGCTGCCCTGCTGCTCATCTCGCTGGCCTTCGCGCAGG
PANX1-136delC_QC-R	CCTGCGCGAAGGCCAGCGAGATGAGCAGCAGGGCAGCCCCACCGCAATGCACGTGACCATCTTGTCC
Casp-Res-F	GGCATGATCAAGATGGCTGTTGTTGCTGGCAAAACTCCCATG
Casp-Res-R	CATGGGAGTTTTGCCAGCAACAACAGCCATCTTGATCATGCC
C265R-F	GCCCGATCAGTTTCAGCGCAAACTCATTGCCGT
C265R-R	ACGGCAATGAGTTTGCGCTGAAACTGATCGGGC
R217H-F	CAAGTACATTAGCTGCCACCTGCTGACACTCATCA
R217H-R	TGATGAGTGTCAGCAGGTGGCAGCTAATGTACTTG
L421H-F	GAATGCCCGACAGAGACATCTGGATTCTTCTTGCT
L421H-R	AGCAAGAAGAATCCAGATGTCTCTGTCGGGCATTC
V290M-F	TCCTGCTGGCTCCCATGGTTGTCTACACG
V290M-R	CGTGTAGACAACCATGGGAGCCAGCAGGA

REFERENCES

1 Stratton, M. R., Campbell, P. J. & Futreal, P. A. The cancer genome. *Nature* **458**, 719-724, doi:10.1038/nature07943 (2009).

2 Stratton, M. R. Exploring the genomes of cancer cells: progress and promise. *Science* **331**, 1553-1558, doi:10.1126/science.1204040 (2011).

3 Mardis, E. R. A decade's perspective on DNA sequencing technology. *Nature* **470**, 198-203, doi:10.1038/nature09796 (2011).

4 Yachida, S. *et al.* Distant metastasis occurs late during the genetic evolution of pancreatic cancer. *Nature* **467**, 1114-1117, doi:10.1038/nature09515 (2010).

5 Vogelstein, B. *et al.* Cancer genome landscapes. *Science* **339**, 1546-1558, doi:10.1126/science.1235122 (2013).

6 DeSantis, C., Siegel, R., Bandi, P. & Jemal, A. Breast cancer statistics, 2011. *CA Cancer J Clin* **61**, 409-418, doi:10.3322/caac.20134 (2011).

7 Gupta, G. P. & Massagué, J. Cancer metastasis: building a framework. *Cell* **127**, 679-695, doi:10.1016/j.cell.2006.11.001 (2006).

8 Talmadge, J. E. & Fidler, I. J. AACR centennial series: the biology of cancer metastasis: historical perspective. *Cancer Res* **70**, 5649-5669, doi:10.1158/0008-5472.CAN-10-1040 (2010).

9 Hanahan, D. & Weinberg, R. A. Hallmarks of cancer: the next generation. *Cell* **144**, 646-674, doi:10.1016/j.cell.2011.02.013 (2011).

10 Chiang, A. C. & Massagué, J. Molecular basis of metastasis. *N Engl J Med* **359**, 2814-2823, doi:10.1056/NEJMra0805239 (2008).

11 Greaves, M. & Maley, C. C. Clonal evolution in cancer. *Nature* **481**, 306-313, doi:10.1038/nature10762 (2012).

12 Fidler, I. J. Selection of successive tumour lines for metastasis. *Nat New Biol* **242**, 148-149 (1973).

13 Minn, A. J. *et al.* Genes that mediate breast cancer metastasis to lung. *Nature* **436**, 518-524, doi:10.1038/nature03799 (2005).

14 Tavazoie, S. F. *et al.* Endogenous human microRNAs that suppress breast cancer metastasis. *Nature* **451**, 147-152, doi:10.1038/nature06487 (2008).

15 Pencheva, N. *et al.* Convergent multi-miRNA targeting of ApoE drives LRP1/LRP8-dependent melanoma metastasis and angiogenesis. *Cell* **151**, 1068-1082, doi:10.1016/j.cell.2012.10.028 (2012).

16 Png, K. J., Halberg, N., Yoshida, M. & Tavazoie, S. F. A microRNA regulon that mediates endothelial recruitment and metastasis by cancer cells. *Nature* **481**, 190-194, doi:10.1038/nature10661 (2012).

17 Oskarsson, T. *et al.* Breast cancer cells produce tenascin C as a metastatic niche component to colonize the lungs. *Nat Med* **17**, 867-874, doi:10.1038/nm.2379 (2011).

18 Gupta, G. P. *et al.* Mediators of vascular remodelling co-opted for sequential steps in lung metastasis. *Nature* **446**, 765-770, doi:10.1038/nature05760 (2007).

19 Meyerson, M., Gabriel, S. & Getz, G. Advances in understanding cancer genomes through second-generation sequencing. *Nat Rev Genet* **11**, 685-696, doi:10.1038/nrg2841 (2010).

20 Ding, L. *et al.* Genome remodelling in a basal-like breast cancer metastasis and xenograft. *Nature* **464**, 999-1005, doi:10.1038/nature08989 (2010).

21 Biankin, A. V. *et al.* Pancreatic cancer genomes reveal aberrations in axon guidance pathway genes. *Nature* **491**, 399-405, doi:10.1038/nature11547 (2012).

22 Gundry, M. & Vijg, J. Direct mutation analysis by high-throughput sequencing: from germline to low-abundant, somatic variants. *Mutat Res* **729**, 1-15, doi:10.1016/j.mrfmmm.2011.10.001 (2012).

23 Adzhubei, I. A. *et al.* A method and server for predicting damaging missense mutations. *Nat Methods* **7**, 248-249, doi:10.1038/nmeth0410-248 (2010).

24 Bao, L., Locovei, S. & Dahl, G. Pannexin membrane channels are mechanosensitive conduits for ATP. *FEBS Lett* **572**, 65-68, doi:10.1016/j.febslet.2004.07.009 (2004).

25 Locovei, S., Bao, L. & Dahl, G. Pannexin 1 in erythrocytes: function without a gap. *Proc Natl Acad Sci U S A* **103**, 7655-7659, doi:10.1073/pnas.0601037103 (2006).

26 Ransford, G. A. *et al.* Pannexin 1 contributes to ATP release in airway epithelia. *Am J Respir Cell Mol Biol* **41**, 525-534, doi:10.1165/rcmb.2008-0367OC (2009).

27 Seminario-Vidal, L. *et al.* Rho signaling regulates pannexin 1-mediated ATP release from airway epithelia. *J Biol Chem* **286**, 26277-26286, doi:10.1074/jbc.M111.260562 (2011).

28 Chekeni, F. B. *et al.* Pannexin 1 channels mediate 'find-me' signal release and membrane permeability during apoptosis. *Nature* **467**, 863-867, doi:10.1038/nature09413 (2010).

29 Sandilos, J. K. & Bayliss, D. A. Physiological mechanisms for the modulation of pannexin 1 channel activity. *J Physiol* **590**, 6257-6266, doi:10.1113/jphysiol.2012.240911 (2012).

30 Corriden, R. & Insel, P. A. Basal release of ATP: an autocrine-paracrine mechanism for cell regulation. *Sci Signal* **3**, re1, doi:10.1126/scisignal.3104re1 (2010).

31 Schumacher, D., Strilic, B., Sivaraj, K. K., Wettschureck, N. & Offermanns, S. Platelet-Derived Nucleotides Promote Tumor-Cell Transendothelial Migration and Metastasis via P2Y2 Receptor. *Cancer Cell* **24**, 130-137, doi:10.1016/j.ccr.2013.05.008 (2013).

32 Bruzzone, R., Barbe, M. T., Jakob, N. J. & Monyer, H. Pharmacological properties of homomeric and heteromeric pannexin hemichannels expressed in Xenopus oocytes. *J Neurochem* **92**, 1033-1043, doi:10.1111/j.1471-4159.2004.02947.x (2005).

33 Ma, W., Hui, H., Pelegrin, P. & Surprenant, A. Pharmacological characterization of pannexin-1 currents expressed in mammalian cells. *J Pharmacol Exp Ther* **328**, 409-418, doi:10.1124/jpet.108.146365 (2009).

34 Gulbransen, B. D. *et al.* Activation of neuronal P2X7 receptor-pannexin-1 mediates death of enteric neurons during colitis. *Nat Med* **18**, 600-604, doi:10.1038/nm.2679 (2012).

35 Sandilos, J. K. *et al.* Pannexin 1, an ATP release channel, is activated by caspase cleavage of its pore-associated C-terminal autoinhibitory region. *J Biol Chem* **287**, 11303-11311, doi:10.1074/jbc.M111.323378 (2012).

36 Silverman, W., Locovei, S. & Dahl, G. Probenecid, a gout remedy, inhibits pannexin 1 channels. *Am J Physiol Cell Physiol* **295**, C761-767, doi:10.1152/ajpcell.00227.2008 (2008).

37 Thompson, R. J., Zhou, N. & MacVicar, B. A. Ischemia opens neuronal gap junction hemichannels. *Science* **312**, 924-927, doi:10.1126/science.1126241 (2006).

38 Qian, B. *et al.* A distinct macrophage population mediates metastatic breast cancer cell extravasation, establishment and growth. *PLoS One* **4**, e6562, doi:10.1371/journal.pone.0006562 (2009).

39 Weiss, L., Nannmark, U., Johansson, B. R. & Bagge, U. Lethal deformation of cancer cells in the microcirculation: a potential rate regulator of hematogenous metastasis. *Int J Cancer* **50**, 103-107 (1992).

40 Wong, C. W. *et al.* Apoptosis: an early event in metastatic inefficiency. *Cancer Res* **61**, 333-338 (2001).

41 Kienast, Y. *et al.* Real-time imaging reveals the single steps of brain metastasis formation. *Nat Med* **16**, 116-122, doi:10.1038/nm.2072 (2010).

42 Weiss, L. Biomechanical interactions of cancer cells with the microvasculature during hematogenous metastasis. *Cancer Metastasis Rev* **11**, 227-235 (1992).

43 Weiss, L., Harlos, J. P. & Elkin, G. Mechanism of mechanical trauma to Ehrlich ascites tumor cells in vitro and its relationship to rapid intravascular death during metastasis. *Int J Cancer* **44**, 143-148 (1989).

44 Li, A. *et al.* Mechanisms of ATP release, the enabling step in purinergic dynamics. *Cell Physiol Biochem* **28**, 1135-1144, doi:10.1159/000335865 (2011).

45 Zhang, M., Piskuric, N. A., Vollmer, C. & Nurse, C. A. P2Y2 receptor activation opens pannexin-1 channels in rat carotid body type II cells: potential role in amplifying the neurotransmitter ATP. *J Physiol* **590**, 4335-4350, doi:10.1113/jphysiol.2012.236265 (2012).

46 Belete, H. A., Hubmayr, R. D., Wang, S. & Singh, R. D. The role of purinergic signaling on deformation induced injury and repair responses of alveolar epithelial cells. *PLoS One* **6**, e27469, doi:10.1371/journal.pone.0027469 (2011).

47 Győrffy, B. *et al.* An online survival analysis tool to rapidly assess the effect of 22,277 genes on breast cancer prognosis using microarray data of 1,809 patients. *Breast Cancer Res Treat* **123**, 725-731, doi:10.1007/s10549-009-0674-9 (2010).

48 Wang, J. & Dahl, G. SCAM analysis of Panx1 suggests a peculiar pore structure. *J Gen Physiol* **136**, 515-527, doi:10.1085/jgp.201010440 (2010).

49 Dennerlein, S., Rozanska, A., Wydro, M., Chrzanowska-Lightowlers, Z. M. & Lightowlers, R. N. Human ERAL1 is a mitochondrial RNA chaperone involved in the assembly of the 28S small mitochondrial ribosomal subunit. *Biochem J* **430**, 551-558, doi:10.1042/BJ20100757 (2010).

50 Goto, S., Kato, S., Kimura, T., Muto, A. & Himeno, H. RsgA releases RbfA from 30S ribosome during a late stage of ribosome biosynthesis. *EMBO J* **30**, 104-114, doi:10.1038/emboj.2010.291 (2011).

51 Datta, P. P. *et al.* Structural aspects of RbfA action during small ribosomal subunit assembly. *Mol Cell* **28**, 434-445, doi:10.1016/j.molcel.2007.08.026 (2007).

52 Vander Heiden, M. G., Cantley, L. C. & Thompson, C. B. Understanding the Warburg effect: the metabolic requirements of cell proliferation. *Science* **324**, 1029-1033, doi:10.1126/science.1160809 (2009).

53 Ishikawa, K. *et al.* ROS-generating mitochondrial DNA mutations can regulate tumor cell metastasis. *Science* **320**, 661-664, doi:10.1126/science.1156906 (2008).

54 Clayton, D. A. Transcription of the mammalian mitochondrial genome. *Annu Rev Biochem* **53**, 573-594, doi:10.1146/annurev.bi.53.070184.003041 (1984).

55 Boettner, B. & Van Aelst, L. Control of cell adhesion dynamics by Rap1 signaling. *Curr Opin Cell Biol* **21**, 684-693, doi:10.1016/j.ceb.2009.06.004 (2009).

56 Cavé-Riant, F. *et al.* Spectrum and expression analysis of KRIT1 mutations in 121 consecutive and unrelated patients with Cerebral Cavernous Malformations. *Eur J Hum Genet* **10**, 733-740, doi:10.1038/sj.ejhg.5200870 (2002).

57 Laberge-le Couteulx, S. *et al.* Truncating mutations in CCM1, encoding KRIT1, cause hereditary cavernous angiomas. *Nat Genet* **23**, 189-193, doi:10.1038/13815 (1999).

58 Sahoo, T. *et al.* Computational and experimental analyses reveal previously undetected coding exons of the KRIT1 (CCM1) gene. *Genomics* **71**, 123-126, doi:10.1006/geno.2000.6426 (2001).

59 Sahoo, T. *et al.* Mutations in the gene encoding KRIT1, a Krev-1/rap1a binding protein, cause cerebral cavernous malformations (CCM1). *Hum Mol Genet* **8**, 2325-2333 (1999).

60 Davenport, W. J. *et al.* CCM1 gene mutations in families segregating cerebral cavernous malformations. *Neurology* **56**, 540-543 (2001).

61 Verlaan, D. J. *et al.* Cerebral cavernous malformations: mutations in Krit1. *Neurology* **58**, 853-857 (2002).

62 Verlaan, D. J. *et al.* CCM1 mutation screen of sporadic cases with cerebral cavernous malformations. *Neurology* **62**, 1213-1215 (2004).

63 Gianfrancesco, F. *et al.* Highly variable penetrance in subjects affected with cavernous cerebral angiomas (CCM) carrying novel CCM1 and CCM2 mutations. *Am J Med Genet B Neuropsychiatr Genet* **144B**, 691-695, doi:10.1002/ajmg.b.30381 (2007).

64 Liquori, C. L. *et al.* Different spectra of genomic deletions within the CCM genes between Italian and American CCM patient cohorts. *Neurogenetics* **9**, 25-31, doi:10.1007/s10048-007-0109-x (2008).

65 Cau, M. *et al.* C329X in KRIT1 is a founder mutation among CCM patients in Sardinia. *Eur J Med Genet* **52**, 344-348, doi:10.1016/j.ejmg.2009.05.002 (2009).

66 Hogan, B. M., Bussmann, J., Wolburg, H. & Schulte-Merker, S. ccm1 cell autonomously regulates endothelial cellular morphogenesis and vascular tubulogenesis in zebrafish. *Hum Mol Genet* **17**, 2424-2432, doi:10.1093/hmg/ddn142 (2008).

67 Glading, A. J. & Ginsberg, M. H. Rap1 and its effector KRIT1/CCM1 regulate beta-catenin signaling. *Dis Model Mech* **3**, 73-83, doi:10.1242/dmm.003293 (2010).

68 Serebriiskii, I., Estojak, J., Sonoda, G., Testa, J. R. & Golemis, E. A. Association of Krev-1/rap1a with Krit1, a novel ankyrin repeat-containing protein encoded by a gene mapping to 7q21-22. *Oncogene* **15**, 1043-1049, doi:10.1038/sj.onc.1201268 (1997).

69 Cavallaro, U. & Christofori, G. Cell adhesion in tumor invasion and metastasis: loss of the glue is not enough. *Biochim Biophys Acta* **1552**, 39-45 (2001).

70 Damsky, W. E. *et al.* β-catenin signaling controls metastasis in Braf-activated Pten-deficient melanomas. *Cancer Cell* **20**, 741-754, doi:10.1016/j.ccr.2011.10.030 (2011).

71 Lunyak, V. V. & Rosenfeld, M. G. No rest for REST: REST/NRSF regulation of neurogenesis. *Cell* **121**, 499-501, doi:10.1016/j.cell.2005.05.003 (2005).

72 Majumder, S. REST in good times and bad: roles in tumor suppressor and oncogenic activities. *Cell Cycle* **5**, 1929-1935 (2006).

73 Weissman, A. M. How much REST is enough? *Cancer Cell* **13**, 381-383, doi:10.1016/j.ccr.2008.04.011 (2008).

74 Wagoner, M. P. *et al.* The transcription factor REST is lost in aggressive breast cancer. *PLoS Genet* **6**, e1000979, doi:10.1371/journal.pgen.1000979 (2010).

75 Andrés, M. E. *et al.* CoREST: a functional corepressor required for regulation of neural-specific gene expression. *Proc Natl Acad Sci U S A* **96**, 9873-9878 (1999).

76 Tapia-Ramírez, J., Eggen, B. J., Peral-Rubio, M. J., Toledo-Aral, J. J. & Mandel, G. A single zinc finger motif in the silencing factor REST represses the neural-specific type II sodium channel promoter. *Proc Natl Acad Sci U S A* **94**, 1177-1182 (1997).

77 Gaj, T., Gersbach, C. A. & Barbas, C. F. ZFN, TALEN, and CRISPR/Cas-based methods for genome engineering. *Trends Biotechnol* **31**, 397-405, doi:10.1016/j.tibtech.2013.04.004 (2013).

78 Burgess, D. J. Technology: a CRISPR genome-editing tool. *Nat Rev Genet* **14**, 80, doi:10.1038/nrg3409 (2013).

79 Trapnell, C., Pachter, L. & Salzberg, S. L. TopHat: discovering splice junctions with RNA-Seq. *Bioinformatics* **25**, 1105-1111, doi:10.1093/bioinformatics/btp120 (2009).

80 Chen, S., Liu JS. Statistical Applications of the Poisson-Binomial and Conditional Bernouilli Distributions. *Statistica Sinica* **7**, 875-892 (1997).

81 Benjamini Y, H. T. Controlling the False Discovery Rate: A Practical and Powerful Approach to Multiple Testing. *Journal of the Royal Statistical Society Series B (Methodological)*, 289-300 (1995).

82 Goya, R. *et al.* SNVMix: predicting single nucleotide variants from next-generation sequencing of tumors. *Bioinformatics* **26**, 730-736, doi:10.1093/bioinformatics/btq040 (2010).

83 Koboldt, D. C. *et al.* VarScan: variant detection in massively parallel sequencing of individual and pooled samples. *Bioinformatics* **25**, 2283-2285, doi:10.1093/bioinformatics/btp373 (2009).

84 Forbes, S. A. *et al.* COSMIC: mining complete cancer genomes in the Catalogue of Somatic Mutations in Cancer. *Nucleic Acids Res* **39**, D945-950, doi:10.1093/nar/gkq929 (2011).

85 Network, C. G. A. Comprehensive molecular portraits of human breast tumours. *Nature* **490**, 61-70, doi:10.1038/nature11412 (2012).

86 Network, C. G. A. Comprehensive molecular characterization of human colon and rectal cancer. *Nature* **487**, 330-337, doi:10.1038/nature11252 (2012).

87 Network, C. G. A. R. Integrated genomic analyses of ovarian carcinoma. *Nature* **474**, 609-615, doi:10.1038/nature10166 (2011).

88 Network, C. G. A. R. Comprehensive genomic characterization of squamous cell lung cancers. *Nature* **489**, 519-525, doi:10.1038/nature11404 (2012).

89 Pellegatti, P., Falzoni, S., Pinton, P., Rizzuto, R. & Di Virgilio, F. A novel recombinant plasma membrane-targeted luciferase reveals a new pathway for ATP secretion. *Mol Biol Cell* **16**, 3659-3665, doi:10.1091/mbc.E05-03-0222 (2005).

90 Biserni, A., Martorana, F., Roncoroni, C., Klaubert, D., Maggi, A., Ciana, P. Identification of Apoptotic Cells in Reporter Mice Using Modified Luciferin. *TOP (TRANSGENIC OPERATIVE PRODUCTS) SRL* (2010).

91 Xu, J. Preparation, Culture, and Immortalization of Mouse Embryonic Fibroblasts. *Current Protocols in Molecular Biology* **28.1**, 8, doi:10.1002/0471142727.mb2801s70 (2005).